EXPERIMENTAL INVESTIGATION INTO CONVECTIVE HEAT TRANSFER IN THE TRANSITION FLOW REGIME BY USING NANOFLUIDS IN A RECTANGULAR CHANNEL

by

SOHAIB MUSTAFA MOHAMMED OSMAN

submitted in partial fulfilment of the requirements for the degree

Philosophiae Doctor in Mechanics

in the

Department of Mechanical and Aeronautical Engineering

Faculty of Engineering, Built Environmental and Information Technology

University of Pretoria

Pretoria

2020

DEDICATION

I dedicate this work to:

my father, Mr Mustafa Mohammed Osman, and my mother, Mrs Fatheia Mohammed Ahmed;

my wife, with special gratitude for her unlimited support and sacrifices throughout my PhD journey; and my beloved children, Weaam, Mustafa and Mohammd.

ACKNOWLEDGEMENTS

- I acknowledge the financial support from the Clean Energy Research Group at the Department of Mechanical and Aeronautical Engineering at the University of Pretoria, and also appreciate and acknowledge the fund provided by the NRF and DST of South Africa.

- I want to express my sincerest gratitude to my supervisor, Prof Mohsen Sharifpur, for his continuous supervision throughout the research period, and his technical guidance and support.

- I appreciate the financial and academic support from my co-supervisor and the head of the Department of Mechanical and Aeronautical Engineering at the University of Pretoria, Prof Josua Meyer.

- I acknowledge the assistance of Mr Charles Moon and Mr Koos Mtoombini in building the test section and modifying the experimental set-up: they were always ready for any technical help or advice.

ABSTRACT

Title: Experimental investigation into convection heat transfer in the transition flow regime by using nanofluids in a rectangular channel

Supervisor: Prof Mohsen Sharifpur

Co-supervisor: Prof Josua Meyer

Department: Mechanical and Aeronautical Engineering

Degree: PhD (Mechanics)

The growing demand for energy worldwide requires attention to the design and operating of heat exchangers and thermal devices to utilise and save thermal energy. There is a need to find new heat transport fluids with better heat transfer properties to increase convective heat transfer, and nanofluids are good alternatives to conventional heat transport fluids. Although extensive research has been done on the properties of nanofluids in recent decades, there is still a lack of research on convection heat transfer involving nanofluids, particularly in the transitional flow regime. This study focused on the application of nanofluids in heat exchangers as heat transport fluids by investigating forced convective heat transfer of alumina-water and titanium dioxide-water nanofluids prepared by using the one-step method. The particle size used was 46 nm and 42 nm for the aluminium oxide and the titanium dioxide respectively. Uniform heat flux boundary conditions were used by uniformly heating the rectangular channel electrically. Nanofluids with volume concentrations of 0.3, 0.5 and 1% were used for the alumina-water nanofluids, and volume concentrations of 0.3, 0.5, 0.7 and 1% were used for the titanium dioxide-water nanofluids. The viscosity of the nanofluids under investigation was determined experimentally, while the thermal conductivity and other properties were predicted by using suitable correlations from the literature. A Reynolds number range of 200 to 7 000 was covered, and the investigated flow rates included the laminar and turbulent flow regimes, as well as the transition regime from laminar to turbulent flow. Temperatures and pressure drops were measured to evaluate heat transfer coefficients, Nusselt numbers and pressure drop coefficients. Heat transfer and hydrodynamic characteristics in the transition flow regime were carefully studied and compared with those in the transition regime when flowing pure water in the same test section.

The study also investigated another approach of enhancing heat transfer in heat exchangers by increasing the heat transfer area of the heat exchanger itself, and this was done by filling the rectangular test section with porous media to increase the heat transfer surface area and thus enhance heat transfer. Hence in this study, the effect of using porous media was also studied by filling the rectangular test section with high-porosity nickel foam. The permeability of the used nickel foam was determined by conducting pressure drop measurements through the nickel foam in the test section, and heat transfer and pressure drop parameters were measured and compared with those in the empty test section.

The results showed that all the nanofluids used enhanced heat transfer, particularly in the transition flow regime. The 1.0% volume concentration alumina nanofluid showed maximum enhancement of the heat transfer coefficient, with values of 54% and 11% in the turbulent regime. The maximum enhancement of the heat transfer coefficient was 29.3% in the transition regime for the 1.0% volume concentration titanium dioxide-water nanofluid. The thermal performance factor in the transition flow regime was observed to be better than that in the turbulent and laminar flow regimes for all the nanofluids.

The results of the nickel foam test section showed that the values of the friction coefficient were 24.5 times higher than the values of the empty test section, and the Nusselt number was observed to be three times higher when using nickel foam than without foam in the test section. No transition regime was observed for the foam-filled test section on either the heat transfer results or the pressure drop results; however, transition from laminar to turbulent was found for the test section without foam. The results of the thermal factor of the foam-filled test section showed a thermal performance factor higher than unity through the entire Reynolds number range of 2 000 to 6 500, with better thermal performance factor at lower Reynolds number.

TABLE OF CONTENTS

DEDICATION i
ACKNOWLEDGEMENTS ii
ABSTRACT iii
TABLE OF CONTENTS v
LIST OF FIGURES viii
LIST OF TABLE xi
NOMENCLATURE xii
PUBLICATIONS IN JOURNALS AND CONFERENCE PROCEEDINGS xiii
CHAPTER 1 INTRODUCTION 1
1.1 Introduction 1
1.2 Background 1
1.2.1 Convection heat transfer of nanofluids 1
1.2.2 Hydrodynamics and heat transfer characteristics of metal foams 5
1.3 Problem statement 8
1.4 Research objectives 8
1.5 Thesis structure 10
CHAPTER 2 LITERATURE REVIEW 11
2.1 Introduction 11
2.2 Preparation of nanofluids 12
2.2.1 One-step method 12
2.2.2 Two-step method 13
2.3 Thermal conductivity of nanofluids 14
2.3.1 Factors affecting the thermal conductivity of nanofluids 15
2.3.2 Experimental investigation into thermal conductivity 17
2.3.3 Analytical investigation and modelling of thermal conductivity 19
2.4 Viscosity of nanofluids 22
2.4.1 Experimental investigation into viscosity of nanofluids 23
2.4.2. Theoretical investigation 26
2.5 Convection heat transfer of nanofluids 28
2.5.1 Experimental investigation into convective heat transfer in laminar flow 29
2.5.2 Experimental investigation into convective heat transfer in turbulent flow 32
2.5.3 Experimental investigation into convective heat transfer in transitional flow regime 37
2.6 Transition in plain horizontal tubes 38
2.7 Conclusion 41

CHAPTER 3 EXPERIMENTAL SET-UP AND TEST SECTION 43
3.1 Introduction 43
3.2 Experimental set-up 43
3.3 Test section 44
3.4 The test section with porous media insert 47
3.5 Instruments 49
3.5.1 Pressure transducers 49
3.5.2 Flow meter 49
3.5.3 Power supply 49
3.5.4 Data acquisition system 50
3.6 Testing procedures 50
3.7 Conclusion 50
CHAPTER 4 DATA REDUCTION AND VALIDATION OF THE SET-UP 51
4.1 Introduction 51
4.2 Data reduction 51
4.2.1 Pressure drop 51
4.2.2 Heat transfer 52
4.3 Uncertainty analysis 54
4.4 Validation of the experimental set-up 55
4.4.1 Validation of friction coefficient results 55
4.4.2 Validation of Nusselt number results 58
4.5 Conclusion 62
CHAPTER 5 NANOFLUID PREPARATION AND PROPERTY ANALYSIS 63
5.1 Introduction 63
5.2 Nanoparticle size and properties 63
5.3 Preparation of nanofluids 65
5.3.1 Preparation and dilution of nanofluids 65
5.3.2 Stability of nanofluids 65
5.4 Thermophysical properties of nanofluids 67
5.4.1 Thermal conductivity 67
5.4.2 Viscosity and other properties 68
5.5 Conclusion 70
CHAPTER 6 RESULTS AND DISCUSSION 71
6.1 Introduction 71
6.2 Heat transfer results of Al_2O_3-water nanofluids 71
6.3 Pressure drop results of Al_2O_3-water nanofluids 73

6.4 Comparison of convective heat transfer and pumping power 75
6.5 Heat transfer results of TiO_2-water nanofluids 76
6.6 Pressure drop and friction coefficient results 79
6.7 Evaluation of the heat transfer performance of nanofluids 80
6.8 Comparison of the two nanofluids 81
6.8.1 Heat transfer coefficient and Nusselt number 81
6.8.2 Pressure drop and friction coefficient results 86
6.8.3 Thermal performance evaluation of nanofluids 88
6.9 Heat transfer results of the porous media insert 89
6.9.1 Pressure drop across the test section with the nickel foam insert 89
6.9.2 Heat transfer evaluation of the test section with the nickel foam insert 91
6.9.3 Heat transfer enhancement evaluation of the nickel foam test section 93
6.10 Conclusion 93
CHAPTER 7 95
CONCLUSION AND RECOMMENDATIONS 95
7.1 Summary 95
7.2 Conclusions 96
7.2.1 Conclusions on aluminium oxide-water nanofluids 96
7.2.2 Conclusions on titanium dioxide-water nanofluids 96
7.2.3 Conclusions on comparison of aluminum with titanium dioxide-water nanofluids 97
7.2.4 Conclusions on nickel foam-filled test section 98
7.3 Recommendations 98
7.4 Challenges 99
REFERENCES 100
Appendix A 110
Calibration of thermocouple and pressure transducers 110
A.1 Results of thermocouple calibration 110
A.2 Results of pressure transducer calibration 118
Appendix B 119
Error estimation and uncertainty analysis 119
B.1 Introduction 119
B.2 Background 119
B.3 Uncertainty results 125
Appendix C 127
Thermal properties of the working fluids 127
C.1 Water properties 127

C.2 Nanofluid properties 128

LIST OF FIGURES

Figure 1. 1: Schematic relating the research aims with the research filed and the lack of knowledge in the area. 9

Figure 2. 1: Aggregation effect on the effective thermal conductivity [78]. 15
Figure 2.2: Exponential decrease to increase in temperature. 24
Figure 2.3: Change of viscosity with the particle diameter [26]. 25
Figure 2.4: Graphical representation of heat transfer coefficient and Reynolds number for various nanoparticles at different volume concentrations for turbulent flow regime. 36
Figure 2.5**:** Representation of flow regimes in terms of Nusselt number against Reynolds number. ... 38

Figure 3.1: Layout of the experimental set-up. 44
Figure 3.2**:** Schematic diagram of the test section. 45
Figure 3.3**:** Distribution of the thermocouple stations over the test section and pressure tap positions. 45
Figure 3.4**:** Thermocouple joint adjacent to the heating wire on the wall of the test section. 46
Figure 3.5**:** Layout of the nickel foam inserted into the test section, and the thermocouple station distribution. 47
Figure 3.6**:** Nickel foam placement in the open rectangular channel. 48
Figure 3.7**:** (a) Top opened test section and the foam, (b) foam inserted tightly into the test section, (c) foam mechanically ponded to the test section after the top of the test section was brazed. 48
Figure 3.8**:** (a) Mechanical ponding of the foam and the test section, (b) brazing of the top of the channel. 48

Figure 4.1: Adiabatic friction coefficient data compared with theoretical correlations. 56
Figure 4.2: Deviation of friction coefficients from correlations in the laminar regime. 56
Figure 4.3**:** Deviation of friction coefficients from correlations in the turbulent regime. 57
Figure 4.4**:** Nusselt number comparison with the correlation in the laminar flow regime. 58
Figure 4.5**:** Ratio of the predicted to the measured value of Nusselt number in the laminar regime. ... 59
Figure 4.6**:** Nusselt number comparison with correlations in the turbulent flow regime. 60
Figure 4.7**:** Ratio of the predicted to the measured value of Nusselt number in the turbulent regime. 61
Figure 4.8: Nusselt number variation with Reynolds number for the entire flow range. 61

Figure 5.1: TEM imaging of Al2O3-water nanofluid. 64
Figure 5.2**:** TEM imaging of TiO_2-water nanofluid. 64
Figure 5.3: Aluminium oxide nanofluid (left) and titanium dioxide nanofluid (right) immediately after the preparation. 65
Figure 5.4: Aluminium oxide nanofluid (left) and titanium dioxide nanofluid (right) after seven days since the preparation. 66
Figure 5.5: Variation of the viscosity of Al_2O_3-water nanofluids with time at 25 ˚C. 66
Figure 5.6: Variation of the viscosity of TiO_2-water nanofluids with time at 20 ˚C. 67

Figure 5.7: Viscosities of Al_2O_3-water nanofluids compared with water viscosity as a function of temperature. 68
Figure 5.8**:** Variation of TiO_2-water nanofluids viscosity with the temperature for different volume concentrations. 69
Figure 5. 9: Comparison of the thermal conductivity for the two nanofluids with the different concentrations at 25 °C 70
Figure 5. 10: Comparison of the viscosity for the two nanofluids with the different concentrations at 25 °C 70

Figure 6.1: Heat transfer coefficient results of Al_2O_3-water nanofluids compared with water against Reynolds number. 72
Figure 6.2: Nusselt number results of Al_2O_3-water nanofluids compared with water against Reynolds number. 73
Figure 6.3**:** Pressure drops of Al_2O_3-water nanofluids compared with water against Reynolds number. 74
Figure 6.4**:** Friction coefficients of Al_2O_3-water nanofluids compared with water against Reynolds number. 74
Figure 6.5**:** Convective heat transfer efficiency of Al_2O_3-water nanofluids in turbulent and transition flow regimes against the volumetric concentration. 75
Figure 6.6**:** Variation of heat transfer coefficients of TiO_2-water nanofluids and water with Reynolds number. 76
Figure 6.7: Nusselt number variation of TiO_2-water nanofluids compared with pure water. 77
Figure 6.8: Heat transfer coefficient enhancement of TiO_2-water nanofluids in transition regime 78
Figure 6.9**:** Nusselt number enhancement of TiO_2-water in trransition regime. 79
Figure 6.10**:** Pressure drop of TiO_2-water nanofluids and pure water as a function of Reynolds number. 79
Figure 6.11**:** Variation of friction coefficient of TiO_2-water nanofluids and water with Reynolds number. 80
Figure 6.12: Thermal performance factor of TiO_2-water nanofluids over Reynolds number through the full flow range. 81
Figure 6.13: Comparison of heat transfer coefficient for Al_2O_3- and TiO_2-water nanofluids at 0.3 vol%. 82
Figure 6.14: Nusselt number comparison of Al_2O_3- and TiO_2- water nanofluids at 0.3 vol%. 83
Figure 6.15: Comparison of heat transfer coefficient of Al_2O_3- and TiO_2-water nanofluids at 0.5 vol%. 84
Figure 6.16: Nusselt number comparison of Al_2O_3- and TiO_2-water nanofluids at 0.5 vol%. 84
Figure 6.17: Comparison of (a) heat transfer coefficient and (b) Nusselt number for Al_2O_3- and TiO_2-water nanofluids at 1.0 vol% 85
Figure 6.18: Comparison of (a) heat transfer coefficient and (b) Nusselt number for Al_2O_3- and TiO_2-water nanofluids at 1.0 vol% 86
Figure 6.19: Variation of friction coefficients with Reynolds number for all nanofluids compared with water 87
Figure 6.20: Variation of pressure drop with Reynolds number for all nanofluids compared with water 88
Figure 6.21: Thermal performance factor variation with volume concentration in the turbulent and the transition regimes for TiO_2- and Al_2O_3-water-based nanofluids 88
Figure 6.22: Linear relation of pressure gradient across the porous media with the velocity. 90

Figure 6.23: Friction coefficient variation with Reynolds number of the empty test section compared with the test section with nickel foam insert. 91
Figure 6.24: Local Nusselt number of two different flow rates through nickel foam in a rectangular test section. 92
Figure 6.25: Nusselt number comparison of flow through an empty rectangular test section and nickel foam-inserted test section. 92
Figure 6.26: Thermal performance factor variation with Reynolds number for flow through nickel foam in a rectangular test section. 93

Figure A.1: Calibration of the thermocouples used to measure the water temperature at (a) the inlet and (b) the outlet of the test section. 110
Figure A.2: Calibration of the four thermocouples in the first station: (a) top thermocouple, (b) thermocouple on the bottom side and (c) thermocouple on the eastern side of the test section. 111
Figure A.3: Calibration of the four thermocouples in the second station: (a) top thermocouple, (b) thermocouple on the bottom side and (c) thermocouple on the eastern side of the test section. 112
Figure A.4: Calibration of the four thermocouples in the third station: (a) top thermocouple, (b) thermocouple on the bottom side and (c) thermocouple on the eastern side of the test section. 113
Figure A.5: Calibration of the four thermocouples in the fourth station: (a) top thermocouple, (b) thermocouple on the bottom side and (c) thermocouple on the eastern side of the test section. 114
Figure A.6: Calibration of the four thermocouples in the fifth station: (a) top thermocouple, (b) thermocouple on the bottom side and (c) thermocouple on the eastern side of the test section. 115
Figure A.7: Calibration of the four thermocouples in the sixth station: (a) top thermocouple, (b) thermocouple on the bottom side and (c) thermocouple on the eastern side of the test section. 116
Figure A.8: Calibration of the four thermocouples in the seventh station: (a) top thermocouple, (b) thermocouple on the bottom side and (c) thermocouple on the eastern side of the test section. 117
Figure A.9: Calibration of high-range pressure transducer (PT2). 118
Figure A.10: Calibration of low-range pressure transducer (PT1). 118

LIST OF TABLE

Table 2.1: Summary of forced convection laminar flow experimental studies on nanofluids under constant heat flux boundary conditions. 32
Table 2.2**:** Summary of forced convection turbulent flow experimental studies on nanofluids under constant heat flux boundary conditions. 36

Table 3. 1: standard specification for the Ni foam supplied by Alantum. 47

Table 4.1: Range and accuracies of instruments. 54
Table 4.2**:** Uncertainties of the measured parameter at high and low Reynolds numbers. 55
Table 4.3: Correlations from the literature for the turbulent regime 59

Table 5.1**:** Properties of the nanofluid materials used 63

Table B.1: Uncertainty of the instruments used in the tests 125
Table B.2: Uncertainty of pure water properties 125
Table B.3: Uncertainty of heat transfer and pressure drop parameters for pure water. 126

NOMENCLATURE

A_c	Cross-section area	m^2
A_S	Surface area	m^2
C_P	Specific heat	J/kg. K
D_h	Hydraulic diameter	m
ΔP	Pressure drop	Pa
h	Heat transfer coefficient	W/m^2 °C
H	Height	m
h(x)	Local heat transfer coefficient	W/m^2 °C
k	Thermal conductivity	W/m °C
L	Length of the tube	m
$\dot{m}$	Mass flow rate	kg/s
p	Perimeter	m
$\dot{Q}$	Heat transfer rate	W
$\dot{q}$	Heat flux	W/m^2
T	Temperature	°C
V	Velocity	m/s
x	Local distance	m
Z	Width	m
$\frac{dP}{dx}$	Pressure gradient	Pa/m

Greek symbols

μ	Dynamic viscosity	kg/m. s
ρ	Density	kg/m^3
$\emptyset$	Volume concentration	
η	Convective heat transfer efficiency	
α	Aspect ratio	
Gr	Grashof number	
β	Expansion coefficient	
σ	Standard deviation	

Non-dimensional numbers

f	Friction coefficient
Re	Reynolds number
Nu	Nusselt number
pr	Prandtl number
Pe	Peclet number
pw	Wall factor
K	Permeability
C	Drag coefficient

Subscripts

Avg.	Average
b	Bulk
bf	Base fluid
e	Exit
Eff.	Effective
i	Inlet
m	Mean
nf	Nanofluid
P	Particles
w	Wall

PUBLICATIONS IN JOURNALS AND CONFERENCE PROCEEDINGS

Journal Articles

1. S. Osman, M. Sharifpur, and J. P. Meyer, Experimental investigation of convection heat transfer in the transition flow regime of aluminium oxide-water nanofluids in a rectangular channel, *International Journal of Heat and Mass Transfer,* vol. 133, pp. 895-902, 2019/04/01/ 2019.

2. S. Osman, M. Sharifpur, and J. P. Meyer, Effect of the thermal properties and nanoparticles size on the convection heat transfer enhancement in transition flow regime of metal oxides nanofluids flowing in a rectangular channel, *submitted to International Communications in Heat and Mass Transfer, manuscript number ICHMT-D-01317.*

3. S. Osman, M. Sharifpur, and J. P. Meyer, The influence of high porosity Nickel foam on the transition flow regime for heat transfer and pressure drop characteristics in a rectangular channel, *submitted to International Journal of Heat and Mass Transfer, manuscript number HMT_2020_791*.

Conference Papers

1. S. Osman, M. Sharifpur, and J. P. Meyer, Experimental examination of the transitional flow of dilute alumina-water nanofluid, *Proceedings of the 16th International Heat Transfer Conference, IHTC-16 August 10-15, 2018, Beijing, China.*

2. S. Osman, M. Sharifpur, and J. P. Meyer, The effect of chopping the boundary layer at the inlet on the transition heat transfer and pressure drop characteristics in smooth horizontal tube, *Proceedings of the 14th International Conference on Heat Transfer, Fluid Mechanics and Thermodynamics (HEFAT), Wicklow, Ireland, 22-24 July 2019.*

CHAPTER 1 INTRODUCTION

1.1 Introduction

Enhancing the heat transfer rate is one of the main issues at the design stage of different thermal devices for various industries, including the transfer rates in chemical processes, and heating and cooling processes. Several techniques have been studied and developed to reduce design and operation costs. All of these techniques revolve around a compromise between the minimisation of flow resistance and the enhancement of heat transfer coefficients. Therefore, it is vital to develop techniques to enhance the heat transfer rate in heat exchangers while attempting to keep the pressure drop as low as possible.

Because of the increasing demand for improvements in the performance of a heat exchanger, new heat transfer transport fluids called nanofluids were introduced towards the end of the last century. The term 'nanofluid' was first introduced by Choi in 1995 [1], after which many researchers investigated (i) the preparation and thermophysical properties of nanofluids [2-7], (ii) forced convection using nanofluids in heat exchangers [8-14], and (iii) natural convection of nanofluids in cavities [15-17].

1.2 Background

1.2.1 Convection heat transfer of nanofluids

Pak and Cho [18] experimentally measured the heat transfer and friction coefficients of Al_2O_3-water and TiO_2-water nanofluids for a fully developed turbulent flow. The addition of Al_2O_3 nanoparticles resulted in a 45% enhancement of the heat transfer coefficients at a volume concentration of 1.3%, with a 75% enhancement at a concentration of 2.7%.

Wen and Ding [19] investigated the heat transfer augmentation provided by Al_2O_3-deionised water nanofluids in the laminar flow regime, considering volume concentrations of 0.6, 1 and

1.6%. The local heat transfer coefficient results for the three nanofluids showed enhancements of heat transfer compared with that of water. The enhancement was significant in the entrance regime, with a value of 45%, and decreased towards the exit of the test section to 14%. The authors concluded that this heat transfer improvement was the result of particle movements and the reduction of the boundary layer thickness.

Anoop et al. [20] performed experiments to investigate the influence of particle size on heat transfer using 45 nm and 150 nm Al_2O_3 nanoparticles and weight concentrations of 1, 4 and 6%. Both sizes of Al_2O_3 nanoparticles showed the potential to increase heat transfer. The 45 nm nanofluid was found to be better than the 150 nm nanofluid as far as the heat transfer was concerned. Heat transfer correlations were developed for both nanofluids.

Hwang et al. [21] measured the convective heat transfer and pressure drop in the laminar flow regime in an experiment with an Al_2O_3-water-based nanofluid prepared using a two-step method. The covered volume concentration had a range of 0.01 to 0.3%. It was found that the heat transfer coefficient increased by 8% when using the 0.3% concentration.

Sahin et al. [22] performed experiments with an Al_2O_3-aqueous nanofluid. Their tests were carried out using volume concentrations of 0.5, 1, 2 and 4% in a circular pipe. It was observed that the heat transfer increased when the Reynolds number increased. It was also noticed that a volume concentration increase contributed to a heat transfer improvement of up to 1%. For a volume concentration higher than 1%, the viscosity increase was much higher than the increase in the thermal conductivity, which negatively affected the heat transfer.

Liu and Yu [23] conducted an experimental study on the single-phase forced convection heat transfer of an Al_2O_3-water nanofluid in a circular mini-channel. Friction factor and convection heat transfer coefficients were measured for nanofluids of various volume concentrations (1, 2, 3.5 and 5%) and compared with those of the base fluid. The Reynolds number range covered in the study was 600 to 4 500. The results showed that the friction factor and convective heat transfer coefficients were both less than those of water at the same Re in the transition flow, with no improvement in the turbulent and laminar regime. However, they failed to examine volume fractions smaller than 1%, which is an essential range for nanofluid applications.

Meyer et al. [24] experimentally investigated the convective heat transfer enhancement provided by multi-walled carbon nanotubes suspended in water, flowing in a straight horizontal circular tube. Nanofluid volume concentrations of 0.33, 0.75 and 1% were tested, and a Reynolds number range of 1 000 to 8 000 was covered. The transition began early compared with that of water, and the nanofluid concentration increased earlier. No heat transfer enhancement was found when comparing the heat transfer coefficients of the nanofluids with those of water, but there was an enhancement when comparing the Nusselt numbers of the nanofluids with those of water. The inefficiency of the nanofluids used was because the increase in the viscosity of the nanofluid was four times the increase in the thermal conductivity.

Kayhani et al. [25] conducted an experimental investigation into convective heat transfer and pressure drop in the turbulent flow of TiO_2-water nanofluid in a horizontal constantly heated pipe. Volume concentrations of 0.1, 0.5, 1.0, 1.5 and 2.0% were used. The results showed that the heat transfer coefficients did not change with Reynolds number but increased with an increase in the volume concentration of the nanofluid. The enhancement of the Nusselt number at Re = 11 800 was 8% when using a volume concentration of 2.0%.

He et al. [26] performed a set of experiments on aqueous suspensions of TiO_2 flowing through a vertical pipe in the laminar and turbulent flow regimes. Results revealed that the heat transfer coefficients of the nanofluid increased with the concentration as well as with the Reynolds number in both the laminar and the turbulent flow regimes. The volume concentrations covered were 0.24, 0.6 and 1.1%. The maximum enhancement achieved in the laminar flow regime was 12% at Re = 1 500 when using a volume concentration of 1.1%, while it was slightly above 40% at Re = 5 900 for the same nanofluid concentration. The effect of the nanoparticle size was also investigated, and the effect on the heat transfer found to be marginal. Thermal conductivity decreased with an increase in the volume concentration unlike the current work because the thermal conductivity increased with the concentration. Also, the Reynolds number was calculated based on the base fluid properties unlike in this research because thermal conductivity was evaluated based on the nanofluid properties. These differences can explain the different results in the laminar and turbulent flow regimes in this work.

Azmi et al. [27] experimentally investigated the convective heat transfer of titanium dioxide-water-based nanofluids in a plain tube and with different twisted-tape inserts. A nanofluid volume concentration range of 0.5 to 3% was studied, and the turbulent flow regime was the focus of the investigation. When nanofluid of 3 vol% flows in the clear tube, the heat transfer coefficient was decreased compared with that of pure water, while a significant enhancement of 23.2% in the heat transfer coefficient at Re = 23 917 was achieved at 1% volume concentration in the clear tube.

Sajadi and Kazemi [28] conducted an experimental investigation into turbulent heat transfer characteristics of titanium dioxide-water nanofluid in a circular tube. The volume concentration was from 0.05 to 0.25%. The heat transfer coefficients of the nanofluids were increased by 22% for 0.25% volume concentration. The study showed that increasing the concentration did not have any influence on the heat transfer enhancement in the studied range of concentration. A correlation was developed for the Nusselt number of the nanofluid because the experimental measurements were not in agreement with those of previous studies.

Duangthongsuk et al. [29] tested a volume concentration of 0.2% of TiO_2-water nanofluid in a double-tube counterflow heat exchanger. The results showed the heat transfer coefficients of the nanofluids were increased by 6 to 11% compared with those of pure water in the turbulent flow regime. In a similar work by Duangthongsuk et al. [30], the heat transfer enhancement in a horizontal double-tube counterflow heat exchanger under turbulent flow conditions was investigated. TiO_2-water nanofluids of 0.2 to 2% volume concentration were used. The results showed that the nanofluids of volume concentration less than 1% resulted in higher heat transfer coefficient than for the base fluid as the heat transfer enhancement was 26% at a volume concentration of 1%. However, at a higher concentration of 2%, the heat transfer coefficient was 14% lower than that of water. The pressure drop of the nanofluids was observed to be slightly higher than that of water when the concentration of the nanofluid was increased.

Arani and Amani [31] studied the effect of particle diameter of TiO_2-water-based nanofluid on the convection heat transfer enhancement for fully developed turbulent flow in a horizontal double-pipe counterflow heat exchanger. The particle sizes used were 10, 20, 30 and 50 nm, and the volume concentrations were 0.01, 0.015 and 0.02%. All particle sizes

showed improvement of Nusselt number compared with that of pure water as a heat transfer fluid. Furthermore, the thermal performance of the 20 nm particle size diameters was found to be the highest. The average Nusselt number increased with an increase in the Reynolds number and particle volume concentration. Similar work was conducted by Arani and Amani [32] to investigate TiO_2 (20 nm)-water-based nanofluid for the volume concentration of 0.002 to 0.02%. The Reynolds number range was 8 000 to 51 000. The results showed that when using a Reynolds number greater than 30 000, the pressure drop became higher than the increase in the heat transfer, making it more viable to use the nanofluid at a Reynolds number lower than this limit. However, for a lower Reynolds number, it was observed that the Nusselt number increased with an increase in the volume concentration or Reynolds number.

Hamid et al. [33] conducted experiments to study the convection heat transfer of TiO_2-water, the range of Reynolds numbers was 3 000 to 24 000 in a test section under constant heat flux. The nanofluid volume concentration was 0.5 to 1.5%, and bulk temperatures of 30 °C, 50 °C and 70 °C were used to evaluate heat transfer performance. Heat transfer coefficient results for a concentration of less than 1.2% were observed to be lower than the base fluid when evaluated at 30 °C. However, the heat transfer coefficients for all concentrations showed improvement at 50 °C and 70 °C. It was further observed that as the bulk working temperature increased, more enhancement was achieved at higher concentrations.

1.2.2 Hydrodynamics and heat transfer characteristics of metal foams

Metal foams are lightweight materials with an irregular cellular and porous structure, and metal foams can be split into (a) open-cell or (b) closed-cell. In the closed-cell metal foams, the cells form a stand-alone enclosure within the material, while in the open-cell metal foams, the cells are all interconnected with no walls permitting the fluid to pass with less pressure drop. The metal foams possess unique properties compared with the traditional porous media. However, not much research was done on metal foams, while many studies reported on conventional porous media [34-39] and some books have also focused on porous media [40, 41].

The type of metal foam used in this research falls under the group of the open-cell metal foams, and is a porous media with high porosity and the following interesting properties [42]:

(1) lightweight because of the high number of voids in the foam;

(2) high specific surface area, which leads to compact heat exchanger design;

(3) machinability and weldability to facilitate the formation of the complex parts;

(4) excellent fluid mixing, which enhances the convective heat transfer.

In the past few decades, several researchers investigated the use of metal foams in heat exchangers to reduce the size of heat exchangers in thermal management applications and to enhance heat transfer. The first study of metal foam was conducted by Beavers and Sparrow [43]. They studied the pressure drop across nickel foams without reporting the pore size and the porosity. The Reynolds number was evaluated based on the permeability. They found that the flow pattern deviated from the Darcy regime at unity Reynolds number. Paek et al. [44] determined the thermophysical properties of aluminium-based metal foams. The permeability and thermal conductivity of the foams were measured while air flowed through the metal foams. They found that permeability was influenced by the pore size and the porosity, while thermal conductivity increased when the porosity decreased and remained unaffected by the pore size. A correlation for the friction coefficient was developed as a function of permeability and inertial forces.

Miwa and Revankar [45] developed an apparatus to investigate the permeability of metal foam. Various nickel foams with different pore size were used. The permeability of nickel foams was experimentally determined by measuring the pressure drop across the foam. A correlation was obtained for this type of metal foam in a Darcian flow regime. The developed friction factor correlation was a function of the Reynolds number based on the permeability as characteristic length and included the effect of the pore size and structure. Calmidi and Mahajan [46] found that heat transfer enhancement was very low for aluminium foam when the working fluid was air, while water enhanced the forced convection heat transfer considerably. Kim et al. [47] studied the effect of metal foam permeability on Nusselt number and friction coefficients, and testing results on aluminium foams revealed that the low permeable foams resulted in high Nusselt number, but high friction factors were noticed.

Nazari et al. [48] studied the heat transfer and pressure drop characteristics of Al_2O_3-water nanofluids flowing in a horizontal circular pipe packed with metal foam, and compared the results with those of the empty tube. The results of the porous media test section showed

remarkable enhancement of heat transfer compared with those of the empty tube with a penalty in the pressure drop. A maximum increase in Nusselt number of 57% was achieved.

Noh et al. [49] conducted an experiment on an annulus filled with aluminium foam and obtained pressure drop, average and local convective heat transfer. The non-Darcy flow in the metal foam showed enhancement in the laminar flow regime compared with the empty annulus. The correlation for friction coefficient and heat transfer was developed to suit the tube-in-tube and shell-in-tube heat exchangers, and was used in the design phase for these heat exchangers.

Wang and Guo [50] investigated the pressure drop and the heat transfer performance of stainless steel metal foam. Three different pore sizes were manufactured using the sintering technique, and the pressure drop of air flowing at high speed was measured. Compared with the low-speed airflow correlations, the pressure drop was found to be highly dominated by inertial drag. The Nusselt numbers data were obtained under the convective boundary conditions and found to be higher than the values of the reported Nusselt number under constant heat flux condition. Mancin et al. [51] investigated the effect of foam height on the heat transfer coefficient and the pressure gradient of air flowing in two different aluminium foams with the same porosity but different heights. The heat flux was also changed, and the results revealed that the heat flux had no effect on the heat transfer, while increasing the foam height had a reverse impact on the heat transfer, and the pressure drop remained unchanged with the foam height.

Hamadouche et al. [52] considered the heat transfer enhancement of a foam-filled channel, which was filled with aluminium foam. The study reported that the heat transfer of air flowing through aluminium foam in the turbulent regime was 300% higher than in the empty channel.

Dukhan et al. [53] investigated flow regime in a metal foam consisting of an aluminium foam pore density of 20 pores per inch and a porosity of 87.6%. A set of points wasere measured to plot the friction coefficient of the foam with Reynolds number, and the square root of the permeability was considered as a characteristic length to evaluate Reynolds number. The transition from pre-Darcy to turbulent flow was investigated and compared with the transition in the traditional porous media found in the literature. The study showed that the permeability and inertial drag coefficient values were different in the various flow regimes for the same foam.

1.3 Problem statement

From the above review, it is clear that only two investigations [23, 24] were reported on the convective heat transfer of nanofluids in the transition flow regime, and both studies used circular channels. The current study is an attempt to close the research gap in convection heat transfer of nanofluids over the entire flow regime, including the transition flow regime. The current work differs from previous studies [23, 24] by using nanofluids prepared by thee one-step method, namely aluminium oxide- and titanium dioxide-aqueous nanofluids. Nanofluids prepared by using the one-step method were chosen because of the stability characteristics as they are generally stable for a longer time than nanofluids prepared by using the two-step method. In addition, the test section used in this work was a rectangular channel, and the concentrations used in this work were lower than those used in the work of Liu and Yu [23] to contribute to the knowledge. Moreover, a Reynolds number range of 200 to 7 000 was investigated in this study.

There is also a lack of research on the influence of high-porosity foams in heat transfer enhancement in rectangular channels. There is also a dearth of research on the transition from the Darcy to the non-Darcy regime. Therefore, this study pays attention to high-porosity nickel foam, and the comparison of heat transfer and pressure drop characteristics, and the transition in the foam-filled test section to the empty test section.

1.4 Research objectives

i. Obtaining heat transfer coefficients and pressure drop values for three Al_2O_3-water nanofluids and four TiO_2-water nanofluids compared with those of water.

ii. Determining the Nusselt number and friction coefficient data for four TiO_2-water nanofluids and Al_2O_3-water nanofluids and then conducting a comparison with pure water.

iii. Identifying the nature of the transition flow regime as well as the start and end of the transition in the rectangular channels and comparing it with the transition in the conventional circular channels found in the literature.

iv. Evaluating the heat transfer enhancement of the nanofluids by comparing the heat transfer capability to the penalty cause due to the pressure drop.

v. Investigating heat transfer and pressure drop characteristics in the nickel foam-filled test section and comparing these with the empty rectangular test section.

vi. Studying whether there is a transition in the porous media-filled test section in the same flow rate range of the empty test section and conducting a comparison between the two test sections regarding the thermal performance factor.

The above-listed objectives of the research can be related to progress in the research field and lack of information needed in the forced convection of nanofluids, the relation is illustrated in Figure 1.1.

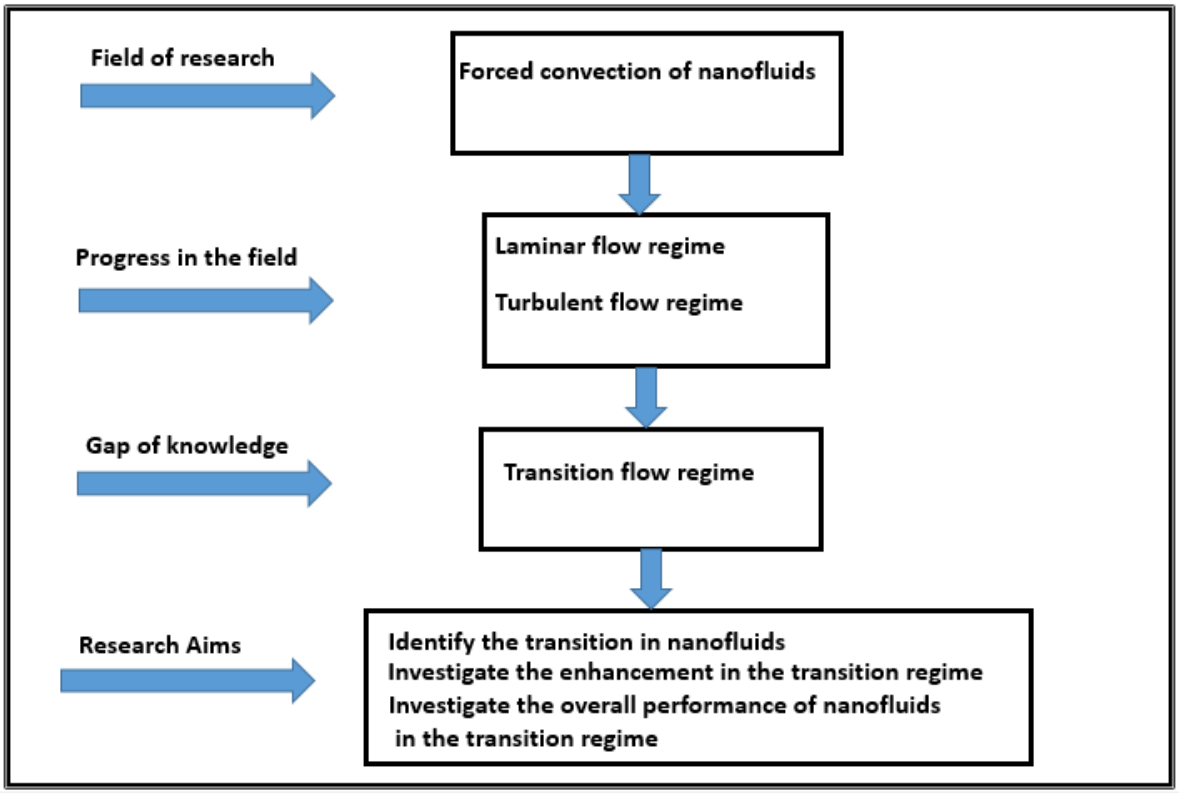

Figure 1. 1: Schematic relating the research aims with the research filed and the lack of knowledge in the area.

1.5 Thesis structure

The thesis consists of seven chapters; the chapters are divided into sections according to the topics relevant to the chapter subject. The structure of each chapter is described in this section.

Chapter 1 presents the definition of nanofluid and emphasises the importance of introducing such a new kind of heat transport fluid. In addition, background knowledge is presented, and the problem statement and the objective of the work are outlined. A literature review of the nanofluid preparation methods, thermal properties and convective heat transfer of nanofluids is presented in Chapter 2. In Chapter 3, a general description of the experimental set-up, experimental procedures and the test section building process are also presented in detail. Chapter 4 presents the data reduction and the validation of the experimental set-up against the available literature. The characteristics and the preparation of the nanofluids, as well as the measurements of the properties, are included in Chapter 5, while Chapter 6 presents the results obtained by the experimental investigations, and the highlight of those results accompanied by the recommendations are provided in Chapter 7.

CHAPTER 2 LITERATURE REVIEW

2.1 Introduction

Over the past quarter-century, researchers have worked to overcome the limitations of conventional heat transfer fluids (HTF) (such as water and air) and to develop alternative fluids with better heat transfer properties than the traditional ones. The need for such improvement is due to the growing demand and the broad applications of HTF in the industry (solar thermal systems, refrigeration, air-conditioning and microelectronics devices, etc.). The term ‘nanofluid’ emerged after the work of Choi [1]. The configuration of dispersed nanoparticles in a base fluid is known as nanofluid. Nanoparticles are metals (nickel, aluminium, copper, silver, etc.), non-metals (carbon nanotubes, graphite, Si, etc.), oxides of metals and oxides of non-metals. The base fluid mostly is water, but there are others that can be used such as ethylene glycol, propylene glycol and engine oil.

Nanofluids possess superior thermal properties such as high thermal conductivity, high specific surface area, mixture stability, and minimal blockage in flow passages when compared with micro- or millimetre-size particles mixing with a fluid [54]. The advantages of nanofluids in comparison with the fluids including micro-size can be summarised as follows:

- high stability of dispersion with principally Brownian motion of particles;
- reduced particle clogging;
- less pumping power required;
- adjustable properties by varying particle concentrations and or size to suit different applications;
- large specific surface area of nanoparticles enabling more heat transfer between particles and fluid.

Heat transfer experiments indicate that thermal conductivity is not the only parameter that influences heat transfer augmentation of the nanofluid [55]. Several mechanisms contribute to the heat transfer enhancement of nanofluids such as Brownian motion, Brownian diffusion, nanolayer interaction between nanoparticles and the base fluids.

2.2 Preparation of nanofluids

Preparation of nanofluids is a crucial process in getting a stable nanofluid, and the stability of nanofluids is the key factor in obtaining a nanofluid possessing superior properties. The following aspects must be considered while preparing a stable nanofluid:

1) The high surface energies of the nanofluids as a multiphase dispersion system lead to a thermodynamically unstable mixture.

2) The strong Brownian motions of the nanoparticles can counteract their sedimentation due to gravity force.

3) The dispersion of the nanoparticles can decline with time due to the aggregation of nanoparticles, which is caused by Van der Waals forces.

4) Chemicals between the base fluid and nanoparticles while using the nanofluid must be prevented.

The above-mentioned aspects indicate that nanofluid preparation is not as simple as mixing some nanoparticles in a base fluid, because aggregation and sedimentation are two critical factors influencing the stability of the nanofluids [56]. Two techniques are mainly used for synthesising nanofluids: the one-step method and the two-step method.

2.2.1 One-step method

The process of incorporating the preparation of nanoparticles into the synthesis of nanofluids is known as a one-step method. In this method, the nanoparticles are produced by a physical vapour deposition (PVD) technique or a liquid chemical method to minimise the agglomeration of nanoparticles and to increase the stability of nanofluids. The limitations of this method are that it is impossible to use in large industrial applications, and it can only be successfully used for low vapour pressure base fluids. The working vapour pressure limits the application of the method. Chang et al. [57] produced nanofluids of TiO_2 nanoparticles dispersed in pure water by using the one-step chemical method with a high-pressure homogeniser. This method is called modified magnetron sputtering.

2.2.2 Two-step method

In this technique, dry nanoparticles/nanotubes are first produced, and then they are dispersed in a suitable conventional liquid as the base fluid. The nanoparticles have high surface energy, aggregation and agglomeration are inescapable and become visible immediately. As a result, particle sediment accumulates at the bottom of the container. Therefore, preparing a homogeneous dispersion by the two-step method remains a substantial technical challenge in the nanofluid research area. However, there are some techniques which diminish this problem, like high shear and ultrasonication techniques.

This method is useful for oxide nanoparticles and high particle concentration (greater than 20 vol.%), but it is less effective with metal nanoparticles, although some surface-treated nanoparticles show excellent dispersion [58]. The disadvantages are due to the rapid agglomeration of the particles. Because nanoparticles disperse partially, the dispersion is weak and sedimentation occurs. Therefore, a high volume concentration is needed to increase the heat transfer (10 times higher than the volume needed in the preparation with the one-step method) and therefore the cost rises [59].

The following methods are used to improve the stability of the nanofluids prepared by the two-step technique:

i. Addition of surfactant:

Surfactants are a group of chemical solutions with the ability to improve dispersion stability by preventing nanoparticles forming sedimentation. The addition of surfactants to the nanofluids changes the surface of the nanoparticles due to the charges forming in the surface. The generation of repulsion force due to the surface charges of the particles helps the particles to move away from each other; this force is known as zeta potential [60-62]. The most common used surfactants are: sodium dodecyl sulfate (SDS) [60, 61], dodecyl trimethyl ammonium bromide (DTAB) and sodium octanoate (SOCT) [63], cetyltrimethylammonium bromide (CTAB)[64, 65].

ii. pH control

The stability of dispersion is directly related to the electrostatic charges of the particle surface (zeta potential). When the particles carry no charges (isoelectric point), the nanoparticles will agglomerate due to the absence of the repulsion force, but any movement from the isoelectric line will prevent the agglomeration and improve the stability. Xie et al. [66] showed that by simple acid treatment, a carbon nanotube suspension gained good stability in water. The reason for this is the change of particle surface geometry from a hydrophobic to a hydrophilic nature.

iii. Ultrasonication

The ultrasonication technique, unlike other device methods (magnetic and high shear stirrer), breaks down the agglomeration of the nanoparticles while the other methods intend to alter the surface properties of dissolved nanoparticles and to suppress the forming of groups of particles . Various apparatuses are used for the ultrasonication process. Ultrasonic bath, processor and homogeniser are potent devices for breaking down the agglomerations in comparison with the other apparatuses. However, sonication time is a critical factor in the process, and it has to be optimised because exceeding the optimum duration of the process will cause more severe problems in the agglomeration and clogging, resulting in fast sedimentation. Hwang et al. [67] proposed a new method to get stable suspensions, which consists of two micro-channels, dividing a liquid stream into two streams. Both streams are then recombined in a reacting container.

2.3 Thermal conductivity of nanofluids

Thermal conductivity is one of the significant parameters for enhancing the heat transfer performance of a heat transfer fluid. Metals have a thermal conductivity higher than those of fluids; therefore, the addition of nanoparticles to the base fluid is anticipated to enhance the conductivity and consequently heat transfer performance. A considerable increase in thermal conductivity can be achieved by the inclusion of only a small percentage of solids as reported by several researchers [56, 59, 68-70].

2.3.1 Factors affecting the thermal conductivity of nanofluids

The mechanisms that affect the conductivity of nanofluids are the aggregation of particles, the Brownian motion, and the interfacial layer. These phonemes have been discussed by [71-75] and are summarised in this section.

Maxwell [76] introduced a theory which considered nanofluid as a two-phase flow mixture and then evaluated nanofluid properties by the mixture theory as a combination of solid and fluid properties. The developed model is based on an effective medium theory that presumes well-dispersed particles in a fluid medium. If the particles in the fluid become agglomerated around particle chains or clusters, then the predicted thermal conductivity by the theory will be significantly higher as noticed by many researchers [77, 78] and might be high depending on the aggregates' dimension and the radius of gyration of the aggregates. This result is based on the three-level homogenisation theory. A validation of heat conduction dependence on aggregates was carried out by researchers [79-81]. Figure 2.1 relates the enhancement of thermal conductivity to nanoparticle agglomeration. an optimum particle structure maximum thermal conductivity has to be attained and the fully dispersed mixture leads to a thermal conductivity value which is much less than the optimum thermal conductivity. This phenomenon shows the importance of nanofluid preparation for the improvement of thermal properties.

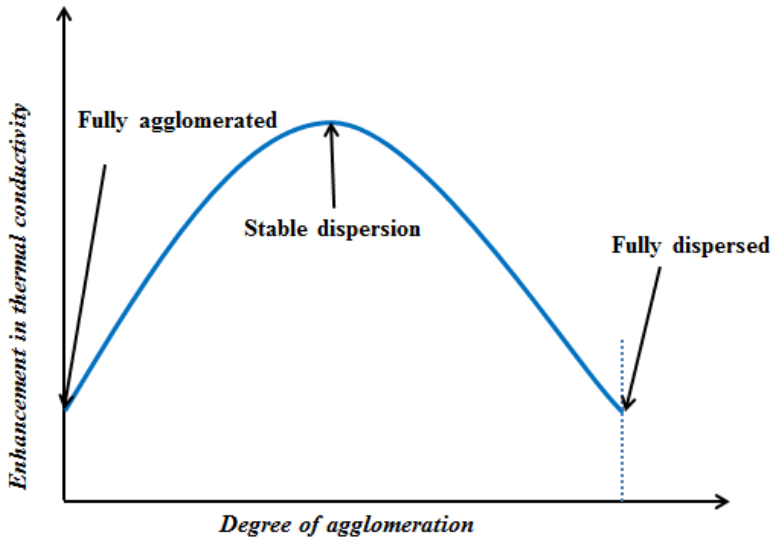

Figure 2. 1: Aggregation effect on the effective thermal conductivity [78].

Colloid chemistry has a critical role in improving the thermal properties of nanofluids as proved by the possible effect of particle agglomeration on conductivity. Hong et al. and Özerinç et al. [82, 83] experimentally proved the theory of lowering the thermal conductivity of aggregation forming by light scattering of iron nanoparticle aggregate. Gao and Zhou [84-86] indicated that the shape of nanoparticles could also influence the effective thermal conductivity increase. They predicted the effective thermal conductivity of nanofluid with non-spherical nanoparticles. Their prediction is based on Bruggeman's model [68], which is built on the phenomena of the interfacial thermal resistance across the solid particles and the base fluids. The study showed that a significant enhancement of effective thermal conductivity could be achieved if the shape of nanoparticles was non-spherical. Koo and Kleinstreuer [87] found that the role of Brownian motion was much more significant than the thermophoretic and osmophoretic motions.

As a conclusion, several investigators state that nanoparticle aggregation influences the thermal transport due to their chain shape [79, 88], while some others believe that the time-dependent thermal conductivity in the nanofluids proves the lowering of thermal conductivity with time due to agglomeration [89].

Experiments performed by Vadasz [90] showed that a transient heat conduction process might cause heat transfer enhancement; and thermal conductivity depends on numerous parameters, such as the chemical composition of the particles and the base fluid, surfactants, particle shape, particle size and concentration. There is still a dearth of research on determining the relation and the trend of the thermal conductivity with these variables.

The increase in temperature enhances the thermal conductivity of the nanofluids, as reported in the many studies that were conducted to find out the effect on CuO, Al_2O_3, TiO_2, ZnO dispersed nanofluids by Mintsa et al.[91] , Roberts and Walker [92], Murshed et al. [93], Yu et al. [94], and Karthikeyan et al. [89]. Nevertheless, the real mechanism of this enhancement has not been reported yet. A lack of reliable data for the conductivity of nanofluid is a major problem in nanofluid industrial applications.

The volume fraction of nanoparticles is another crucial factor affecting thermal conductivity enhancement [54], although this relationship is generally non-linear for nanoparticles with a high aspect ratio [88]. Wang et al. [59] investigated the thermal conductivity augmentation for aqueous suspensions. The results showed a notable increase in thermal conductivity compared with the results of Lee et al. [95] and Yang et al. [96].

Oh et al. [97] performed experiments for EG-based nanofluids. Their results showed relatively low thermal conductivity values compared with those of Lee et al. [98] and Wang et al. [59]. Thermal conductivity was observed to be constant when the volume of surfactant varied. Therefore, the property improvement is highly dependent on the particles when dispersing the nanoparticles into the water. The general behaviour of the particle-water interaction depends on the properties of the particle surface. A dose of surfactant may cause high or low pH value, resulting in a lower surface charge and a weaker repulsion between particles. Therefore, this action leads to stronger coagulation [99].

Xuan et al. [100] suggested the Brownian motion mechanism and the diffusion limited aggregation model for random movement of suspended nanoparticles. The influence of temperature on this characteristic is also mentioned in their work. Lee et al. [95] reported the effect of particle surface charge in thermal conductivity, the stability of the suspended particles confirmed to be improved and the thermal conductivity of nanofluid was enhanced when the pH of the solution moved from the isoelectric point of particles. Moreover, their research showed that there was a domination factor in controlling nanofluid aggregation by surface charge. Lee et al. [95] proposed a new interpretation of the charged sites and ion densities in the diffuse layer as the number and efficiency of channels for phonon transport respectively. Wang et al. [99, 101] proved the same theory.

2.3.2 Experimental investigation into thermal conductivity

Several experimental studies were conducted on the thermal conductivity of nanofluids. Three methods were used to measure the thermal conductivity of nanofluids, namely the transient hot-wire method, temperature oscillation and the steady-state parallel-plate method. The transient hot-wire method is the most commonly used technique. This method uses the temperature/time response measure for the wire corresponding to an instantaneous electrical pulse, then the derivation of Fourier's law and temperature data are used to calculate the thermal conductivity. The results obtained from experimental studies showed that the addition of a small quantity of nanoparticles caused much higher thermal conductivity than those of base fluids.

All the experiments performed by using Al_2O_3 and CuO as nanoparticles showed enhancement of the thermal conductivity for different sizes and shapes of the nanoparticles. Wang et al. [59] experimented with measuring the thermal conductivity of nanofluids

composed of Al_2O_3 and CuO nanoparticles. The technique of the steady-state parallel-plate method was used to measure the thermal conductivity of the nanofluids. The nanoparticles were dispersed in water, ethylene glycol, vacuum pump oil and engine oil. Experimental data showed that the thermal conductivity of all nanofluids was higher than that of the base fluids. The thermal conductivity of the nanofluids was enhanced with an increasing volume concentration of the nanoparticles. For a specific volume concentration, the increase of thermal conductivity was different for each base fluid.

Xuan and Li [102] studied the thermal conductivity of a nanofluid containing copper nanoparticles and base liquid. The results showed that the suspended nanoparticles increased the thermal conductivity of the base liquid. The thermal conductivity of the nanofluid increased with an increasing volume concentration of nanoparticles. When the volume concentration of the nanoparticles increased from 2.5 to 7.5%, the effective thermal conductivity (ratio of thermal conductivity of the nanofluid to that of the base fluid) increased from 1.24 to 1.78.

Xie et al. [103] investigated the effects of pH value, the specific surface area, the crystalline phase of the solid phase, and the thermal conductivity of the base fluid on the thermal conductivity of Al_2O_3 nanoparticle suspensions. The results showed that the addition of nanoparticles into the liquid led to higher thermal conductivity than that of the base fluid. The increase in the volume concentration also increased the thermal conductivity of Al_2O_3 nanofluid. The enhancement was more when the difference between the pH value and the isoelectric point of Al_2O_3 increased. The specific surface area was found to significantly influence the thermal conductivity of the suspensions containing the same base fluid. For the suspensions using the same nanoparticles, the enhanced thermal conductivity ratio decreased with the increased thermal conductivity of the base fluid, while the crystalline phase of the solid phase was found not to affect the effective thermal conductivity.

Das et al. [70] conducted investigations into the relation between thermal conductivity and temperature. They used aqueous Al_2O_3 and CuO nanofluids, and the thermal conductivity measured by temperature oscillation technique. The volume-weighted average value of particle diameter was 38.4 nm for Al_2O_3, while it was 28.6nm for CuO. The experimental results showed that the thermal conductivity increased with an increase in temperature. Smaller particle nanofluids (CuO) showed substantial enhancements of thermal conductivity with temperature than larger particles (Al_2O_3). They explained the increase in the thermal

conductivity by the random motion of nanoparticles because the smaller particles mobilised easier and generated a higher level of stochastic motion.

The effects of the nanoparticle size, temperature and chemical characteristics of particle coatings on the thermal conductivity of nanofluids were investigated by [104]. Gold (Au) and silver (Ag) nanoparticles with two kinds of coatings, thiolate and citrate, were used in this experiment with water- and toluene-based fluids. The thermal conductivities of the nanofluids were higher than those of their base fluids. For the polynomial function, the increments in thermal conductivity of the nanofluids correlated well with the temperature and an almost linear equation was found to correlate the enhancement with particle concentrations. Although silver particles had higher thermal conductivity and concentration, the thermal conductivity enhancement of the silver nanofluids was less than that of the gold nanofluids. Particle surface area per unit volume was used to describe the mechanism of thermal conductivity enhancement. The nanofluids with particles with thiolate coating had less thermal conductivity enhancement than those with particles with citrate coating. This showed that the effective heat transfer at metal surface contact was connected to the type of coating.

Choi et al. [105] measured the thermal conductivity of carbon nanotube-oil mixture nanofluid at room temperature. The thermal conductivity enhancement ratio was more than 2.5 1 vol.% of nanotube concentration. Xie et al. [66] dispersed carbon nanotube in distilled water, ethylene glycol and they obtained the same results; nanofluids containing a small amount of carbon nanotubes had considerably higher thermal conductivities than their base liquids. The thermal conductivity of the nanofluids was non-linear with higher nanotube concentrations. The thermal conductivity enhancement increased with increasing nanotube concentrations but reduced with increasing thermal conductivity of the base fluids. They also found that the size and shape of nanotubes caused the non-linear phenomenon. Compared with other nanostructure materials, nanotubes provided the highest thermal conductivity enhancement.

2.3.3 Analytical investigation and modelling of thermal conductivity

The thermal conductivity nanofluids is a function of thermal conductivity of the nanoparticle material and the base fluid, the volume fraction, the shape of the nanoparticles suspended in the liquid, and the surface area. There is still a lack of proper correlation and model that can predict the thermal conductivity well. The Maxwell model [106], which is an existing

traditional model for thermal conductivity, was proposed for the mixtures of solid-liquid with relatively large particles, as shown in Equation 2.1.

$$K_{eff,Maxwell} = \frac{k_p + 2k_1 + 2(k_p - k_1)\,\phi}{k_p + 2k_1 + (k_p - k_1)\phi}\, k_1 \qquad (\mathbf{2.1})$$

Many models proposed later were based on the Maxwell model. The effective thermal conductivity, $k_{eff,}$ is a function of k_p, the thermal conductivity of the particle, k_1, the thermal conductivity of the liquid and ϕ is the particle volume fraction of the suspension. From Maxwell's model, it is clear that the effective thermal conductivity of suspensions depends on the thermal conductivity of spherical particle, base liquid and the volume fraction of the solid particles. Maxwell's model is not a good model because it does not include particle size.

For non-spherical particles, nanofluid thermal conductivity depends on the shape of the particles as well as the volume fraction of the particles. Hamilton and Crosser [107] developed a model for the effective thermal conductivity of two-component mixtures. The model is a function of the conductivity of both the particle and base fluid and the shape of the particles. The thermal conductivity of two-component mixtures, in which the ratio of conductivity of two phases is larger than 100, can be determined as follows:

$$k_{eff,Hamilton} = \frac{k_p + (n-1)k_1 + (n-1)(k_1 - k_p)\phi}{K_p + (n-1)k_1 + (k_1 - k_p)\phi}\, k_1 \qquad (\mathbf{2.2})$$

where Ψ is the sphericity factor, n is the shape factor given by n = 3/Ψ, and defined by the ratio of the surface area of a sphere, having a volume equal to that of the particle, to the surface area of the particle.

Keblinski et al. [108] provide four factors explaining the mechanism of enhancing the thermal conductivity of the nanofluids, namely the Brownian motion of particles, molecular-level layering of the liquid at the interface between liquid and particle, the nature of heat transport in the nanoparticles, and the effects of nanoparticle clustering. They show that the

nanoparticle mobility due to Brownian motion is very slow in transferring much heat across a nanofluid. The existence of layering of liquid at the liquid-particle interface leads to higher thermal conductivity of the nanofluid. When the particle size is small, the thickness has more effect on the enhancement of thermal conductivity. The nature of heat transport in the nanoparticle is ballistic rather than diffusive. The clustering of particles can hurt thermal conductivity enhancement. The thermal conductivity enhancement of unattached packed clusters is higher than that of tightly packed clusters.

Wang et al. [109] proposed the fractal model to predict the thermal conductivity of nanofluids. The model is based on the effective medium approximation and the fractal theory. The thermal conductivity can be calculated as follows:

$$k_{eff,Wang} = \frac{(1-\phi) + 3\phi \int_0^{\infty} \frac{k_{cl}(r)n(r)}{k_{cl}(r)+2k_1}\, dr}{(1-\phi) + 3\phi \int_0^{\infty} \frac{k_{cl}n(r)}{k_{cl}(r)+2k_1}\, dr}\, k_1 \qquad (\mathbf{2.3})$$

where $n(r)$ is the radius distribution function and $k_{cl}(r)$ is the thermal conductivity of particle clusters. The model considers the effect of size and surface adsorption of nanoparticles. The proposed model matches well the achieved experimental data for 50 nm CuO particles suspended in deionised water with particle volume concentrations lower than 0.25 vol.%.

Xue [110] proposed a model for predicting the thermal conductivity of nanofluids. The model developed was based on the Maxwell theory and average polarisation theory, assuming that there was an interfacial film between the nanoparticles and liquid, and all nanoparticles were of the same rotational ellipsoid. They compared results from this prediction with experimental data of Choi et al. [105] for carbon nanotube-oil nanofluid and Xie et al. [103] for Al_2O_3 nanoparticle-water nanofluid. The model predicted the thermal conductivity well when compared with the experimental data for the same assumed interfacial shell thickness of 3 nm, but differed from the thermal conductivity of the interfacial layer. However, no explanation of the reasons for using the assumed values of thickness and thermal conductivity of the interfacial shell was given.

Yu and Choi [111] developed an alternative formula for calculating the effective thermal conductivity of solid-liquid mixtures. They assumed the mixture as a structural model of nanofluids might consist of a bulk liquid, solid nanoparticles and solid-like nanolayers. The

solid-like nanolayer acts as a thermal bridge between a solid nanoparticle and a bulk liquid [111]. The suggested expression yields:

$$k_{eff,Hamilton} = \frac{k_p + 2k_1 + 2(k_p - k_1)(1+\beta)^3\phi}{k_p + 2k_1 + (k_p - k_1)(1+\beta)^3\phi}\, k_1 \qquad (\mathbf{2.4})$$

where β is the ratio between the nanolayer thickness to the original particle radius and k_p is the equivalent thermal conductivity of the equivalent particle. In this model, the prediction is more valid when the nanoparticles have a diameter of less than 10 nm. Jang and Choi [112] proposed another model for predicting the thermal conductivity of nanofluids. The fundamental role of a dynamic nanoparticle is predicting thermal conductivity, which considers four modes of energy transport in the nanofluid. They are the collision between base fluid molecules, the thermal diffusion of nanoparticles in the fluid, the collision between nanoparticles due to Brownian motion, and the thermal interactions of dynamic nanoparticles with base fluid molecules. As with the results discussed in Keblinski et al. [108], they found that the Brownian motion had less effect than the other modes and could be neglected. This is because the collision of nanoparticles due to Brownian motion is a prolonged process. The expression is:

$$k_{eff,Jang} = k_1(1-\phi) + 2k_p\phi + 3C\frac{d_1}{d_p}k_1 Re_{d_p}^2 Pr\phi \qquad (\mathbf{2.5})$$

where Re_{d_p} is the Reynolds number defined by $Re_{d_p} = (\overline{C}_{RM} d_p)/v$, C is a proportional constant, $\overline{C}_{RM}$ is the random motion velocity of nanoparticles, v is the dynamic viscosity of the base fluid, Pr is the Prandtl number. The predictions from this model were in agreement with the experimental data of Lee et al. [98].

2.4 Viscosity of nanofluids

Viscosity is defined as the internal resistance of a fluid to flow, and it is an essential property for all thermal devices involving the flow of fluids [113]. The viscosity also has a significant effect on pumping power. The pressure drop in laminar flow is directly proportional to viscosity. Moreover, viscosity also influences the convective heat transfer coefficient. Hence viscosity is as vital as thermal conductivity in engineering systems involving fluid flow [114]. Much research has been done on nanofluids recently, but most research is related to heat transfer properties.

2.4.1 Experimental investigation into viscosity of nanofluids

In this section, the effect of the different parameters on the viscosity is studied. These parameters are temperature, particle size and shape, and volume fraction.

i. Effect of temperature

Yang et al. [9] conducted experiments to study the effect of temperature on nanofluid viscosity. They investigated experimentally the temperature effect of viscosity at four temperatures (35, 43, 50 and 70 °C) for four nanofluid solutions taking graphite as nanoparticles. They experimentally showed that kinematic viscosity decreased with an increase in temperature and important observations were made such as the corresponding viscosity of 2 wt% graphite with ATF at 35 and 70 °C was found to be 41.4 and 12.2 (cSt) respectively.

Chen et al. [115] prepared a nanofluid consisting of multi-walled carbon nanotubes with distilled water. They studied the temperature effect of the viscosity for a temperature range of 5 °C to 65 °C and showed that relative viscosity increased significantly with temperature after 55 °C.

Nguyen et al. [113, 116] conducted an experimental study to determine the temperature effect of nanofluid viscosity for Al_2O_3-water and CuO-water over a temperature range of 21 °C to 75 °C. The researchers reported that nanofluid viscosity decreased with an increase in temperature.

Anoop et al. [117] studied the viscosity of CuO-ethylene glycol, Al_2O_3-ethylene glycol and Al_2O_3-water for the temperature range of 20 °C to 50 °C with volume concentrations of 0.5, 1, 2, 4 and 6 vol.%. They confirmed that viscosity declined with an increase in temperature.

Naik et al. [118] experimentally showed that the viscosity of CuO/PG-water nanofluids decreased exponentially with an increase in temperature for a range of 258 to 335 K. Namburu et al. [119] indicated that CuO nanoparticles in an ethylene glycol and water mixture behaved like Newtonian fluids with the temperature ranging from 35 °C to 50 °C with a volume fraction of 0 to 6.12%. Moreover, viscosity decreased exponentially with an increase in temperature, as indicated in Figure 2.2. They also conducted a separate study [120] to investigate the influence of the temperature of nanofluids containing SiO_2 nanoparticles, and the same trend was observed.

Similarly, Kulkarni et al. [121] reported that viscosity decreased exponentially with an increase in temperature. They analysed CuO, $Al2O_3$ and SiO_2 as nanoparticle with EG/water-based fluid for a temperature range of 35 °C to 50 °C, as shown in Figure 2.2.

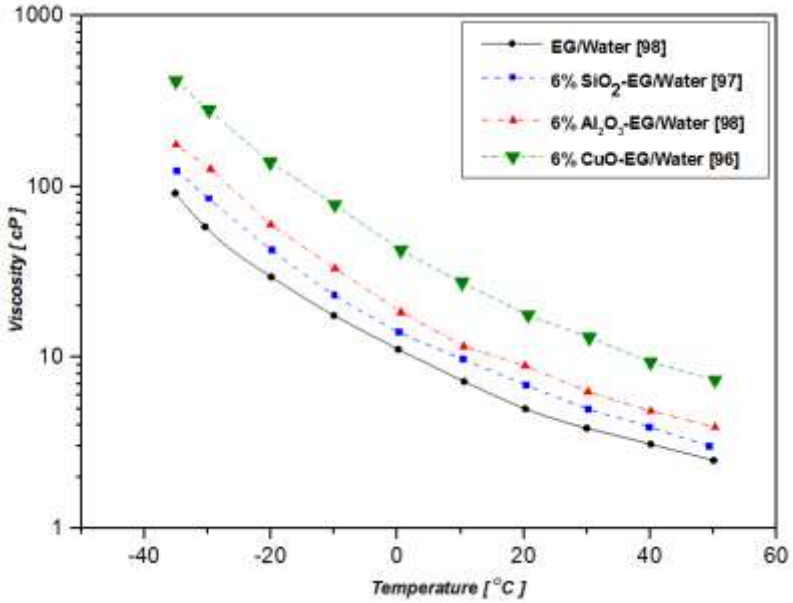

Figure 2.2: Exponential decrease to increase in temperature.

ii. Effect of particle size and shape

Few investigations have been conducted into the effect of particle size on nanofluid viscosity. Nguyen et al. [113] reported particle size effect of Al_2O_3-water nanofluid and noticed that particle size had a significant effect particularly for the nanofluids of high volume concentration. Their studies reported that for low volume concentrations such as below 4%, viscosities of 36 nm and 47 nm particle size Al_2O_3-water nanofluids were nearly equal. Moreover, for higher particle volume concentrations, viscosities of 36 nm particle size were lower than those of 47 nm size. In another study, Nguyen et al. [116] found that viscosity values of 36 nm particles were 5% lower than the value of 47 nm particle sizes. Also, the particle size effect was more significant for a higher particle fraction. Also, He et al. [26] reported an increase in shear viscosity with an increase in particle size. They measured TiO_2-distilled-water nanofluids viscosity for different volume concentrations and three different nanoparticle sizes (95,145, 210 nm). Figure 2.3 shows the increasing trend of viscosity with an increase in particle diameter for nanoparticle sizes (95,145, 210 nm).

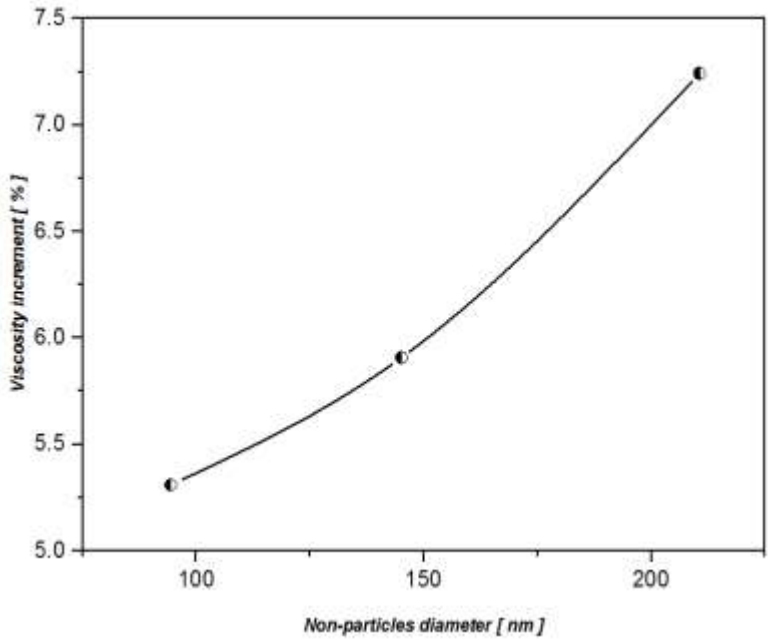

Figure 2.3: Change of viscosity with the particle diameter [26].

Lu and Fan [122] examined viscosity of Al_2O_3 with water and ethylene glycol for many sizes of nanoparticles both numerically (simplified molecular dynamic (MD) simulation) and experimentally. They noticed that the viscosity of nanofluids decreased with an increase in the diameter of the particle. Also, for diameters more than 30 nm, the change in shear viscosity was relatively less.

Chevalier et al. [123] took viscosity measurements of SiO_2 with ethanol for three different sizes of particle diameter, 35, 94 and 190 nm, and observed that viscosity rose with a reduction in particle size.

Pastoriza-Gallego et al. [124] also measured the viscosity of CuO in water for different particle sizes and volume concentrations. They utilised two different samples of CuO of 3 to 37 nm and other 11 ± 3 nm diameter and measured the viscosity of both samples for 0 to 10 wt.%. They measured the viscosity in the temperature range of 283.15 to 323.15 K and they found that the sample containing the smaller size exhibited larger viscosity.

Prasher et al. [125] reported a different result from earlier investigations, and they indicated that nanofluid viscosity was not a rigorous function of nanoparticle diameter. They studied 27, 40 and 50 nm of Al_2O_3 with propylene glycol and found that nanofluid viscosity changed slightly with particle diameter.

Timofeeva et al. [126] studied the shape of the particles and found that elongate particles such as platelets and cylinders produced higher viscosity at the same volume fraction. Furthermore, they suggested the use of spherical particles or lower aspect ratio spheroids for lower viscosities. Fewer results are available in the research about particle shape impact on the viscosity of nanofluids. Nevertheless, the viscosity of nanofluids has a huge dependency on nanoparticle shape [126, 127].

iii. Effect of volume fraction

Most of the available results about the viscosity of nanofluids regarding the effect of volume fraction acknowledge that viscosity of nanofluids increases with increasing volume fractions. Das et al. [128] proved Newtonian behaviour of Al_2O_3-water nanofluid between 1% and 4% particle volume concentration and pointed out that viscosity of nanofluid increased with increasing the particle concentration. Prasher et al. [125] noted that viscosity was proportionally enhanced when the nanoparticle volume fraction started to increase. They also determined that viscosity enlarged around (10 times) as the volume fraction increased. Chevalier et al. [123] measured the viscosity of SiO_2 in ethanol at room temperature with three different nanoparticle sizes, 35, 94 and 190 nm, and for a volume concentration of 1.4% to 7%. The viscosity was found to increase substantially with an increase in volume concentrations.

Some researchers reported a noticeable increase in viscosity with the addition of nanoparticles. For example, in the case of 12 vol.% of Al_2O_3 with water, viscosity increased 5.3 times [116], for 12 vol.% of TiO_2 with water, viscosity increased 1 200 times [129] and for 3 vol.% of SiC with DIW, viscosity increased 102% compared with that of DIW [130]. Metal oxide-based nanofluids have been extensively studied, and Al_2O_3- and TiO_2-related research makes up most of the available literature concerning the viscosity of nanofluids.

2.4.2. Theoretical investigation

There are several theoretical formulae in the literature to determine the particle suspension viscosities. Among them, the formula proposed by Einstein [131] is one of the more popular ones. His hypotheses are based on the linear viscous fluid-carrying dilute, suspended,

spherical particles and low particle volume concentration (less than 2%). The suggested formula is as follows:

$$\mu_{nf} = \mu_{bf}(1 + 2.5\phi) \qquad (\mathbf{2.6})$$

where $\mu_{nf}$is the viscosity of suspension, μ_{bf} is the viscosity of the base fluid and ϕ is the volume concentration of particles in the base fluid. In this equation, the viscosity is in direct proportion to the volume concentration and the size of the nanoparticles is not involved.

The more recognised equation was developed by Brinkman in 1952 [132]. The formula is an extended form of Einstein's formula, and it can be used with moderate particle concentrations, considering the effect of the addition of one solute molecule to an existing solution, which is considered as a continuous medium. The expression is valid for particle concentrations less than 4%, and is formulated as follows:

$$\mu_{nf} = \mu_{bf}(1 - \phi)^{2.5} \qquad (\mathbf{2.7})$$

Krieger and Dougherty in 1959 [133] obtained a semi-empirical relation for the shear viscosity including the full range of particle volume fraction:

$$\mu_{nf} = \mu_{bf}\left(1 - \left({}^{\phi}/_{\phi_m}\right)\right)^{-\lfloor\eta\rfloor\phi_m} \qquad (\mathbf{2.8})$$

where ϕ_m is the highest particle packing fraction, which ranges from 0.495 to 0.54 under still conditions, and is about 0.605 at high shear rates and $\lfloor\eta\rfloor$ is the intrinsic viscosity, of which the standard value for monodisperse suspensions of hard spheres is 2.5.

Lundgren [134] proposed the following equation in 1972 under the form of a Taylor series in ∅:

$$\mu_{nf} = \mu_{bf}\left(1 + 2.5\phi + \frac{25}{4}\phi^2 + f(\phi^3)\right) \qquad (\mathbf{2.9})$$

In 1977, Batchelor [135] proposed a formula by taking into account the effect due to the Brownian motion of particles on the bulk stress of a nearly isotropic suspension of rigid and spherical particles. The developed formula is as follows:

$$\mu_{nf=}\mu_{bf}(1 + 2.5\phi + 6.5\phi^2) \qquad (\mathbf{2.10})$$

A generalised form of the Franken and Acrivos formula was suggested by Graham in 1981 [136] to involve the particle radius and interparticle spacing, following Einstein's formula for small ∅. Graham's formula is expressed as follows:

$$\mu_{nf} = \mu_{bf}\left(1 + 2.5\phi + 4.5\left[1\Big/\left(\frac{h}{d_p}.\left(2 + \frac{h}{d_p}\right)\right).\left(1 + \frac{h}{d_p}\right)^2\right]\right) \qquad (\mathbf{2.11})$$

where h is the interparticle spacing and d_p is the particle radius.

In 2003, Tseng and Lin [129] correlated the relative viscosity versus the particle concentration at shear rate γ = 100 s-1 and found that the relative viscosity exponentially increased with the concentration for TiO2-water nanofluid:

$$\mu_{nf} = \mu_{bf} \times 13.47e^{35.98\phi} \qquad (\mathbf{2.12})$$

2.5 Convection heat transfer of nanofluids

Enhancing and understanding heat transfer rate are the main concerns at the design stage of different thermal devices for various industries, including chemical processes, heating, and cooling processes and even electronic devices. Diverse techniques were studied and developed to decrease operating cost. The most vital parameters in reducing the size and cost of heat transfer equipment are heat transfer coefficient and pressure drop or flow resistance. The primary purpose of the equipment design is to compromise between the minimisation of flow resistance and the enhancement of heat transfer coefficients. Therefore, it is crucial to develop methods and techniques to enhance the performance of heat exchangers. This section presents various experimental investigations into convective heat transfer for the various nanofluids, because there are many works of literature on laminar flow and turbulent flow, but only a few publications about the transition flow regime.

2.5.1 Experimental investigation into convective heat transfer in laminar flow

Li and Xuan [8] prepared a nanofluid of Cu nanoparticles in water as a base fluid and experimented with evaluating the heat transfer coefficients in the laminar flow regime. They compared the results with water and found that for the same Reynolds number, the convective heat transfer coefficient of the nanofluid was improved by about 60% for the volume concentration of 2%. They also developed a Nusselt number correlation, as follows:

$$Nu = 0.4328\left(1 + 11.258\,\phi^{0.754}{Pe_d}^{0.218}\right)Re^{0.333}Pr^{0.4} \qquad (\mathbf{2.13})$$

$$800 < Re < 4000\,, 0 < \phi < 2\%$$

Wen and Ding [19] conducted experiments in the entrance flow regime under laminar flow circumstances. The authors observed that convective heat transfer was enhanced in the laminar flow regime when using Al_2O_3 nanoparticles, which were scattered in the water. The convective heat transfer exhibited enhancement with Reynolds number, as well as particle volume concentration. The improvement was especially significant in the entrance regime and decreased with axial distance. The reasons for the enhancement of the convective heat transfer could be the increase in the effective thermal conductivity, the non-uniform distribution of thermal conductivity and viscosity field, the particle movement, and the reduction in the thermal boundary layer thickness.

Yang et al. [9] experimentally investigated the convective heat transfer of graphite-water nanofluids under laminar flow conditions. For a 2.5 wt %, they encountered an increase in heat transfer of 22% over the base fluid at a temperature of 50 °C and 15% at a temperature of 70 °C. They predicted the Nusselt number as follows:

$$Nu = aRe^{b}Pr^{1/3}\left(\frac{D}{L}\right)^{1/3}\left(\frac{\mu_w}{\mu_b}\right)^{1/3} \qquad (\mathbf{2.14})$$

$$5 < Re < 120\,, \qquad 0 < \phi < 2.5\%$$

where a and b can be determined by the nanofluid type and the working temperature.

Ding et al. [10] conducted experimental work to understand the parameters that affect the behaviour of heat transfer in aqueous suspensions flowing through a horizontal tube. They performed the experiments using carbon nanotubes (CNT), and it was found that concentration, flow conditions and pH level had a significant influence on heat transfer, but the effect of pH was observed to be small. The augmentation mainly relied on the axial distance from the inlet of the test section. The augmentation showed an increase which reached to the highest and then declined with growing axial distance.

Murshed et al. [11] examined TiO_2-water nanofluids under laminar flow conditions experimentally. The results showed that for Reynolds numbers of 1 100 and 1 700 and the volume concentration of 0.8 vol.%, the local heat transfer coefficient of the nanofluid was about 12% and 14% higher than the deionised water respectively at the location of x/D = 25.

The effect of ultrasonication on viscosity and heat transfer enhancement was studied by Garg et al. [5]. They examined multi-walled carbon nanotubes (MWCNT)-based aqueous nanofluids. The maximum percentage enhancement of thermal conductivity was a 20% increase considerably after 24 °C. At the Reynolds number (500-700), the most significant percentage improvement in heat transfer coefficient was 32%. There was a continuous increase in heat transfer coefficient with axial distance. The participation of the significant increase in thermal conductivity with an increase in bulk temperature with axial distance was the reason for this behaviour.

Kim et al. [137] experimented with a circular, straight tube. They used water-based alumina nanofluids and aqueous amorphous carbonic. The flow was controlled to be in the laminar flow regime. The increment in thermal conductivity and convective heat transfer coefficient was 8% and 20% respectively in alumina nanofluids holding 3 vol.% of suspended particles. For amorphous carbonic nanofluids, the thermal conductivity was similar to that of water, and the convective heat transfer coefficient increased by only 8%. The convective heat transfer enhancement at the entrance regime was due to the immigration of nanoparticles.

Anoop et al. [20] studied the effect of particle size on convective heat transfer. They used an aqueous solution of given nanoparticles in their experiments and the flow in the pipe was in the developing regime. It was noted that the nanofluid with 45 nm particles showed a better

heat transfer coefficient than with 150 nm particles. It was concluded that the observed increase in convective heat transfer with nanofluids was not only due to the enhancement of thermal conductivity but was also because of the effects of particle movement and thermal dispersion. They obtained the following correlation for Nusselt number:

$$Nu = 4.36 + \left[ax_*^{-b}(1+\phi^c)exp^{(-dx_*)}\right]\left[1+e(\frac{d_p}{d_{ref}})^{-f}\right] \qquad (\mathbf{2.15})$$

where $a = 6.219 \times 10^{-3}, b = 1.1522,\ c = 0.1533,\ d = 2.5228,\ e = 0.57825,\ f = 0.2183,\ d_{ref} = 100nm,\ x_* = \frac{x}{RePrD},\ 50 < \frac{X}{D} < 200,\ 500 < Re < 2000,\ 0 \leq \phi \leq 4\%$

Suresh et al. [138] examined the hybrid water-based nanofluid of Al_2O_3-Cu. They worked with a volume concentration of 0.1% and found that the enhancement of heat transfer was 13.56% at Reynolds number of 1 730. They proposed a correlation to relate the Nusselt number with the various parameters, and it is as follows:

$$Nu = 0.031\ (RePr)^{0.68}(1+\phi)^{95.73} \qquad (\mathbf{2.16})$$

$$Re < 2300, \qquad 0 \leq \phi \leq 0.1\%$$

Rea et al. [139] reported a heat transfer enhancement of 27% with alumina nanofluid at a volume concentration of 6%. They also experimented with zirconia nanofluid, and 3% enhancement was achieved at 1.32% volume concentration. A correlation for fully developed vertical pipe under laminar condition was obtained as follows:

$$Nu = 1.619\ (x^+)^{1/3} \qquad (\mathbf{2.17})$$

$$x^+ < 0.01, x^+ = \frac{2(x/D)}{RePr}$$

For Al_2O_3 nanofluids, $431 < Re < 2000, 0 < \phi < 6\%$

For ZrO2 nanofluids, $140 < Re < 362, 0 < \phi < 3\%$

Table 2.1: Summary of forced convection laminar flow experimental studies on nanofluids under constant heat flux boundary conditions.

Author	Nanofluid	Mechanism of enhancement
Li and Xuan (2002)	Cu-water	By increasing the particle volume concentration
Wen and Ding (2004)	ɣ-Al_2O_3	Non-uniform distribution of thermal conductivity due to particle migration effect and thermal boundary layers Thickness reduced with effect of viscosity field
Yang et al. (2005)	Graphite-water	Particle weight concentration (wt.%)
Ding et al. (2006)	MWCNT-water	Particle rearrangement, due to the presence of nanoparticles there was reduction of thermal boundary layer, shear-induced Thermal conduction enhancement
Murshed et al. (2008)	TiO_2-water	Particle volume concentration and the position (x/D)
Garg et al. (2009)	MWCNT-water	Increase in axial distance
Kim et al. (2009)	Alumina-water Carbonic nanoparticle-water	Disturbances of thermal boundary layer
Anoop et al. (2009)	Al_2O_3-water	Thermal dispersion and particle migration effects
Suresh et al. (2012)	$Al_2O_{3\text{-}cu}$-water	Brownian diffusion and thermophorises
Rea et al. (2009)	Al_2O_3- and ZrO2-water	Thermal conductivity enhancement

2.5.2 Experimental investigation into convective heat transfer in turbulent flow

Pak and Cho [18] conducted an experimental investigation using ɣ-Al_2O_3-water and TiO_2-water nanofluids for fully turbulent flow and reported a 45% enhancement of the heat transfer coefficient with the ɣ -Al_2O_3-water nanofluid at a volume concentration of 1.34% and for TiO_2-water nanofluid, a 75% enhancement of the heat transfer coefficient at a volume concentration of 2.78%. However, at the same concentration, the heat transfer enhancement for TiO_2-water nanofluid was less than that of the ɣ-Al_2O_3-water nanofluid. They suggested a correlation-related Nusselt number with Reynolds and Prandtl number, as follows:

$$Nu_{nf} = 0.021 Re_{nf}^{0.8} Pr_{nf}^{0.5} \qquad (\mathbf{2.18})$$

$$10^4 \leq Re \leq 10^5, \qquad 6.54 < Pr < 12.33, \qquad 0 \leq \phi \leq 3\%$$

Vajjha et al. [140] introduced new correlations for convective heat transfer and friction factor from the experiments of nanoparticles composed of aluminium oxide, copper oxide and silicon dioxide scattered in 60% ethylene glycol and 40% water by mass. The heat transfer coefficient of nanofluids recorded an increase with the volumetric particle concentration. For instance, at a Reynolds number of 7 240, the percentage increase in the heat transfer coefficient over the base fluid for a 10% Al_2O_3 nanofluid was 81.74%. The pressure loss of nanofluids also increased with an increase in particle volume concentration since the rise in pressure loss for a 10% Al_2O_3 nanofluid at a Reynolds number of 6 700 was about 4.7 times than for the base fluid. This loss was due to the growth in the viscosity of the nanofluid with concentration.

$$Nu = 0.065\ (Re^{0.65} - 60.22)(1 + 0.0169\phi^{0.15})Pr^{0.542} \qquad (\mathbf{2.19})$$

$$R^2 = 0.97, 3000 < Re < 16000$$

$$0 \leq \phi \leq 0.06\ \%\ \text{ for } CuO_2 \text{ and } SiO_2$$

$$0 \leq\ \phi \leq 0.1\ \%\ \text{ for } Al_2O_3 \text{ nanofluid}$$

Ferrouillat et al. [141] examined SiO_2-water nanofluids for the entire flow with special focus on the turbulent flow results. Results showed that at a volume concentration of 18.9%, the heat transfer was enhanced by 50% for a Reynolds number greater than 1 000. Sundar et al. [142] conducted tests for a horizontal circular tube with and without twisted-tape inserts. They studied the convection heat transfer and friction factor characteristics of magnetic nanofluid in the turbulent flow regime. At of 0.6 vol%, the heat transfer augmentation was 51.88% when working with a twisted-tape insert of twist ratio H/D = 5, while the friction factor of the same volume concentration of nanofluid was 1.231 times more than water flowing in a plain tube for the same twist ratio and Reynolds number. They developed the following correlation as a result of their experiments:

$$Nu = 0.02172\ Re^{0.8}Pr^{0.5}(1 + \phi)^{0.5181} \qquad (\mathbf{2.20})$$

$$3000\ \leq Re \leq 22000, \qquad 3.72 < Pr < 6.5, \qquad 0 \leq\ \phi \leq 0.6\%$$

Azmi et al. [143] studied forced convection heat transfer and friction factor using SiO_2 nanofluid in the turbulent flow regime. They reported an enhancement of the Nusselt number because at a volume concentration of 3.0%, the Nusselt number was enhanced by 32.7%. Moreover, the friction factor at the same nanofluid particle concentration was 17.1% greater than for water. They also observed that the pressure drop decreased when the particle volume concentration increased more than for pure water. The friction factor of the nanofluid was found to reduce with an increase in Reynolds number at any concentration. Kayhani et al. [144] conducted an experimental study on convective heat transfer and pressure drop in the turbulent flow regime. They did the tests on water-based nanofluids that contained a given nanoparticle of (15 nm) size through a heated continuously horizontal circular tube containing 0.1, 0.5, 1.0, 1.5 and 2.0 vol% of nanoparticles. The results showed an enhancement of 8% in Nusselt number at a Reynolds number of 11 800 and nanoparticle volume concentration of 2.0 %. They also observed an increase in heat transfer coefficients with an increase in the nanofluid volume concentration; however, no change was noticed in changing the Reynolds number. Sahin et al. [145] studied the influence of Al_2O_3-water nanofluid on the convective heat transfer and the pressure drop characteristics. Nanofluid volume concentrations of 0.5%, 1%, 2% and 4% was used inside a circular tube in the turbulent flow regime. All concentrations below 2% showed an enhancement of heat transfer number. Furthermore, heat transfer was noticed to increase with Reynolds number. The particle volume fraction up to the particle volume concentration smaller than 1 vol% also showed positive results concerning the heat transfer. They reported the unsuitability of nanofluids with a volume concentration higher than 1 vol.% because the viscosity growth of the nanofluids influenced the heat transfer enhancement much more than the thermal conductivity of the nanofluids. The friction factor increased with a rise in the particle volume concentration, due to an increase in the viscosity. The volume concentration of 0.5% recorded the highest heat transfer enhancement achieved at Reynolds number of 8 000.

Suresh et al. [146] experimented with nanofluids in a clear and helically dimpled pipe. The convective heat transfer and friction factor characteristics of CuO-water under turbulent flow were considered. The results showed that the use of the helically dimpled pipe contributed to the heat transfer augmentation with the use of the nanofluids. The improvement in the heat transfer was associated with a negligible increase in friction factor compared with the clear pipe. The enhancement of Nusselt number due to the nanofluids for the dimpled tube compared with the clear tube was 19%, 27% and 39% at 0.1%, 0.2% and 0.3 vol% respectively. The experimental results determined that the dimpled tube friction factors were

about 2 to 10% higher than those of the plain tube of isothermal pressure drop. They presented the following correlation:

$$Nu = 0.00105Re^{0.984}Pr^{0.4}(1+\phi)^{-80.78}(1+\frac{p}{d})^{2.089} \qquad (\mathbf{2.21})$$

$$2500 < Re < 6000, \qquad 0 < \phi < 0.3\%$$

Yu et al. [147] conducted an experimental investigation into convective heat transfer with Therminol 59-based nanofluids under turbulent flow regime. They dispersed copper nanoparticles at particle volume concentrations of 0.50% and 0.75%. The heat transfer coefficients were enhanced by 18% when using low concentrations (<2.00 vol.%) of nanoparticles for high temperature circumstances.

Asirvatham et al. [148] performed experiments in a horizontal tube-in-tube test section. Silver-water nanofluids were used. They showed that the nanoparticles significantly increased the heat transfer coefficient by 28.7% for 0.35 vol.% and 69.3% for 0.9 vol.%. They also developed the following correlation for Nusselt number:

$$Nu = 0.0023\ Re^{0.8}Pr^{0.3} + (0.617\phi - 0.135)Re^{(0.445\phi - 0.37)}Pr^{(1.081\phi - 1.305)} \qquad (\mathbf{2.22})$$

$$900 < Re < 12100, \qquad 0 < \phi < 0.9\%$$

Sajadi and Kazemi [28] investigated the use of TiO_2-water nanofluid. They reported an increase in heat transfer coefficient of 22% at 0.25 vol.%. They developed the following correlation:

$$Nu = 0.067\ Re^{0.71}Pr^{0.35} + 0.0005Re \qquad (\mathbf{2.23})$$

$$5000 < Re < 30000, \qquad 0 < \phi < 0.25\%$$

The results obtained from the experimental investigation into the turbulent regime are presented in Figure 2.4.

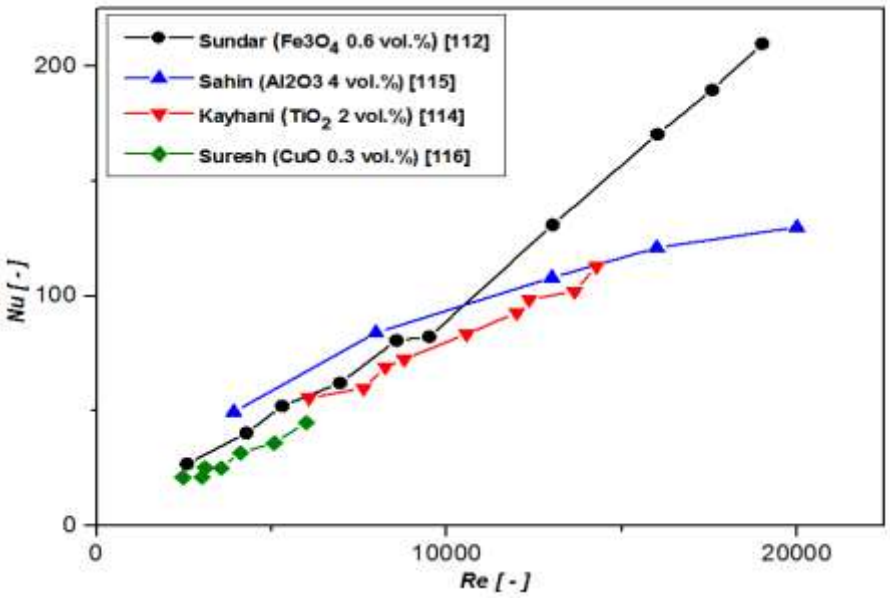

Figure 2.4: Graphical representation of heat transfer coefficient and Reynolds number for various nanoparticles at different volume concentrations for turbulent flow regime.

Table 2.2**:** Summary of forced convection turbulent flow experimental studies on nanofluids under constant heat flux boundary conditions.

Author	**Nanofluid**	**Flow regime (Range of Reynolds numbers)**	**Heat transfer enhancement mechanisms**
Pak and Cho (1998)	ɣ-Al2O_3	10 000 to 100 000	Increasing the particle volume concentration
Vajjha et al. (2010)	Al_2O_3/EG-water CuO/EG-water SiO_2/Eg-water	2 200 to 16 000	Particle volume concentration
Ferrouillat et al (2011)	SiO_2-water	200 to 10 000	Particle weight concentration
Sunder et al.	Fe_3O_4-water	3 000 to 22 000	Use of twisted-tape insert of twist ration H/D=5
Azmi et al. (2013)	SiO_2-water	5 000 to 27 000	Increment in particle volume concentration
Kayhani et al. (2012)	TiO_2-water	7 000 to 15 000	Particle volume concentration
Sahin et al. (2013)	Al_2O_3-water	4 000 to 20 000	Particle volume concentration and Reynolds number
Suresh et al. (2012)	CuO-water	2 500 to 6 000	Increasing volume concentration in plain tube, Reynolds number and dimpled tube in geometry
Yu et al. (2013)	Copper in Therminol 59	3 000 to 8 000	Nanoparticle volume fraction
Asirvatham et al. (2011)	Silver-water	1 000 to 12 000	Enhancement of thermal conductivity by the chaotic movement of the nanoparticles
Sajadi and Kazemi (2011)	TiO_2-water	5 000 to 30 000	Nanoparticle scattering

2.5.3 Experimental investigation into convective heat transfer in transitional flow regime

Meyer et al. [24] did experiments to investigate the convective heat transfer enhancement of multi-walled carbon nanotubes suspended in water. They tested the nanofluid in a straight horizontal tube covering Reynolds number range of 1 000 to 8 000, which included the transition flow regime. Experiments were conducted at a constant heat flux of 13 kW/m2 with 0.33, 0.75 and 1.0 vol% of multi-walled carbon nanotubes. The nanotubes had an outside diameter of 10 to 20 nm, an inside diameter of 3 to 5 nm and a length of 10 to 30 lm. It was found that heat transfer was enhanced when comparing the data on a Reynolds-Nusselt graph.

Li et al. [149] performed tests on zinc oxide/ethylene glycol-water (ZnO/EG-water) and heat transfer and pressure drop were investigated in a circular pipe. The range of Reynolds number was from 1 000 to 6 000, including the transition from laminar to turbulent. The mass concentration and particle size for the nanofluid were from 0 to 5 wt.% and 26 nm respectively. It was found that the nanofluid had a maximum of 30% higher heat transfer coefficient than base fluid at mass fraction of 2.5 wt.%, whereas at higher values of the nanoparticle mass concentration of 5 wt.%, the heat transfer coefficient decreased. There was an optimal value of the concentration for the nanoparticles to have the maximal enhancement of the heat transfer. The measurements also showed that the pressure drop of nanofluid was higher than that of the base fluid in a turbulent flow regime.

Naik et al. [150] tested CuO-propylene glycol nanofluid with less than 50 nm particles size and volume concentrations of 0.05, 0.1 and 0.5%. The experiments were carried out in a plain circular tube with helical inserts having aspect ratio from 0 to 9 for the Reynolds number range from 2 500 to 10 000. The enhancement of Nusselt number at 0.5% concentration was 28% higher in a plain tube and increased by 5.4 times over the base fluid when using helical insert with aspect ratio of three. On the other hand, the friction factor increased by 10% for the plain tube and 140% for the helical insert. Liu and Yu [23] conducted a set of experiments of Al_2O_3-water nanofluid in a circular mini-channel. The volume concentrations used were 1, 2, 3.5 and 5%, and the Reynolds number range covered the laminar, transition and early turbulent regimes. The starting of transition was found to be delayed with the v in

the volume concentration and the heat transfer enhanced in the laminar flow regime with a penalty in the pressure drop. Ma et al. [151] performed experimental work on Fe_3O_4-water nanofluids. The fluid flowed through a horizontal copper tube in the transition regime (2 500-5 000), the volume concentrations were 0.05, 0.16 and 0.24% and the average and local heat transfer coefficients were presented against Reynolds number. The results showed that the average heat transfer coefficient of water cannot be enhanced by adding Fe3O4 nanoparticles. However, it was also observed for the local heat transfer coefficient results that the enhancement was slightly significant at the outlet of the test section, while it became steady in the developed regime. Chougule and Sahu [152] examined the forced convective heat transfer of Al_2O_3-water and CNT-water nanofluids through a uniformly heated horizontal circular tube in the transition regime with helically twisted-tape inserts estimated experimentally. Tests were conducted with a varied range of particle volume concentrations (0.15%, 0.45%, 0.60% and 1%) and helical tape inserts of twist ratio (TR) = 1.5, 2.5 and 3. It was observed that the heat transfer performance of both the nanofluids increased with an increase in the particle volume fraction. The average increase in Nusselt number of CNT-water nanofluids at 1vol% was 75.02%, while it was 39.03% for Al_2O_3-water nanofluid at the same volume concentration.

2.6 Transition in plain horizontal tubes

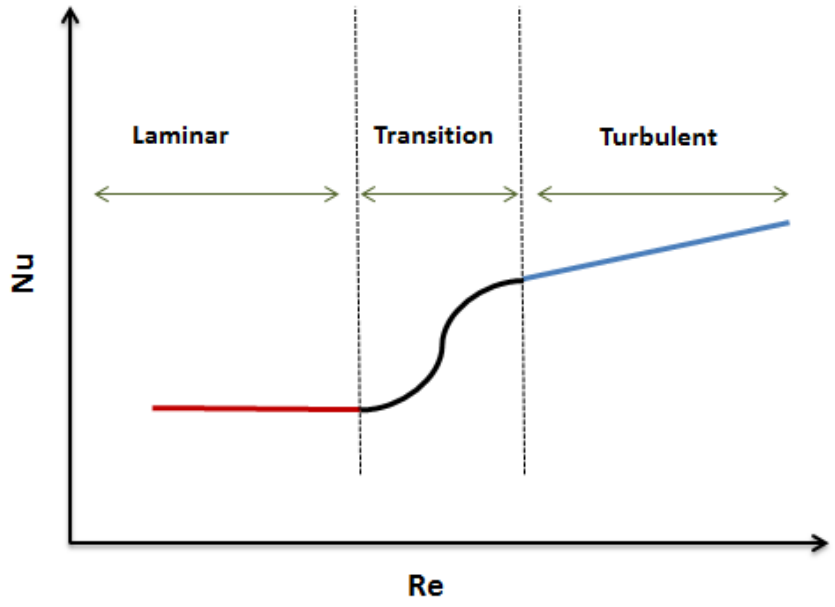

Figure 2.5**:** Representation of flow regimes in terms of Nusselt number against Reynolds number.

The regime where the flow manifests from the laminar to turbulent is known as the transition flow regime, as shown in Figure 2.5. In this regime, a drastic increase in the pressure drop takes place, and the flow fluctuates in the form of eddies and pulses. There is still a lack of design information on this regime, and that is the reason for the recommendation by designers to avoid operating in this regime [153, 154].

Ghajar and Tam were the first researchers to study the effect of the inlet geometry on the transition flow regime [155]. They measured the pressure drop in a horizontal circular test section, a straight tube with re-entrant, square-edged and bell-mouth inlets under adiabatic flow conditions. They reported a Reynolds number range of 500 to 15 000. The fully developed friction coefficient data for the three inlet configurations revealed that the range of Reynolds number values for which transition flow endured was 1 980 to 2 600 for the re-entrant inlet, 2 070 to 2 840 for the square-edged inlet, and 2 125 to 3 200 for the bell-mouth inlet. The authors also developed a correlation to predict the friction coefficient for the fully developed flow in the transition regime for each inlet. A variation of the laminar friction factor with tube length for different inlets was presented and qualitative results were given. The local friction factor results showed that for low laminar Reynolds numbers, the friction factor did not depend on (x/D) only, as reported by other researchers, but it also had a strong dependence on Reynolds number.

Ghajar and Tam [156] studied the influence of inlet geometry on forced and mixed convection heat transfer. They experimented with re-entrant, square-edged and bell-mouth inlets under uniform heat flux conditions. The local heat transfer coefficients were presented for a Reynolds number range of 280 to 49 000, Prandtl number changed from 4 to 158, and the range of Grashof number was from about 1 000 to 2.5 x 105. The heat transfer transition Reynolds number was found to be 2 000 to 8 500 for the re-entrant inlet, 2 400 to 8 800 for the square-edged inlet, and 3 800 to 10 500 for the bell-mouth inlet. They proposed heat transfer coefficient correlations for developing and fully developed forced and mixed convection for the three inlets. In a separate study, the same authors [157] developed a flow regime map to identify the forced convection zone from the mixed convection. The flow map is valid for all flow regimes for the case of uniform heat flux. The map can identify the buoyancy effect at a particular location (X/D) by determining the value of Grashof × Prandtl for a specific Reynolds number.

Tam and Ghajar [158] investigated the effect of heating on the friction factor coefficient in the fully developed transition regime. They used a horizontal circular, straight test section with re-entrant, square-edged and bell-mouth inlets under uniform heat flux flow conditions. The working fluid used was a mixture of ethylene glycol-water inlet. The Reynolds number of 1 000 to 17 000 was covered to include the laminar, transition and turbulent regimes. The results revealed that the range of Reynolds number values for which transition occurred was 2 900 to 3 500 for the re-entrant inlet, 3 100 to 3 700 for the square-edged inlet, and 5 100 to 6 100 for the bell-mouth inlet. Different heat fluxes were used to examine the effect of heating on the friction factor. The results showed that the friction factor increased with an increase in the heating rate for the same Reynolds number due to the secondary flow caused by heating. The heating also affected the transition because at the highest heating value of 16 kW/m2, the transition took place at a Reynolds number range of 4 100 to 5 900 for the re-entrant inlet, 4 500 to 6 400 for the square-edged inlet, and 7 300 to 9 600 for the bell-mouth inlet.

Olivier and Meyer [159] and Meyer and Olivier [160] performed experiments by cooling water in a smooth horizontal pipe with diameters of 15.88 and 19.02 mm. They used four inlet configurations: hydrodynamically fully developed, square-edged, re-entrant and bellmouth. Adiabatic and diabatic friction factor results were presented for a Reynolds number range of 1 000 to 20 000, Prandtl number varied between four and six, and Grashof number was 105. Adiabatic measurements showed that transition was well dependent on the inlet shape, with the transition delayed to Reynolds number of 12 000. Diabatic results revealed that transition was independent of the inlet, and transition occurred at Reynolds number of 2 100. They explained that the reason for the inlet configuration not influencing the transition in diabatic results was due to the secondary flow overcoming the disturbance of the inlets. Laminar heat transfer and friction factors were also considerably higher than their theoretical equivalents. This could also be connected to secondary flows.

Olivier and Meyer [159] reported adiabatic friction factor coefficient data for fully developed and developing flow in the transition regime. They used enhanced tubes and three inlet configurations, square-edged, re-entrant and bellmouth inlets. Results proved that the inlet influenced transition in the same way as for the smooth tube. The transition was delayed for the three, and the most delayed one was the bellmouth inlet. The authors developed a correlation to predict the critical Reynolds number and the fully developed friction factors in the transition regime. The same authors investigated heat transfer and diabatic friction

coefficients [161]. They added the hydrodynamically fully developed inlet to the inlets in the previous study. It was found, unlike the first study, that the inlet shape did not affect the transition as it was started at Reynolds number of 2 000 and ended at 3 000.

Everts and Meyer [162] obtained heat transfer and pressure drop data in the transition flow regime for both fully and developing flow under constant heat flux. The study covered the Reynolds numbers between 700 and 10 000 at various heat fluxes. They found that the critical Reynolds number was not a function of axial location, and the transition happened at the same time throughout the test section length. Nonetheless, the end of transition was dependent on axial position and happened earlier as the flow neared fully developed flow. Free convection effects induced both the start and end of the transitional flow regime and prompted the Reynolds number range of the transitional flow regime to reduce. They developed correlations to predict the beginning and end of the transitional flow regime. Meyer and Everts in parallel work to the previous research [163] investigated mixed convection laminar flow, as well as the impact of free convection on the transition along the tube length. They also described and developed a correlation for the relationship between heat transfer and pressure drop in all flow regimes including the transition regime [164]. The same authors, in a separate paper, presented flow regime maps. The maps were not limited to the fully developed flow, but were also included in the developing flow [165].

2.7 Conclusion

The literature review presented research into the enhancement of heat transfer when using nanofluids. The factors influencing this improvement are the thermal conductivity, the heat capacity of the base fluid, Brownian motion, flow pattern, the viscosity and density of the volume fraction of the suspended particles, the size and shape of the particles, and the nanolayer thermal conductivity. Because of the importance of the preparation process in having an effective nanofluid, nanofluid preparation techniques were discussed in the literature review.

Thermal conductivity of the nanofluids was also discussed, and some of the theoretical and experimental investigations were reviewed. Thermal conductivity models and the empirical correlation were presented. Various factors affecting the viscosity of nanofluids were discussed, and the section covered both experimental and theoretical investigations into nanofluid viscosity. The convective heat transfer of nanofluids was reviewed and presented

under all three regimes, and the enhancement of nanofluids during heat transfer was reported. It was found that there was not enough research on the transition flow regime. In the last section of this chapter, the transition in plain tubes was discussed, and the work of Ghajar and his co-authors showed the significant influence of the inlet geometry on the transition flow regime. Meyer and his co-authors continued the practice of Ghajar, and they focused on the developing flow. They developed a relationship between pressure drop and heat transfer and they presented flow regime maps for the developed and developing a flow.

There is limited literature on heat transfer enhancement and pressure losses in the transition flow regime for nanofluids. Therefore, this study will contribute to knowledge in this area.

CHAPTER 3 EXPERIMENTAL SET-UP AND TEST SECTION

3.1 Introduction

In this chapter, a general description of the experimental set-up is given including specifications for the equipment used for measuring the necessary parameters needed for the analysis. The procedures followed to run the experiments are presented and the test section building process is explained. The data reduction method is described to illustrate the method used to determine the Nusselt number, heat transfer coefficients and friction coefficients from the first principle. The instrument accuracies and an outline of the anticipated uncertainties are presented, the specification for the porous media used in the second test section is presented, and the building procedures of filling the test section with nickel foam are also described.

3.2 Experimental set-up

The basic layout of the experimental set-up is illustrated in Figure 3.1. The test rig consisted of a 10-litre tank (1), which was used to store and supply the nanofluid through the variable speed pump magnetic gear pump (2) to the test section (3). The test section was connected to the power supply to produce a uniform heat flux along the test section so that the water was heated up from T_i to T_e. To prevent the heat from being lost, the heat exchanger was insulated using thermal insulation (4) with a thickness of 50 mm (four layers). The water left the test section at a higher temperature through the flow meter (5), which was used to measure the mass flow rate. The temperature at the inlet to the test section was maintained at 20 $^{\circ}$C by cooling the hot water leaving the test section in a heat exchanger (8), where the heat was transferred to cold water from a chiller (6) through a circulating pump (7). The system was provided with a data acquisition system to receive signals from the thermocouples, pressure transducers, flow meters, and power supply and then to process these in a computer (9). A Lab View program was used for logging the data.

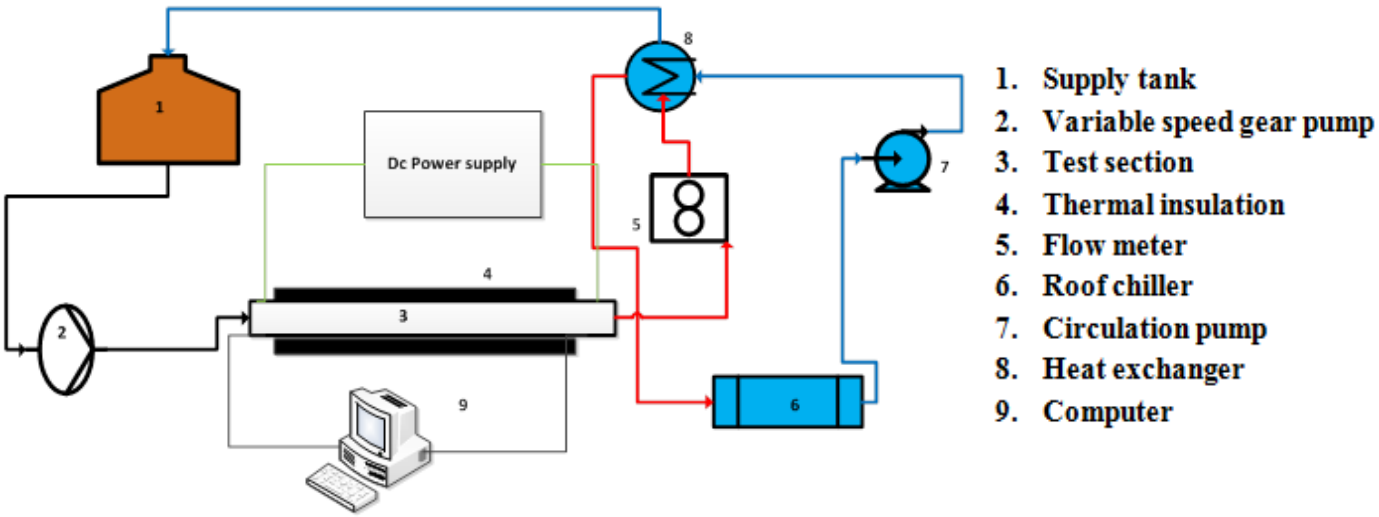

Figure 3.1: Layout of the experimental set-up.

3.3 Test section

Figure 3.2 presents a schematic diagram of the test section, which is a rectangular copper channel with a width of 8 mm, height of 5 mm, and length of 450 mm. The test section was heated by Constantine wire at 200 W using a DC power supply at a current of 0.75 A and voltage of 125 V.

The test section was joined to the test rig using a rectangular channel with the same size and a length of 700 mm as a developing length to ensure that the flow was fully developed hydraulically as presented in Figure 3.2. An acetyl bush was used to separate the developing section from the test section to avoid any axial heat transfer loss. The hydrodynamic entry length was used to ensure that the flow was hydraulically fully developed in the laminar and turbulent flow regimes. The length was determined according to Kays and Crawford [166], as follows:

$$L_{entry} = 0.05\, Re\, D_h \qquad (\mathbf{3.1})$$

The entry length was found to be 600 mm and it was made from the same material and with the same cross-section size as the test section.

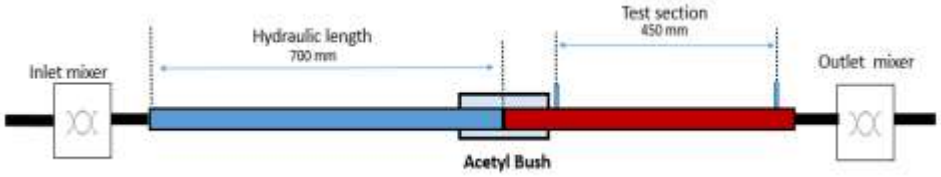

Figure 3.2**:** Schematic diagram of the test section.

Two mixers, as shown in Figure 3.2, were placed in the test section. The first was at the inlet of the test section before the entry length and the second mixer connected the outlet of the test section to the test rig, The mixtures were used in such a way to ensure the temperature at the inlet and the outlet of the test sections was uniform. The mixture consisted of four copper plates, each one positioned perpendicular to the other to assist in splitting and therefore mixing the streams of the flow. The design was adapted from the work of Galaktionov et al. [167]. The plates were 25 mm each inserted into 12.1 mm diameter pipe of 100 mm length.

Figure 3.3 shows that seven thermocouple stations were attached to the test section wall (with four thermocouples at each station) to measure the average wall surface temperature, and two thermocouples were attached to the inlet and outlet to measure the inlet and outlet fluid temperatures respectively.

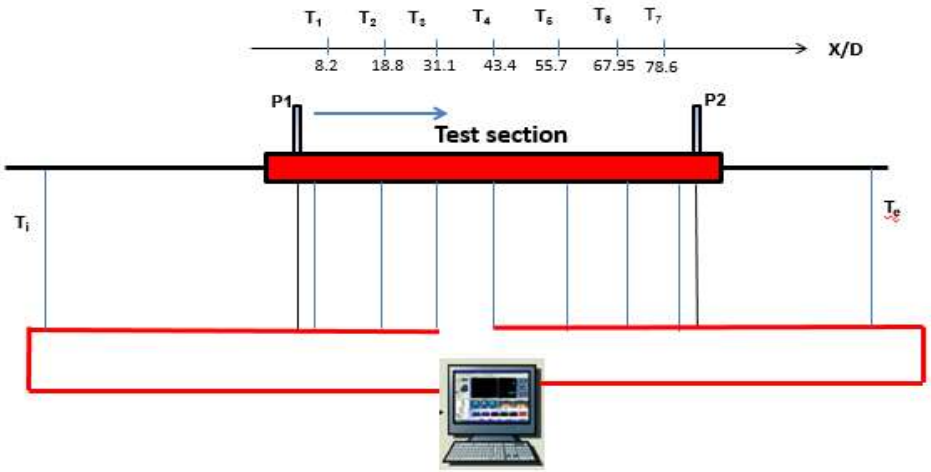

Figure 3.3**:** Distribution of the thermocouple stations over the test section and pressure tap positions.

A small pilot dent of 1 mm diameter was drilled into the test section to attach the thermocouple to the test section. The pilot dents were filled with solder, and then the test section was heated up to melting point to join the thermocouple end into the hole by applying a drop of solder. Figure 3.4 shows the joined thermocouple with the tightly coiled heating wire, and also shows the adjacent coiling of the heating wire to the thermocouple to ensure that the heat flux throughout the test section was uniform.

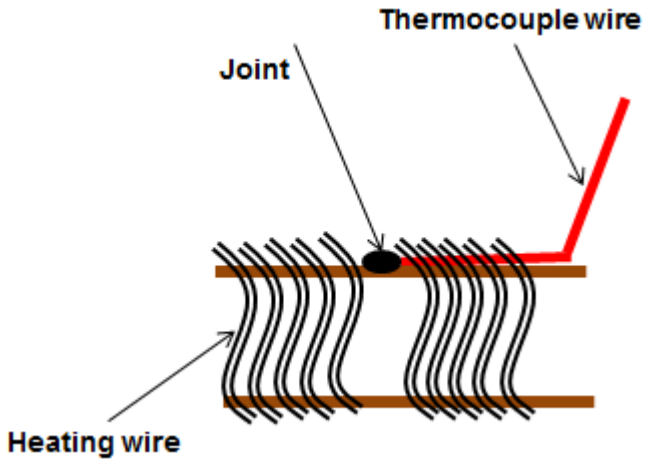

Figure 3.4**:** Thermocouple joint adjacent to the heating wire on the wall of the test section.

The thermocouples were attached to the test section wall, then calibration was done by circulating water from a thermal bath into the test section, the thermal bath was thermostat-controlled, and the temperature was varied from 15 to 50 $^{\circ}$C with an increment of 5 $^{\circ}$C. A digital thermometer was inserted into the thermal bath to log the temperature and to compare it with the thermocouple readings. The measurements were taken when the difference in the temperature between the inlet and the outlet thermocouples was less than 0.1 ^{0}C.
The uniform heat flux on the section was achieved by attaching Constantine wire to an 800 W power supply. The Constantine wire has a resistivity of $5\times10^{-7}\Omega$. The diameter of the wire was 0.24 mm, and 30 m of it was used. The wire was coiled tightly and uniformly throughout the test section. The use of 125 V and current of 0.75 A resulted in a heat flux of 6.9 kW/m^2.

To measure the pressure drop across the test section, two pressure taps were attached to the two ends of the test section, as shown in Figure 3.3. They were 30 mm long and 4 mm diameter copper tubes. The pressure taps were joined to the test section by using silver solder, and then a 0.5 mm hole was drilled into the test section through the taps. Burrs were removed

after the drilling was completed to avoid any eddy formation, which could result in measurement error. The use of such small-hole diameters was to obtain accurate pressure readings because the small diameter would help to avoid flow disturbance [168].

3.4 The test section with porous media insert

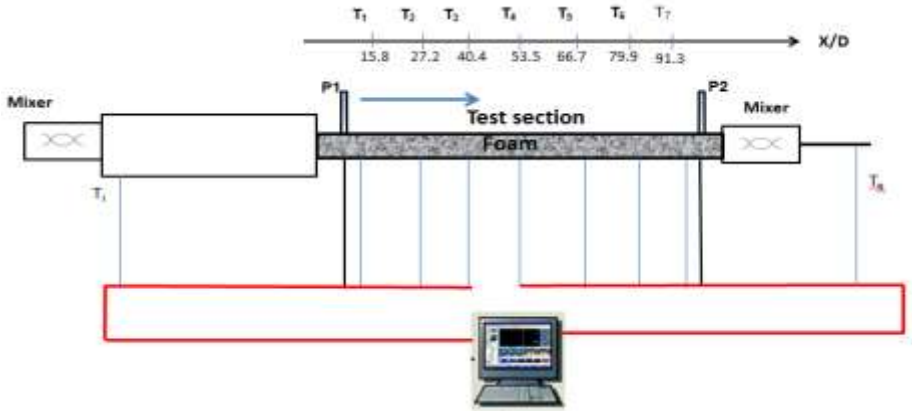

Figure 3.5**:** Layout of the nickel foam inserted into the test section, and the thermocouple station distribution.

The same test section was filled with a porous media insert of rectangular shape to assist in the heat transfer enhancement by increasing the contact surface area with the channel. The porous media was high-porosity foam procured from Alantum, Korea. The supplied foam was initially a rectangular sheet of 200 x 300 mm, the standard specification of the nickel foam is listed in Table 3.1.

The foam was cut into strips with the same dimensions as those of the test section to place it in the test section. Figure 3.6 shows the foam strips placed in the rectangular channel.

Table 3. 1: standard specification for the Ni foam supplied by Alantum.

Pore size (mm)	**Area density (g/mm^2)**	**Porosity (%)**	**Thickness (mm)**	**Permeability**
3	800	98	3.5	

The strips were cut accurately to the required size by using water jet cutting technology; the strip height was made to be slightly higher than the channel height to produce strong, tight bonding with the channel. The dimensions of the cut foam and the open channel are illustrated in Figure 3(a), and the placement of the foam in the channel before and after mechanical bonding of the top of the channel is shown in Figure 3(b) and Figure 3(c) respectively.

Figure 3.6**:** Nickel foam placement in the open rectangular channel.

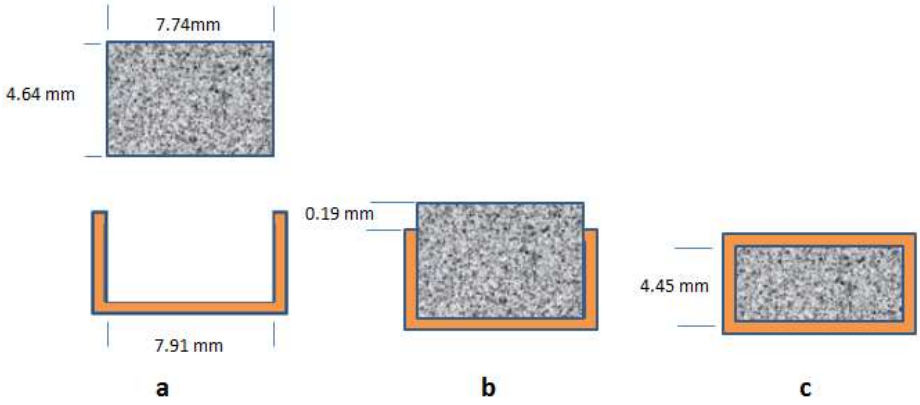

Figure 3.7**:** (a) Top opened test section and the foam, (b) foam inserted tightly into the test section, (c) foam mechanically ponded to the test section after the top of the test section was brazed.

Figure 3.8**:** (a) Mechanical ponding of the foam and the test section, (b) brazing of the top of the channel.

For the placement of the nickel porous foam in the test section, the top of the channel was opened, as shown in Figure 3.6, by using a bench saw, and then the top was machined to ensure a smooth surface to assist bonding the top of the channel to the test section, and then the foam was placed along the channel length by mechanical bonding, as shown in Figure 3.8 (a). To secure the foam inside the channel, the plate was also brazed carefully, as shown in Figure 3.8 (b), to avoid any solder droplet to leak into the channel, preventing the clogging of porous media, and preventing any leaks of the nanofluids while testing. The porosity of the test section foam arrangement was calculated again to count for any changes occurring to the porous media because of the foam insertion to the channel. The porosity was found to be 3% less than the original foam porosity, and this value was considered for the calculation.

3.5 Instruments

3.5.1 Pressure transducers

The pressure transducer of 0.08% accuracy at full scale was used to measure the pressure drop, the full scale of the pressure transducer was 17 kPa. The pressure transducer was calibrated using a water manometer, which had an accuracy of 50 Pa. Seven calibration points were obtained for the calibration. The calibration was conducted, and the calibration given by the supplier of the pressure transducer differed by 2%. Nylon tubing was then used to connect the pressure tap to the pressure transducer.

3.5.2 Flow meter

One Coriolis flow meter of a maximum flow rate of 250 l/h was used to measure the flow rate. The factory calibration uncertainty of the flow meter was 0.05%.

3.5.3 Power supply

A direct current (DC) power supply of 800 W rated power was used to supply the heating wire with a heat source in the form of a DC. The maximum voltage used was 250 V at a current of 0.75 A.

3.5.4 Data acquisition system

The data acquisition system consisted of a personal computer using National Instruments LabVIEW software, and it was utilised to record the data from thermocouples (temperatures), pressure transducers (pressure drops) and flow meters (mass flow rates). The data acquisition system also recorded the mass flow rate signal from the pump.

3.6 Testing procedures

The system was switched on by starting the pump first. The tank was filled with the testing fluid (either water or nanofluid), and all the valves of the circulating loop were in the correct position for the fluid to circulate from the tank through the test section and the other instruments back to the tank again. The flow rate was set at a value to correspond to the maximum Reynolds number before the heat flux was applied by switching the power supply and adjusting the required voltage. Steady-state conditions were monitored, and it was reached after 40 minutes, steady-state conditions were recognised when the temperature, pressure drop and the flow rate measurements remained unchanged for three minutes. When steady state was achieved, a group of data points were captured including the inlet and outlet temperatures, wall temperatures, pressure drop and the flow rate. A total of 200 data points were captured with a 1-second interval, then the flow rate was decreased and the same procedures were followed. In the transition regime, more data points were captured because the decrement of the flow rate was less than in the turbulent and the laminar flow regimes.

3.7 Conclusion

The test section was built by attaching the thermocouples along the test section, the heating wire was coiled carefully around the test section, and the whole test section was covered by thermal insulation of 50 mm. To ensure accurate measurements, the thermocouple and pressure transducers were calibrated and the calibration detailed in Appendix A. Special care was given to the nickel foam strips by cutting them into the correct size to fit tightly into the rectangular test section to ensure efficient contact for the heat transfer improvement.

CHAPTER 4 DATA REDUCTION AND VALIDATION OF THE SET-UP

4.1 Introduction

The data reduction and the equations used in the calculation are presented in the first part of this chapter. The uncertainty results of the instruments and the analysis parameters are also listed. In the last section of this chapter, detailed validation results are given by comparing the water measurements for the heat transfer and the pressure drop with the well-established correlations in the open literature.

4.2 Data reduction

4.2.1 Pressure drop

The average velocity (V) of a fluid of calculated density (ρ) and a mass flow rate ($\dot{m}$) across a rectangular cross-section of measured width (z) and measured height (h) can be calculated from the following equation:

$$V = \frac{\dot{m}}{\rho\, A_c} \qquad (\mathbf{4.1})$$

Cross-sectional area of the test section,

$$A_c = Zh \qquad (\mathbf{4.2})$$

then,

$$V = \frac{\dot{m}}{\rho\, zh} \qquad (\mathbf{4.3})$$

The hydraulic diameter of the rectangular test section can be expressed as:

$$D_h = \frac{4A_c}{p} \qquad (\mathbf{4.4})$$

Perimeter:

$$p = (2z + 2h) \quad (\mathbf{4.5})$$

The hydraulic diameter is formulated as follows:

$$D_h = \frac{4Zh}{2Z+2h} \quad (\mathbf{4.6})$$

The Darcy equation is used to calculate the friction coefficient as a function of the measured hydraulic diameter (D_h), measured pressure drop (ΔP), measured length (L) of the test section and measured fluid density (ρ), as shown in the following equation:

$$f = \frac{2\ \Delta P\ D_h}{\rho L\ V^2} \quad (\mathbf{4.7})$$

4.2.2 Heat transfer

The heat gained by the water (Q_{Water}) as a function of the measured inlet temperature (T_I) and the measured outlet temperature (T_e), the calculated specific heat of the water is (C_P) :

$$\dot{Q}_{Water} = \dot{m}\ .\ C_P\ .\ (T_e - T_i) \quad (\mathbf{4.8})$$

The heat generated by the heating wire (Q_{Elec}), the measured voltage across the wire and the measured current are (V) and (I) respectively:

$$\dot{Q}_{Elec} = VI \quad (\mathbf{4.9})$$

Energy balance (EB) can be estimated as follows:

$$EB = \frac{\dot{Q}_{elec} - \dot{Q}_{Water}}{(\dot{Q}_{elec} + \dot{Q}_{water})/_2} \quad (\mathbf{4.10})$$

The heat flux ($\dot{q}$) :

$$\dot{q} = \frac{\dot{Q}_{water}}{A_s} \quad (\mathbf{4.11})$$

Heat transfer area,

$$A_s = (2z + 2h)L \qquad (\mathbf{4.12})$$

The heat flux is calculated from the following equation:

$$\dot{q} = \frac{\dot{m} \,.\, C_P \,.\, (T_e - T_i)}{(2Z + 2h)L} \qquad (\mathbf{4.13})$$

The wall thermal resistance (R_{wall}) of the copper of thermal conductivity (K_{cu}) and measured hydraulic outer and inner diameter of (D_{hO}) and (D_{hi}) respectively:

$$R_{wall} = \frac{\ln(D_{ho}/D_{hi})}{2\pi K_{cu} L} \qquad (\mathbf{4.14})$$

The inner-wall surface temperature (T_{wi}) is obtained from the measured outer-wall surface temperature as:

$$T_{wi} = T_{wo} - Q_{water} R_{wall} \qquad (\mathbf{4.15})$$

The mean fluid temperature at a station located at x distance from where the inlet temperature was measured can be evaluated as follows:

$$T_m(x) = T_i + \frac{\dot{q}\, x\, (2Z + 2h)}{\dot{m} C_P} \qquad (\mathbf{4.16})$$

To calculate the average convective heat transfer coefficient ($h_{avg.}$), the local heat transfer coefficient ($h(x)$) at each thermocouple station is determined as follows:

$$h(x) = \frac{\dot{q}}{[T_{wi}(x) - T_m(x)]} \qquad (\mathbf{4.17})$$

The average conductive heat transfer ($h_{avg.}$) is calculated from the local convective heat transfer coefficient at each thermocouple station along the test section as in the following expression:

$$h_{avg} = \frac{h(x_1) + \cdots \ldots \ldots \ldots + h(x_n)}{n} \qquad (\mathbf{4.18})$$

Nusselt number for a fluid of calculated thermal conductivity (k):

$$Nu = \frac{h_{avg} D_h}{k} \qquad (\mathbf{4.19})$$

Reynolds number is calculated as follows, and the properties were measured at the fluid bulk temperature.

$$Re = \frac{\rho V D_h}{\mu} \qquad (\mathbf{4.20})$$

4.3 Uncertainty analysis

The procedures suggested by Dunn [169] were used to calculate all the uncertainties of the measured and calculated parameters, where all the uncertainties were evaluated within the 95% confidence interval. The details of the uncertainty analysis are presented in Appendix B. Table 4.1 lists the instrument accuracies which used bias error in the uncertainty analysis, along with their ranges and accuracies. The uncertainties were calculated at a higher Reynolds number of 7 800 and lower Reynolds number of 650. The uncertainty values of the main experimental parameters are given in Table 4.2

Table 4.1: Range and accuracies of instruments.

Instrument	Range	Accuracy
Power supply Current Voltage	 0–12.5 A 0–320 V	 0.5% of the measured value 0.1% of the measured value
Thermocouples	-200–350 °C	0.1 °C
Flow meter	0–252 L/h	0.1%
Pressure transducer	0–17 kPa	0.16%

Table 4.2**:** Uncertainties of the measured parameter at high and low Reynolds numbers.

	Re	ΔP	*f*	*h*	*Nu*
High Re	4.46%	1.15%	1.15	4.48%	4.93%
Low Re	4.63%	16.76%	16.70	0.85%	2.23%

4.4 Validation of the experimental set-up

Friction coefficients and Nusselt number measurements were considered to compare the measured data with the predictions. The data in the laminar and turbulent flow regimes were plotted and compared against the well-established correlations found in the literature. Only water was considered for validation because of a lack of correlations for similar nanofluids as the ones used in this work as well as the geometry of the test section.

4.4.1 Validation of friction coefficient results

A total of 43 data points were captured to plot the adiabatic friction coefficient against Reynolds number ranging from 500 to 8 000 to include the entire flow range including the transition flow regime. Figure 4.1 presents the variation adiabatic friction coefficient with Reynolds number. The data were compared with Leon and Roman [170] for laminar and turbulent flow regimes. As shown in Equation 4.21 and Equation 4.22 respectively, the two correlations were modified from the conventional Poiseuille correlation [171] for laminar flow and Blasius correlation [172] for turbulent flow to suit the rectangular cross-section channels:

$$f_{lamiar} = \frac{64}{Re^*} \quad \textbf{(4.21)}$$

$$f_{turbulent} = 0.316(Re^*)^{-0.25} \quad \textbf{(4.22)}$$

where α is the aspect ratio of the rectangular cross-section, and Re^* is the modified Reynolds number, which can be found as follows:

$$Re^* = \frac{Re}{2\alpha^{0.16}} \quad \textbf{(4.23)}$$

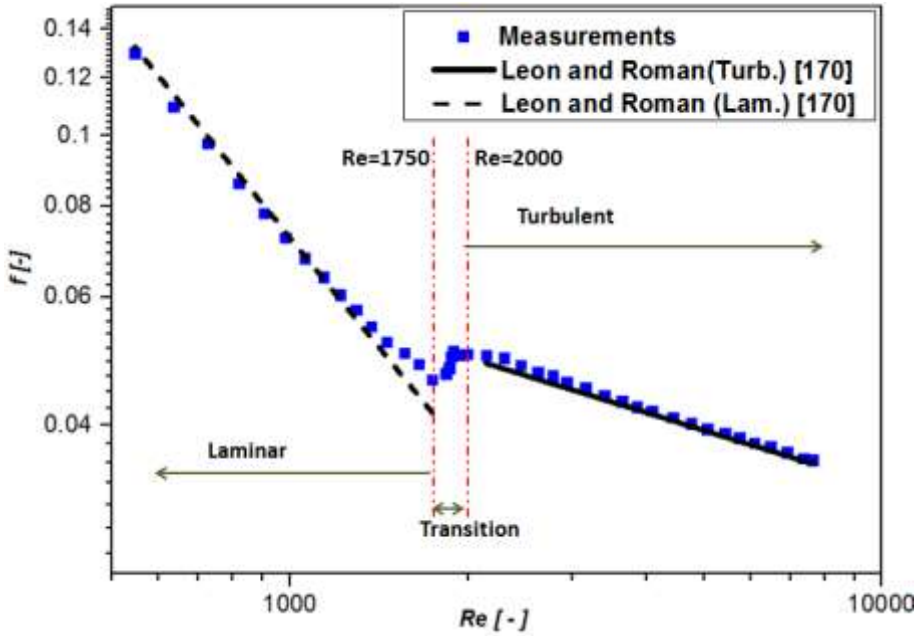

Figure 4.1: Adiabatic friction coefficient data compared with theoretical correlations.

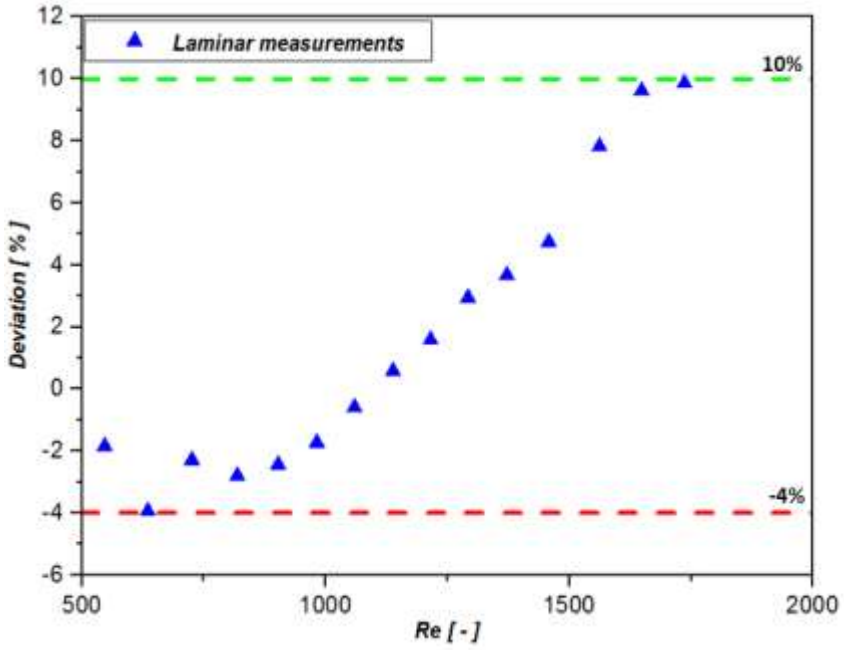

Figure 4.2: Deviation of friction coefficients from correlations in the laminar regime.

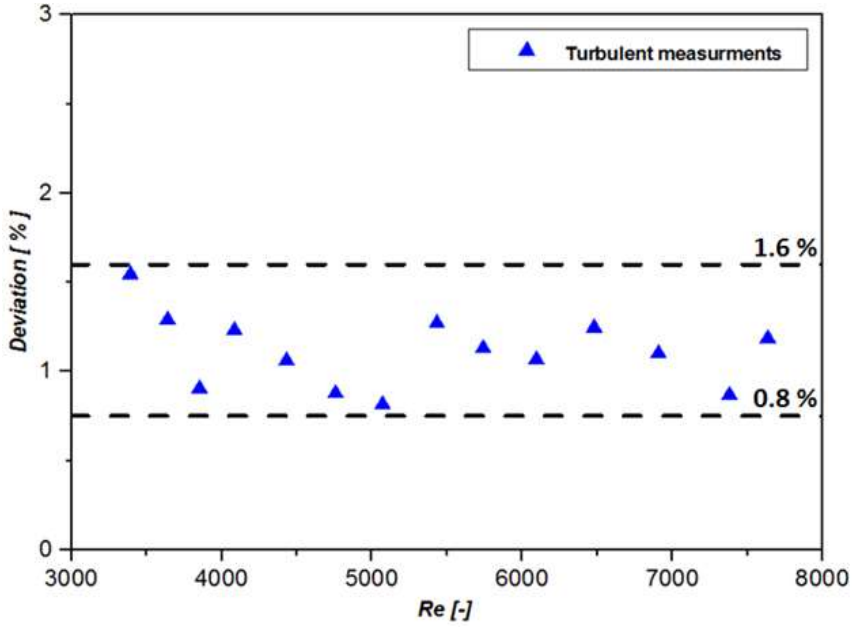

Figure 4.3**:** Deviation of friction coefficients from correlations in the turbulent regime.

The deviation of the measurements in the laminar regime from the correlation is shown in Figure 4.2, indicating that the maximum deviation was 10% at Reynolds number of 1 700. The deviation was in the acceptable range because it was less than the uncertainty value of 16.7% for the friction coefficient in the laminar regime at the lower Reynolds number values. On the other side of the turbulent regime, the deviation was bounded between the values of 1.6 and 0.8% throughout the turbulent zone. The measurements were in good agreement with the correlation, as presented in Figure 4.3.

The transitional flow regime for pure water in the rectangular channels started at a Reynolds number of 1 827, as shown in Figure 4.1, and the length of transition was noticed to be a Reynolds number of 150, while the critical Reynolds number (where transition starts) in a circular tube is 2 300, as reported by Cengel [173]. The earlier transition was due to the geometry of the test section used and the type of inlet because the inlet of the test section had significant effects on the critical Reynolds number, transition pattern and transition length [155, 156, 158].

4.4.2 Validation of Nusselt number results

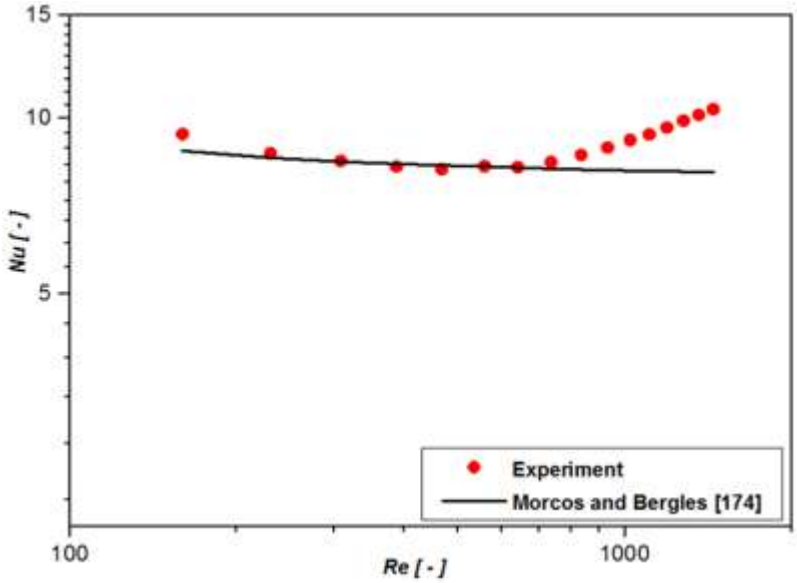

Figure 4.4**:** Nusselt number comparison with the correlation in the laminar flow regime.

The average Reynolds number was calculated by measuring the inlet and the outlet temperature, and then calculating the Reynolds number base on the thermophysical parameters evaluated at the fluid bulk temperature. The validation of the Nusselt number data was carried out in the Reynolds number range of 500 to 1 700. The measured data in the laminar regime are presented in Figure 4.4, a comparison with the Morcos and Bergles [174] correlation was conducted. Morcos and Bergles [174] developed the correlation for the mixed convection laminar, which was the case in this work because the flow was not thermally fully developed. The correlation is as follows:

$$Nu = \sqrt{\left[(4.36)^2 + \left[0.145\left(\frac{Gr_f^* \, pr_f^*}{Pw_f^{*0.25}}\right)^{0.265}\right]^2\right]} \qquad \textbf{(4.24)}$$

Gr_f^* is the modified Grashof number and is expressed as follows:

$$Gr_f^* = GrNu = \frac{g\beta\rho^2 d^3 (T_w - T_b)}{\mu^2} \qquad \textbf{(4.25)}$$

By applying the correlation in Equation 4.24, the measurements matched the correlation very well because the correlation underpredicted the measurements in the range of Reynolds

number greater than 600, as shown in Figure 4.5. The maximum deviation was 0.8% below the measured value and was observed at Reynolds number of 1 440.

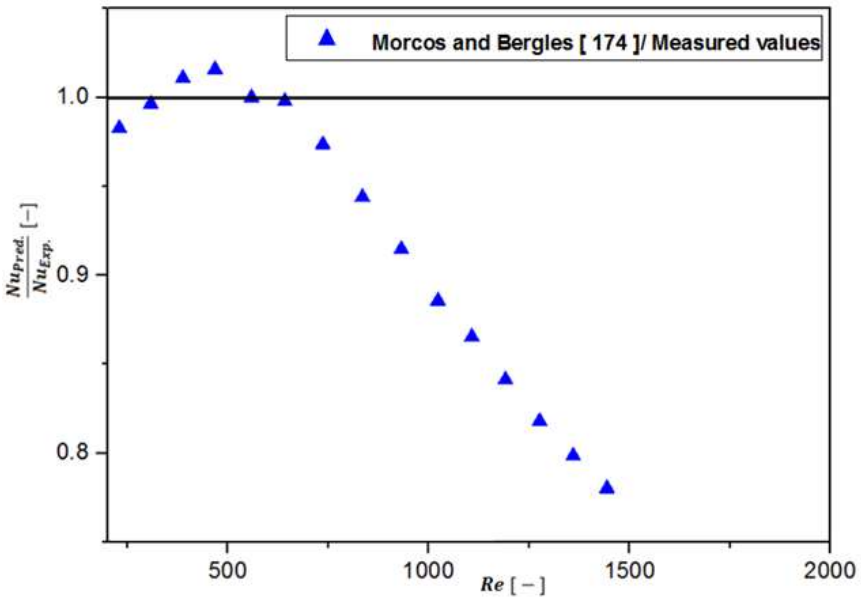

Figure 4.5**:** Ratio of the predicted to the measured value of Nusselt number in the laminar regime.

The Nusselt number data were measured by applying a heat flux of 13 kW/m^2 on the test section and the results were compared with the correlation of Everts and Meyer [164], Olivier and Meyer [159] and Gnielsiki [175], as shown in Figure 4.6. The correlations and their limitation are listed in Table 4.3.

Table 4.3: Correlations from the literature for the turbulent regime .

Author	**Correlation**	**Limitations**
Gnielinski [175]	$Nu = \frac{\frac{f}{8}(Re - 1000)pr}{1 + 12.7\left(\frac{f}{8}\right)^{0.5}(pr^{\frac{2}{3}} - 1)}$ $f = (0.79 \ln Re - 1.64)$	$0.5 \leq Pr \leq 2000$ $3000 \leq Re \leq 500.10^3$
Olivier and Meyer [159]	$Nu = 0.023\, Re^{0.788} pr^{1/3} (\frac{\mu_b}{\mu_w})^{0.14}$	$3.73 \leq Pr \leq 5.06$ $3000 \leq Re \leq 17800$
Everts and Meyer [164]	$Nu = 0.011597\ (pr)^{0.42} (Re)^{0.8607} (\frac{pr_b}{pr_w})^{0.11}$	$5.5 \leq Pr \leq 6.9$ $2804 \leq Re \leq 9787$

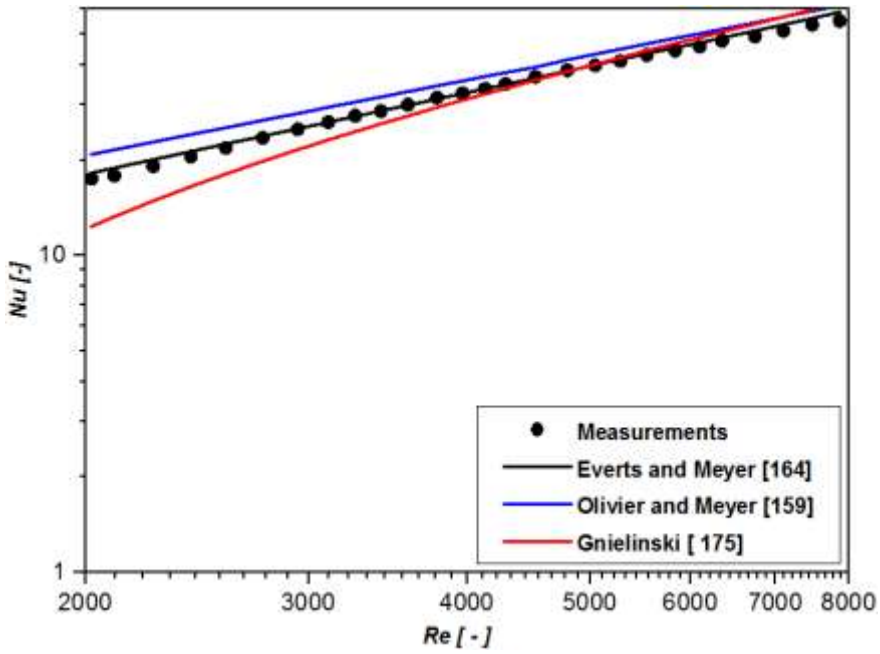

Figure 4.6**:** Nusselt number comparison with correlations in the turbulent flow regime.

The Nusselt number measurements in the turbulent regime were compared with the correlations of Gnielinski [175], Olivier and Meyer [159] and Everts and Meyer [164]. The comparison of the prediction with the measured data, as shown in Figure 4.7, revealed that the average Nusselt number correlated very well with the correlation of Everts and Meyer [164], which overpredicted the results by an average of 1.8%. The correlation of Olivier and Meyer [159] overpredicted the data by an average of 3.8%, which was a good prediction. Gnielinski [175] underpredicted the data by 6% in the Reynolds number range of 3 000 to 5 000, and over-predicted the data by 7% for Reynolds numbers greater than 5 000. The correlations of both Olivier and Meyer [159] and Gnielinski [175] failed to predict the data on the turbulent side between Reynolds numbers of 2 000 and 3 000 because they underpredicted the data in this range by 12% and 21% respectively. This significant difference occurred because the two correlations were developed to predict the turbulent regime of flow for Reynolds numbers greater than 3 000.

The entire flow regime is presented in Figure 4.8 because a set of data of Nusselt number was plotted against Reynolds number to identify the transition zone. The transition from laminar to turbulent was started at a Reynolds number of 1 750 and ended at a Reynolds number of 2 000. Comparing the transition in this test section (rectangular profile) with the circular test

section, an early transition in the rectangular cross-section is noticed. The heat transfer results and the pressure drop results indicate that the starting and the ending of transition are the same on both plots, as shown in Figure 4.1 and Figure 4.8.

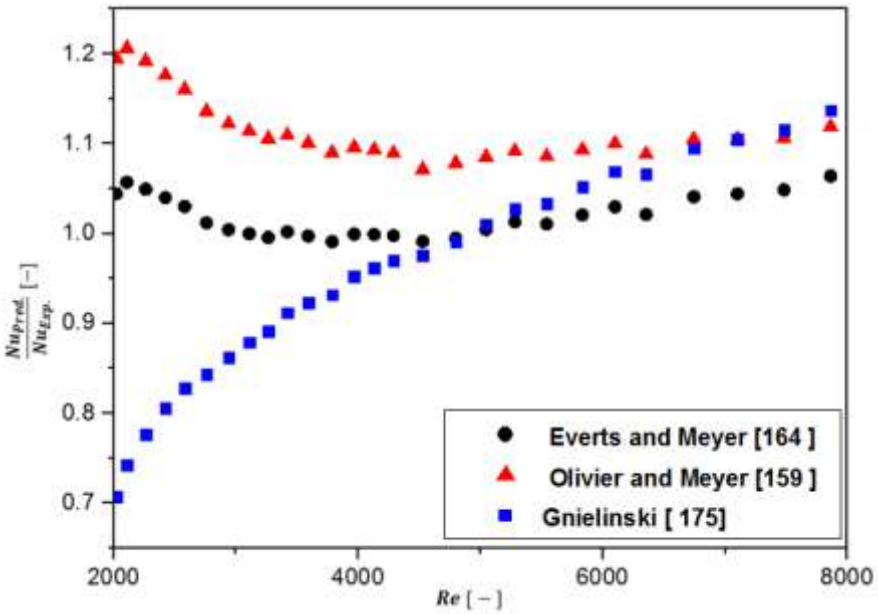

Figure 4.7**:** Ratio of the predicted to the measured value of Nusselt number in the turbulent regime.

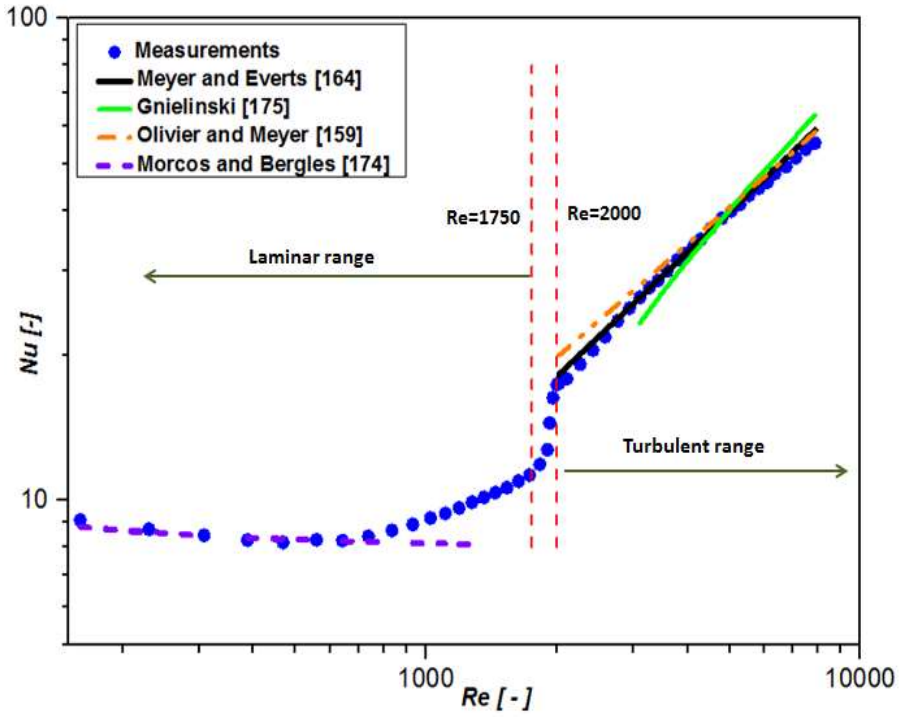

Figure 4.8: Nusselt number variation with Reynolds number for the entire flow range.

4.5 Conclusion

The experimental set-up was explained in detail including the various instruments used for measuring the different parameters. The construction procedures of the rectangular test section used in this work were presented, and the calibration of the thermocouples and the pressure transducers was stated. The accuracies of the equipment and the uncertainties of the measured parameters were tabulated, and the experimental procedures were explained.

The experimental set-up was validated by comparing the laminar and turbulent regime measurements against the reliable correlations found in the literature. The deviation in the laminar regime was good as 0.8%, and the best agreement in the turbulent regime was an average deviation of 1.8%. Therefore, the experimental set-up is reliable and can be used to investigate the heat transfer and the pressure drop characteristics in the transition flow regime for the water and the nanofluids.

CHAPTER 5 NANOFLUID PREPARATION AND PROPERTY ANALYSIS

5.1 Introduction

In this chapter, the characteristics and properties of the nanoparticle materials are presented. The preparation of Al_2O_3-water and TiO_2-water nanofluids is discussed, after which the stability of the nanofluids is judged by visual inspection and through the viscosity measurements over some time for all nanofluids. Both methods and the nanofluid thermal properties are evaluated and discussed at the end of this chapter.

5.2 Nanoparticle size and properties

Two different nanofluids were employed in this study, aluminium oxide-water nanofluid (Al_2O_3-water) and titanium dioxide-water nanofluid (TiO_2-water). Three different concentrations (0.3, 0.5 and 1%) were used from Al_2O_3-water nanofluid, while four different volume concentrations (0.3, 0.5, 0.7 and 1%) were examined. Table 5.1 presents the main thermal properties for both materials used.

Table 5.1**:** Properties of the nanofluid materials used.

Property	**Unite**	**Al_2O_3 particles**	**TiO_2 particles**
Density	kg/m^3	3970	4175
Specific heat	J/kg.K	765	710
Thermal conductivity	W/m.K	46	8.4
Particle size	nm	46	42

Transmission electron microscopy (TEM) imaging of Al_2O_3-water and TiO_2-water nanofluid was conducted to determine the particle sizes. The aggregation between the particles was avoided by adding acetone to the sample for quick-drying. The acetone was applied to 0.1% volume concentration of each case.

From the pictures in Figure 5.1 and Figure 5.2, the size of the nanoparticles for both nanofluids was calculated. The average particle size was considered by recording 10 different measurements for each nanoparticle, and it was found to be 46±1 nm and 42±1 nm for Al_2O_3 and TiO_2 nanoparticles respectively. TEM pictures for Al_2O_3 revealed that the shape was rod-

like and the size was determined by measuring the width and the length of the rod. The shape of TiO_2 particles was observed to be semi-spherical, and the size was determined by measuring the diameter. The standard deviation (σ) for both nanoparticle measurements was evaluated using Equation -5.1- and was found to be 4.3, and 16.2 for Al_2O_3 and TiO_2 respectively.

$$\sigma = \sqrt{\frac{\sum_{i=1}^{i=N}(X - \overline{X})^2}{N}} \qquad (\mathbf{5.1})$$

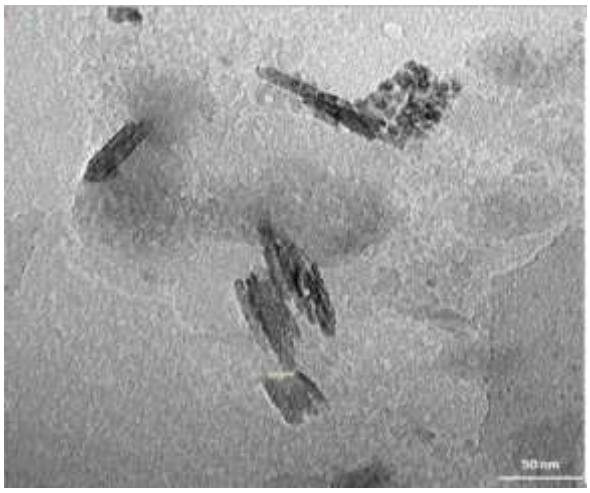

Figure 5.1: TEM imaging of Al2O3-water nanofluid.

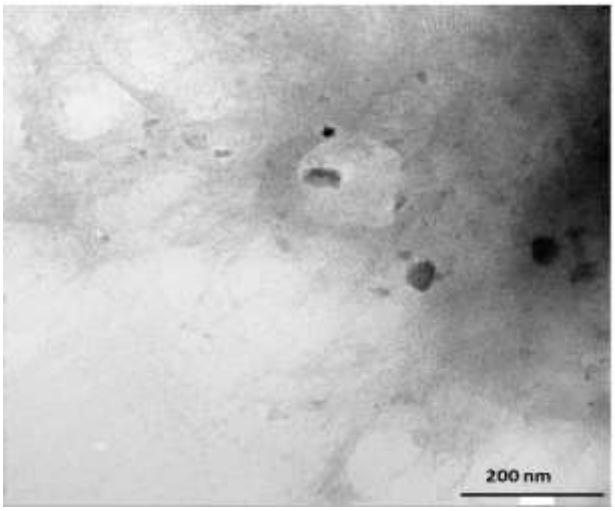

Figure 5.2**:** TEM imaging of TiO_2-water nanofluid.

5.3 Preparation of nanofluids

5.3.1 Preparation and dilution of nanofluids

A 20 wt% (5.9 vol %) aluminium oxide (gamma) nanofluid and 15 wt% (4.2 vol %) titanium dioxide nanofluid prepared using a one-step method was ordered from US Research Nanomaterial (USA). The one-step method nanofluid was used because of the longer stability time. Aluminium oxide-water nanofluids of volume concentrations of 0.3, 0.5 and 1% were prepared by diluting the high-concentration nanofluid. Each nanofluid was prepared by adding deionised water to the concentrated nanofluid and breaking down particle agglomerations using an ultrasonicator (Qsonice Q700) set at an amplitude of 60% for 20 minutes, using 3 s pulse on and 1 s pulse off intervals. For the titanium dioxide nanofluid, four different volume concentrations of 0.3, 0.5, 0.7 and 1% were prepared by diluting the high-concentration nanofluid prepared by using the one-step method. Each nanofluid was prepared by adding deionised water to the concentrated one-step nanofluid and homogenising the diluted nanofluid by using an ultrasonicator (Qsonice Q700). Ultrasonication time of 15 minutes and amplitude of 70% were used, with an interval of 2 s pulse on and 1s pulse off.

5.3.2 Stability of nanofluids

The stability was confirmed by capturing a picture of the nanofluids directly after the preparation and comparing it with pictures after one week. Figure 5.3 and Figure 5.4 illustrate the visual inspection of the stability for 1.0 vol% of Al_2O_3-water and TiO_2-water nanofluid because no sedimentation was observed for one week.

Figure 5.3: Aluminium oxide nanofluid (left) and titanium dioxide nanofluid (right) immediately after the preparation.

Figure 5.4: Aluminium oxide nanofluid (left) and titanium dioxide nanofluid (right) after seven days since the preparation.

To confirm and verify the stability of the nanofluids, one of the properties needed to be measured over a period of time during which there was no change, to confirm the stability in addition to the visual inspection. Therefore, this was accomplished by measuring and observing the viscosity of the aluminium oxide-water and the titanium dioxide-water nanofluids. Figure 5.5 shows the viscosity of three various Al_2O_3-water nanofluid concentrations at a constant temperature of 25 °C. The viscosity over time was constant, indicating the stability of the nanofluids over that period. Similarly, the stability of TiO_2-water nanofluids was investigated, the viscosity measured at a temperature of 20 °C, and the measurement was observed over one day. Figure 5.6 displays the viscosity of all four concentrations over time as unchanged confirming the stability of the nanofluids over that period.

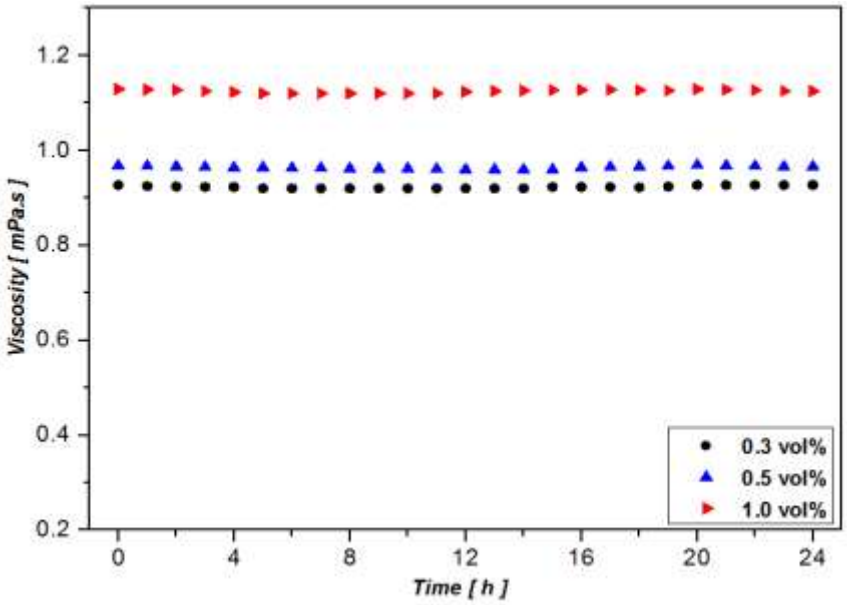

Figure 5.5: Variation of the viscosity of Al_2O_3-water nanofluids with time at 25 °C.

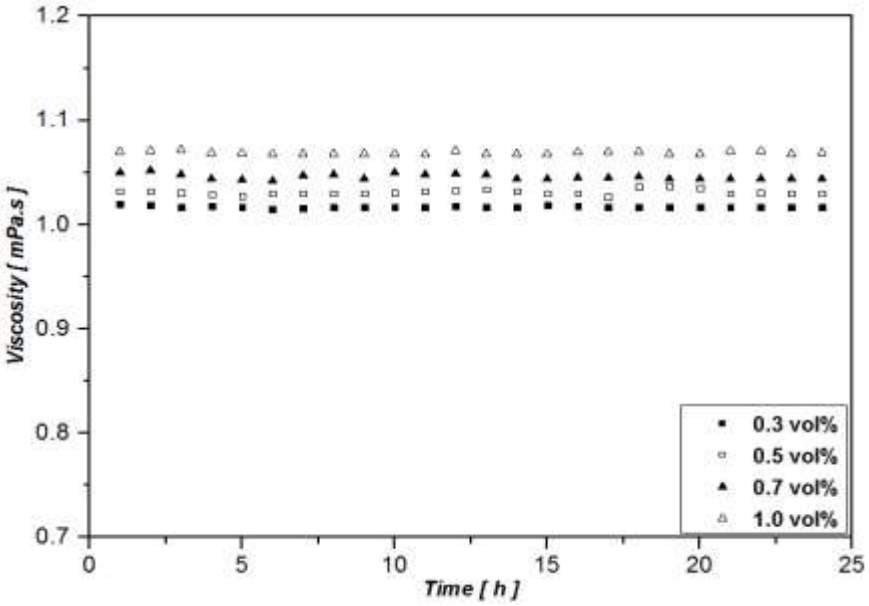

Figure 5.6: Variation of the viscosity of TiO_2-water nanofluids with time at 20 °C.

5.4 Thermophysical properties of nanofluids

5.4.1 Thermal conductivity

Mintsa et al. [91] developed a correlation for the effective thermal conductivity of Al_2O_3-water nanofluids by measuring the thermal conductivities of nanofluids at various volume concentrations up to 9%, and for two different nanoparticle sizes at a wide temperature range. In this study, the thermal conductivity of the nanofluid was calculated using their developed linear correlation [91], as shown in Equation 5.2.

$$\frac{K_{nf}}{K_{bf}} = 1.72\emptyset + 1 \qquad (\mathbf{5.2})$$

The model of He et al. [176] was considered for the thermal conductivity of the nanofluids in this work, which was developed for different TiO_2-water-based nanofluids, as shown in Equation 5.3.

$$\frac{K_{nf}}{K_{bf}} = 125.62\emptyset^2\ 4.82\emptyset + 1 \qquad (\mathbf{5.3})$$

5.4.2 Viscosity and other properties

The viscosity of the nanofluid was measured using a vibro-viscometer (SV-10, A&D, Japan), with 5.0% uncertainty at the full range. Figure 5.7 compares the nanofluid viscosities with the water viscosity predicted by Popiel and Wojtkowiak [177]. It can be observed that the nanofluid viscosity increased with the volume concentration. Previous studies [178-184] reported similar results for the viscosities and thermal conductivities of nanofluids.

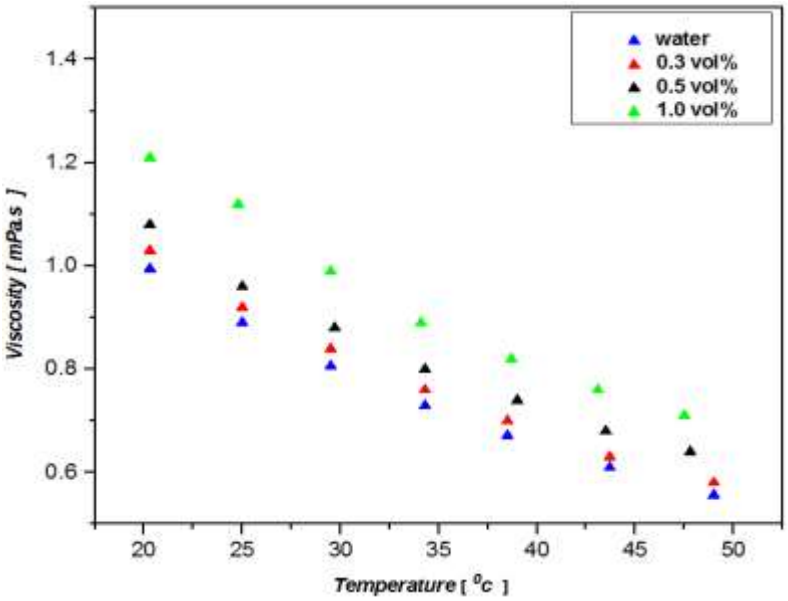

Figure 5.7: Viscosities of Al_2O_3-water nanofluids compared with water viscosity as a function of temperature.

The properties of the water were also determined using the equation developed by Popiel and Wojtkowiak [177]. The viscosity of the nanofluids was measured with a vibro-viscometer (SV-10, A&D, Japan) with 5.0% uncertainty at full range. Figure 5.8 compares the viscosity of the nanofluids with the water viscosity predicted by the correlation of Popiel and Wojtkowiak [177]. The comparison shows that the viscosity of nanofluids increased with volume concentrating. Previous studies [178-184] reported the same observation for the viscosity and thermal conductivity of nanofluids. The viscosity, as shown in Figure 5.8, increased by increasing the volume concentration and temperature of the nanofluids. The viscosity increase was 1.6, 2.8, 4.2 and 6.6% for 0.3, 0.5, 0.7 and 1.0 vol% of the nanofluids respectively.

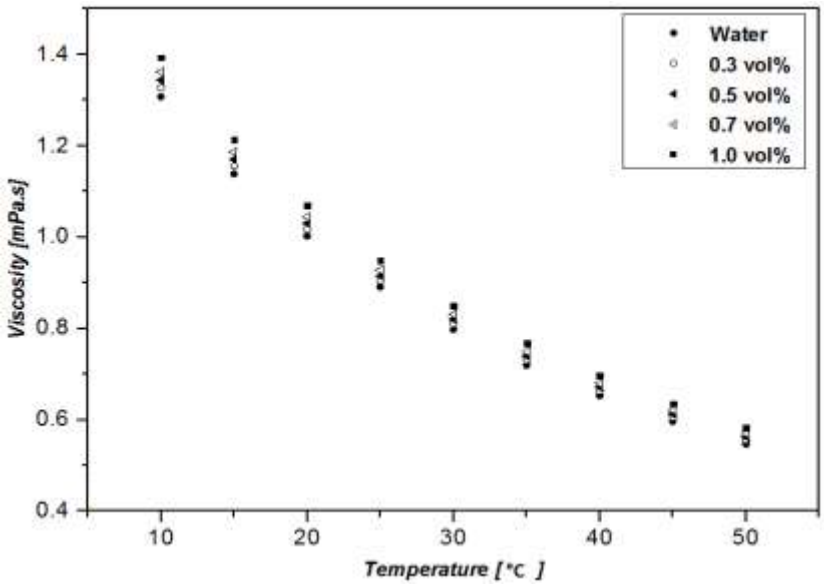

Figure 5.8**:** Variation of TiO_2-water nanofluids viscosity with the temperature for different volume concentrations.

The density and specific heat of the nanofluid were calculated using the following mixing theory equations:

$$\rho_{nf} = \emptyset.\rho_p + (1 - \emptyset) * \rho_{bf} \qquad (\mathbf{5.4})$$

$$(C_p)_{nf} = \frac{\emptyset.(\rho.C_p)_p + (1-\emptyset).(\rho.C_p)_{bf}}{\rho_{nf}} \qquad (\mathbf{5.5})$$

A comparison between the two nanofluids is conducted for the thermal conductivity and the viscosity as illustrated in Figures 5.9 and 5.10, the comparison results showed that the thermal conductivity of the titanium dioxide nanofluid is greater than the aluminium oxide nanofluid for all the concentrations covered in this work. However, the viscosity for the aluminium oxide nanofluid showed higher values compared to the titanium dioxide nanofluid throughout the covered concentration.

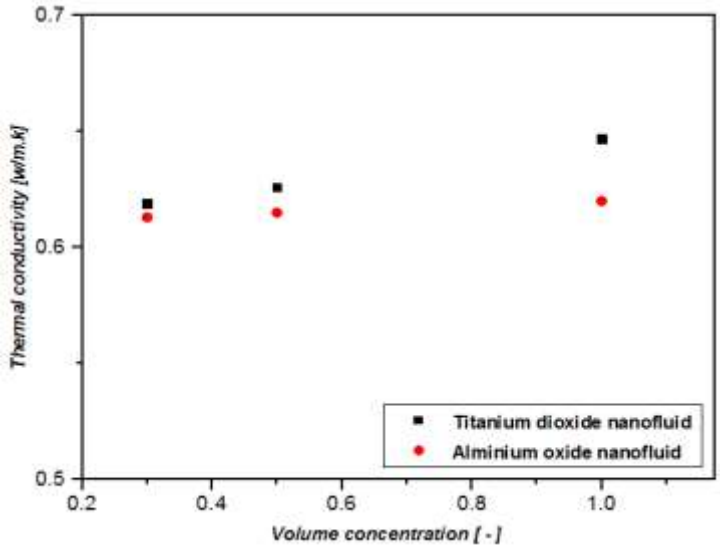

Figure 5. 9: Comparison of the thermal conductivity for the two nanofluids with the different concentrations at 25 °C

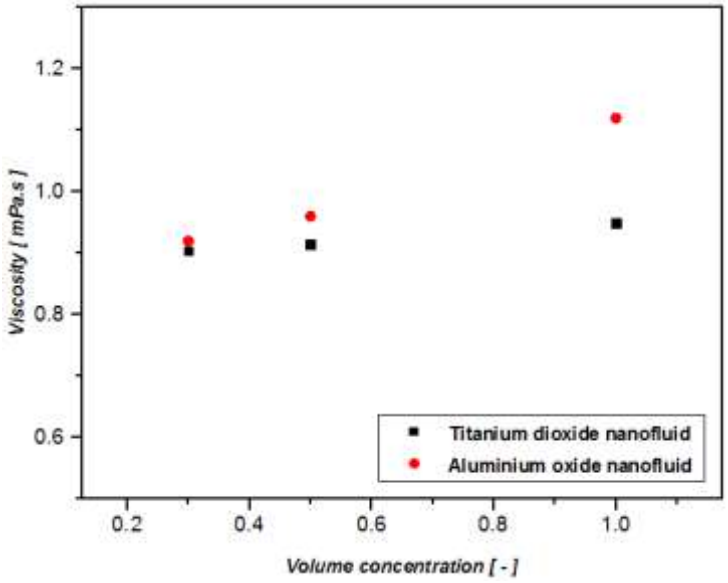

Figure 5. 10: Comparison of the viscosity for the two nanofluids with the different concentrations at 25 °C

5.5 Conclusion

The transmission electron microscopy imaging showed that the actual particle size for Al_2O_3 and TiO_2 were 46 nm and 42 nm respectively, higher than the values provided by the supplier (30 nm for both). The nanofluids were prepared by diluting the procured dispersions. The stability was confirmed by recording the viscosity measurements for all the nanofluids, and it was found that the viscosity values remained constant. Visual inspection of the nanofluids was also considered to ensure the stability. The properties of the nanofluids were determined as the viscosity was obtained experimentally, and the other properties were predicted by using suitable correlations from the literature.

CHAPTER 6 RESULTS AND DISCUSSION

6.1 Introduction

In this chapter, the variation in pressure drop, friction coefficients, heat transfer coefficient, and Nusselt number with Reynolds number are presented and discussed for Al_2O_3-water nanofluids and TiO_2-water nanofluids. A thermal performance factor is also presented. The heat transfer and pressure drop results, as well as the thermal performance analysis, are also discussed for the nickel foam-filled test section. The uncertaintiy of the reported enhancement parameters in this chapter were calculated and listed in Appendix B

6.2 Heat transfer results of Al_2O_3-water nanofluids

The average heat transfer coefficients and the average Nusselt number measurements of Al_2O_3-water nanofluids of 0.3, 0.5 and 1.0 vol% were compared with pure water in a Reynolds number range of 200 to 7 000.

The heat transfer coefficient results, as shown in Figure 6.1, showed an enhancement of the heat transfer in the fully developed turbulent regime, with values of 1.0% at a Reynolds number of 6 364 for the 0.3 vol% nanofluid, 4.0% for the 0.5 vol%, and 11% for the 1.0 vol%. The average enhancements of the heat transfer coefficient in the turbulent flow regime were 3.1% for the 0.3 vol% nanofluid, 6% for the 0.5 vol%, and 16% for the 1.0 vol% nanofluid. The average enhancements of the Nusselt number in the turbulent regime, as shown in Figure 6.2, were 2.5% for the 0.3 vol% nanofluid, 4.6% for the 0.5 vol% nanofluid, and 12.5% for the 1.0 vol%. The same results for the heat transfer enhancements in the turbulent flow regime were observed by Pak and Cho [18]. The random motion of nanoparticles within the fluid decreased the thermal boundary layer thickness and made a significant contribution to the enhancement of the convection heat transfer rate. This could be the reason for the enhancements of the heat transfer coefficient and Nusselt number in the turbulent regime [30, 137].

Two features were observed in the transition flow regime in the rectangular channel when using Al_2O_3-water nanofluid. First, the critical Reynolds number (starting the transition) was earlier when using the nanofluid and occurred at a smaller Reynolds number than that of pure water when a higher concentration nanofluid was used. As shown in Figure 6.1 and Figure 6.2, the transition began at Reynolds numbers of 1 731 for the 0.3 vol% nanofluid, 1 723 for

the 0.5 vol% nanofluid, and 1 705 for the 1.0 vol% nanofluid, and the ranges of Reynolds numbers over which the transition occurred were 125, 110 and 125 respectively. For all three nanofluids, the transition flow regime began earlier than for pure water. This early transition could be justified by the higher viscosity of the nanofluid because a higher viscosity led to a shift in the position of the transition for pure water to a new position, as shown in Figure 6.2. This early transition feature matched that found in the work of Meyer et al. [24], where the results of the nanofluids were represented as a Re-Nu graph.

The second feature in the transition flow regime was the enhancement of the heat transfer coefficients for the three nanofluids, with values of 15%, 24% and 54% for the 0.3, 0.5 and 1.0 vol% nanofluids respectively.

The enhancements of the Nusselt number in the transition flow regime, as shown in Figure 6.2, were found to be 14% for the 0.3 vol% nanofluid, 22% for the 0.5 vol% nanofluid and 50% for the 1.0 vol% nanofluid.

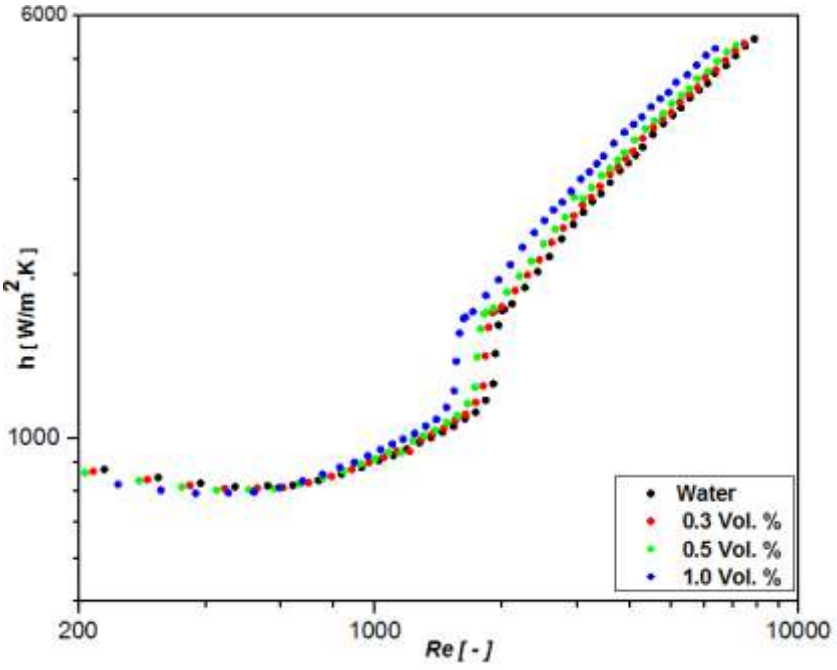

Figure 6.1: Heat transfer coefficient results of Al_2O_3-water nanofluids compared with water against Reynolds number.

A comparison of the heat transfer enhancements in the turbulent flow regime and transition flow regime revealed that the heat transfer was more enhanced in the transition regime than in the turbulent regime. It is possible that the Brownian motion of the nanoparticles and the flow randomness assisted in mixing the nanoparticles with the base fluid, which contributed

to the better heat transfer performance in the transition flow regime. Another reason for the better enhancement in the transition flow regime was that the addition of small particles to the base fluid suppressed turbulence by playing the role of an additional source of dissipation, as proposed by Hetsroni [185].

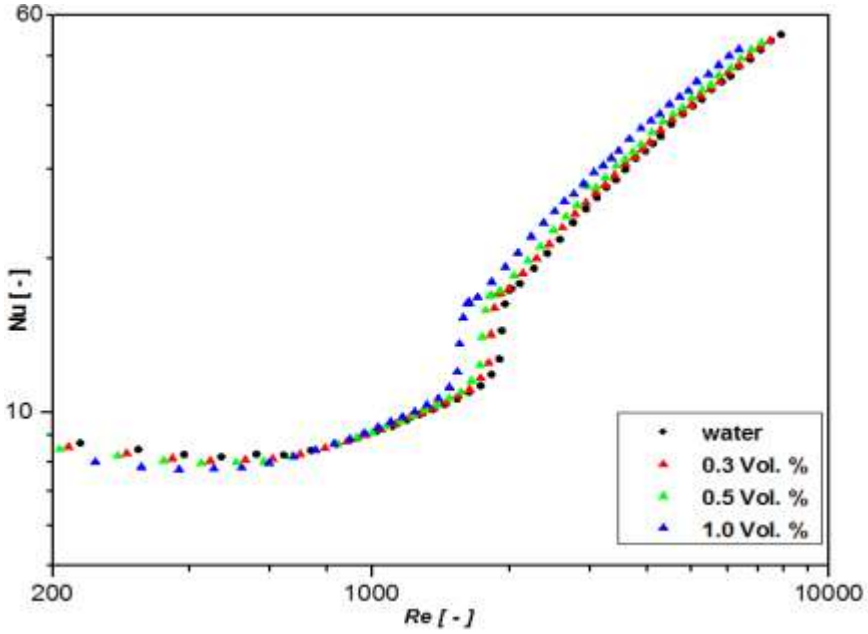

Figure 6.2: Nusselt number results of Al_2O_3-water nanofluids compared with water against Reynolds number.

6.3 Pressure drop results of Al_2O_3-water nanofluids

The pressure drop for the water compared with the three Al_2O_3-water nanofluids against the Reynolds number for the entire flow range is shown in Figure 6.3. The pressure drop of the nanofluid in the turbulent flow regime increased with the volume concentration, with values of 11%, 19% and 46% for the 0.3, 0.5 and 1.0 vol% nanofluids respectively.

The increase in the pressure drop was significant in the transition flow regime, with values of 7.9%, 14% and 61% for the 0.3, 0.5 and 1.0 vol% nanofluids respectively. In the laminar flow regime, the pressure drop increased by 1.8% for the 0.3 vol%, 9.3% for the 0.5 vol% and 29% for the 1.0 vol %.

The friction factor for the water compared with the three Al_2O_3-water nanofluids against the Reynolds number for the entire flow range is presented in Figure 6.4. The friction factor of the nanofluid in the laminar flow regime decreased with an increase in the volume concentration, and the values for all the nanofluids were lower than those for pure water at

the same Reynolds number. Towards the turbulent regime, the friction coefficient results for the nanofluids and water became difficult to distinguish because of the effect of the nanoparticles on the flow physics at this regime.

The transitions shown in Figure 6.3 and Figure 6.4 occurred at the same Reynolds number as those seen in the Nusselt number and heat transfer coefficients results, and the range of Reynolds numbers over which the transitions occurred was also the same as that seen in the Nusselt number and heat transfer coefficient results.

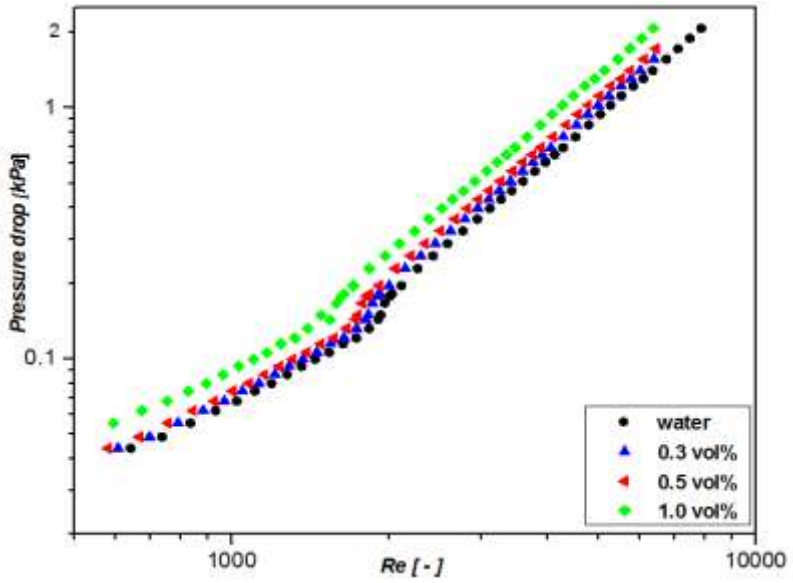

Figure 6.3**:** Pressure drops of Al_2O_3-water nanofluids compared with water against Reynolds number.

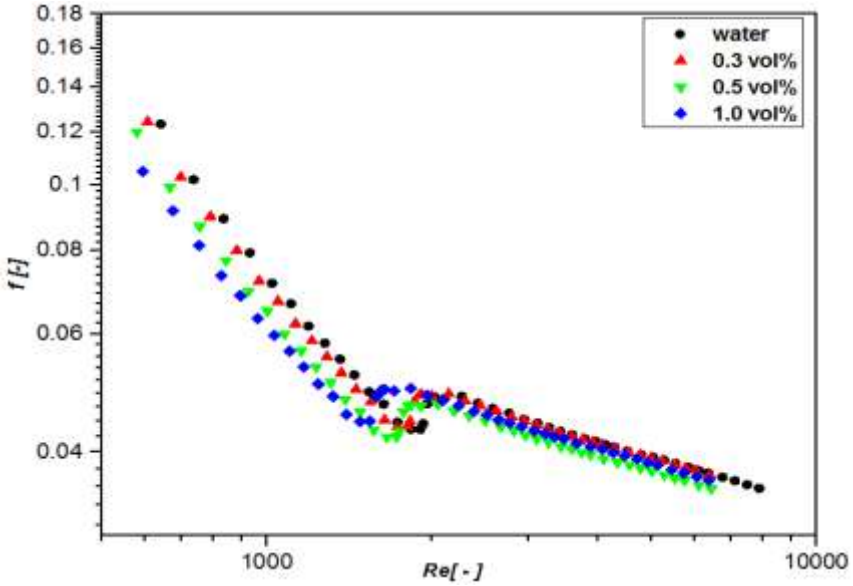

Figure 6.4**:** Friction coefficients of Al_2O_3-water nanofluids compared with water against Reynolds number.

6.4 Comparison of convective heat transfer and pumping power

The heat transfer performance of the nanofluid could be evaluated by comparing the convection heat transfer obtained by the nanofluid to the pumping power required to send the nanofluid to the laminar, transition, or turbulent flow regime. The following expression for the convective heat transfer efficiency (η) was used by Meriläinen et al. [186]:

$$\eta = \frac{(Q_{conv.})_{nf} / (P_{pumping})_{nf}}{(Q_{conv.})_{bf} / (P_{pumping})_{bf}} \qquad (\mathbf{6.1})$$

where $Q_{conv.}$ and $P_{pumping}$ are the convective heat transfer and pumping power respectively; and the subscriptions nf and bf indicate the nanofluid and base fluid respectively.

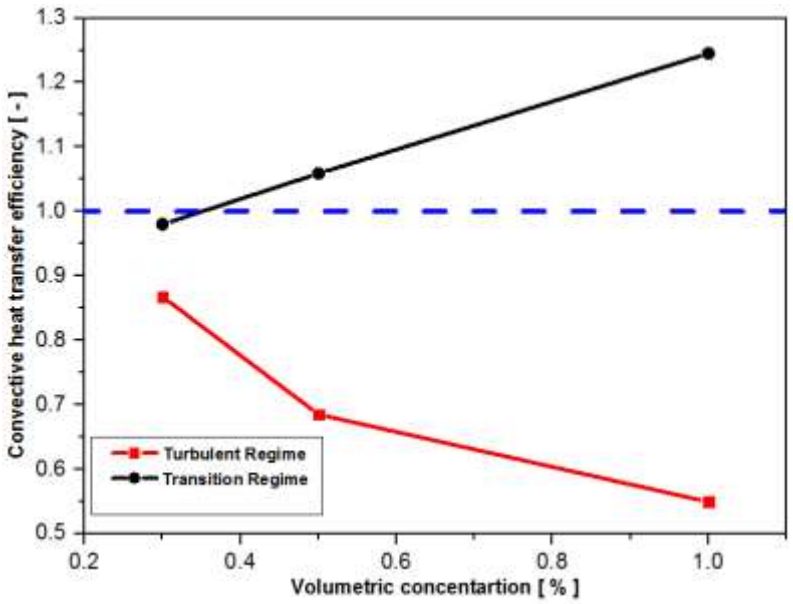

Figure 6.5**:** Convective heat transfer efficiency of Al_2O_3-water nanofluids in turbulent and transition flow regimes against the volumetric concentration.

The heat transfer efficiency, as defined in Equation 6.1, was determined by calculating the average convection heat transfer and pressure drop values in the transition and turbulent flow regimes. The results were plotted against the nanofluid volumetric concentration in Figure 6.5. The laminar regime was not included in the comparison because of the inefficiency of the nanofluids in this regime, as stated in Section 4.2.1. Figure 6.5 shows that the efficiency of the nanofluids in the transition regime was greater than unity for a volume concentration

greater than 0.3 vol%, whereas it was less than unity in the turbulent regime. These observations show that the nanofluids used were more efficient in the transition flow regime because the convective heat transfer dominated the pressure drop, and adding Al_2O_3 nanoparticles to the water was more efficient than simply increasing the flow rate of the pump.

6.5 Heat transfer results of TiO_2-water nanofluids

The average heat transfer coefficient for the four nanofluids compared with pure water over the Reynolds number range of 200 to 8 000 is presented in Figure 6.6. The volume concentrations of 0.7 and 1.0% showed an average improvement in the heat transfer coefficient in the turbulent flow regime, the average enhancement of the heat transfer coefficients was 4.5 and 1.1% respectively. The heat transfer coefficient measurements for the 0.3 and 0.5 vol% overlaid the pure water plot. The small enhancement could explain the reason for the non-improvement of the smallest concentration nanofluid (0.3 and 0.5 vol%) in the thermal conductivity of the nanofluid (0.38% and 0.82%), and such a small increase of nanoparticles could not contribute to the overall heat transfer enhancement in the turbulent flow regime.

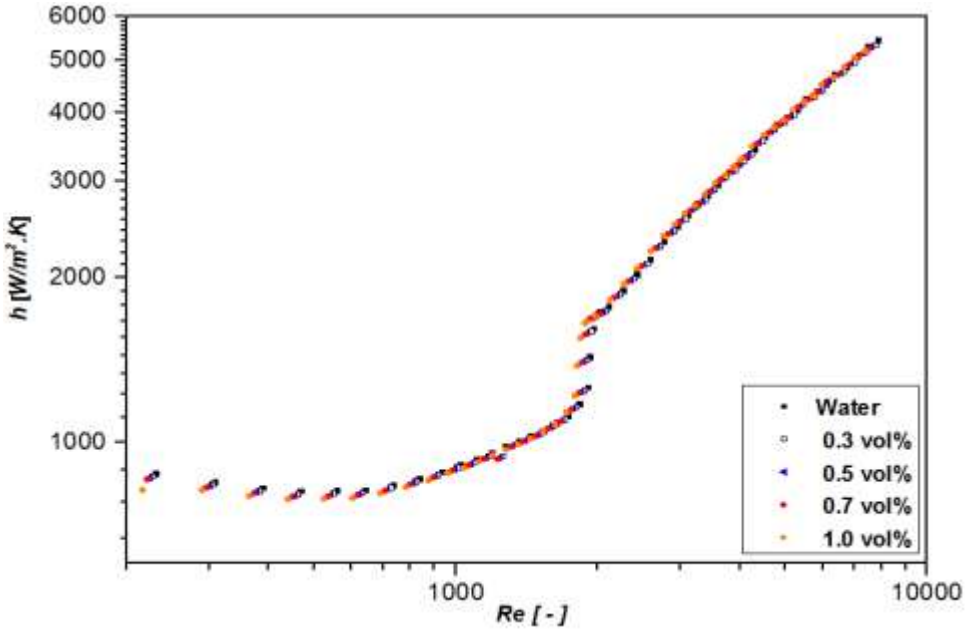

Figure 6.6**:** Variation of heat transfer coefficients of TiO_2-water nanofluids and water with Reynolds number.

The Nusselt number of the nanofluids compared with the base fluid over Reynolds number span of 200 to 8 000 is depicted in Figure 6.7. The Nusselt number was enhanced when using

only the 0.7 vol% nanofluids with an increase of 0.5%. However, the Nusselt number decreased by 1.5%, 2.6% and 4.6% for the 0.3, 0.5 and 1.0 vol% nanofluids.

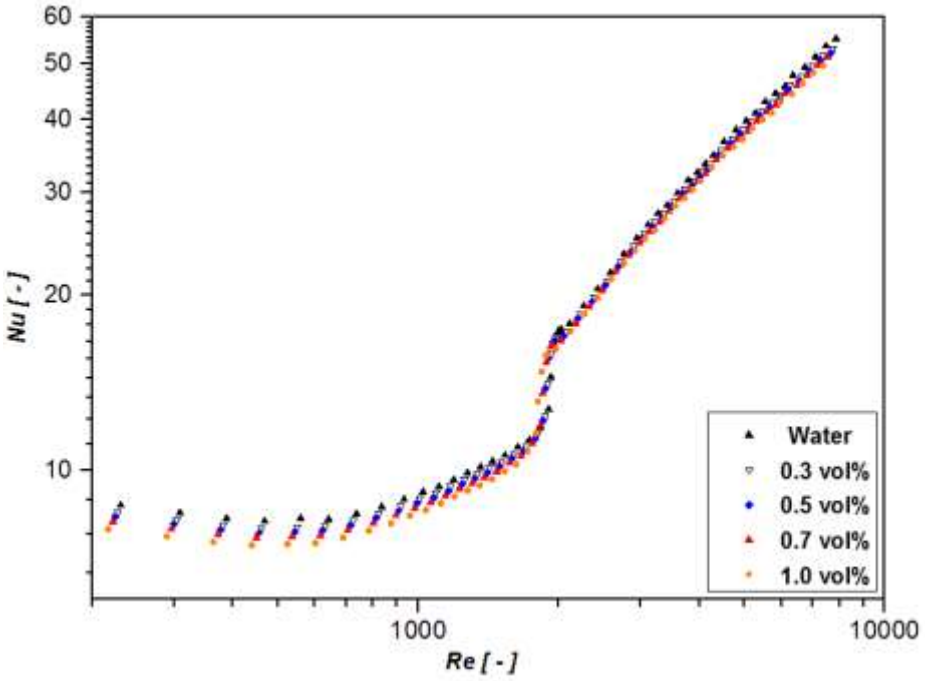

Figure 6.7: Nusselt number variation of TiO_2-water nanofluids compared with pure water.

The augmentation of heat transfer coefficients when experimenting with TiO_2-water nanofluids in the turbulent regime was due to shrinkage in the boundary layer because of Brownian movement of nanoparticles in the base fluid [30, 137].

A magnified view is given to illustrate the transition, as shown in Figure 6.8 and Figure 6.9, and two aspects were noticed when transitioning from laminar to turbulent in the rectangular channels when using TiO2-water nanofluids. The first aspect is that the nanofluid concentration influenced the onset of transition, and it was found to be taking place at a smaller Reynolds number with an increase in the volume concentration. Figure 6.8 and Figure 6.9 illustrate the transition onset as it started at Reynolds number of 1 799 for the 0.3 vol% nanofluid, at Reynolds number of 1 778 for the 0.5 vol% nanofluid, at Reynolds number of 1 754 for the 0.7 vol% nanofluid and at Reynolds number of 1 714 when using 1.0 vol% nanofluid; the length of transition in terms of Reynolds number measured was 191, 189, 186 and 182 respectively.

The transition flow regime for all four nanofluids started earlier compared with that of pure water. The early transition linked to the greater nanofluids viscosity, which shifted the position of transition from what it is in Figure 6.5 to a new transition situation, as presented in Figure 6.7. The quicker transition agreed with the work of Meyer et al. [24]. Another note

concerning the transition behaviour of the current test nanofluids is the significant enhancement of the heat transfer of the four nanofluids, particularly in the transition zone, because the enhancement was 3.9% for the 0.3 vol% nanofluid, 14.8% for the 0.5 vol% nanofluid, 29.26% for the 0.7 vol% nanofluid and 29.33% for the 1.0 vol% nanofluid. The same observation was made for the Nusselt number in the transition flow regime as presented in Figure 6.7, namely 4.6% for the 0.3 vol% nanofluid, 11.7% for the 0.5 vol% nanofluid, 24.3% for the 0.7 vol% and 21.9% for the 1.0 vol% nanofluid.

Heat transfer enhancement in the transition regime was much higher than in the turbulent regime. The reasons for the substantial enhancement were the nanoparticles' Brownian movement, assistance from flow eddies and vortexes from the transition flow nature in mixing the nanoparticles with the base fluid, and the existence of small particles in the host fluid, breaking turbulence by an extra source of dissipation, as suggested by Hetsroni [185].

The heat transfer enhancement in the laminar regime was negligible due to the agglomeration of nanoparticles associated with the low rate of flow.

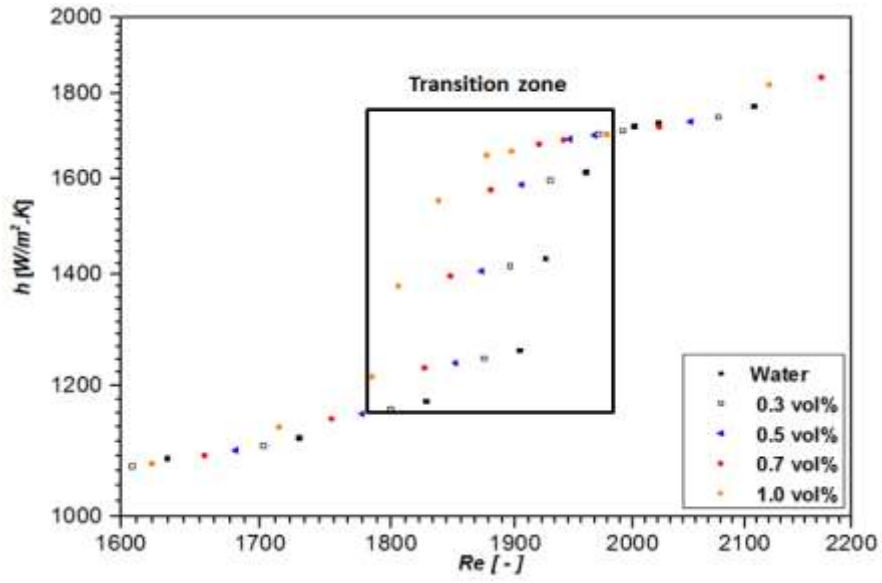

Figure 6.8: Heat transfer coefficient enhancement of TiO_2-water nanofluids in transition regime

.

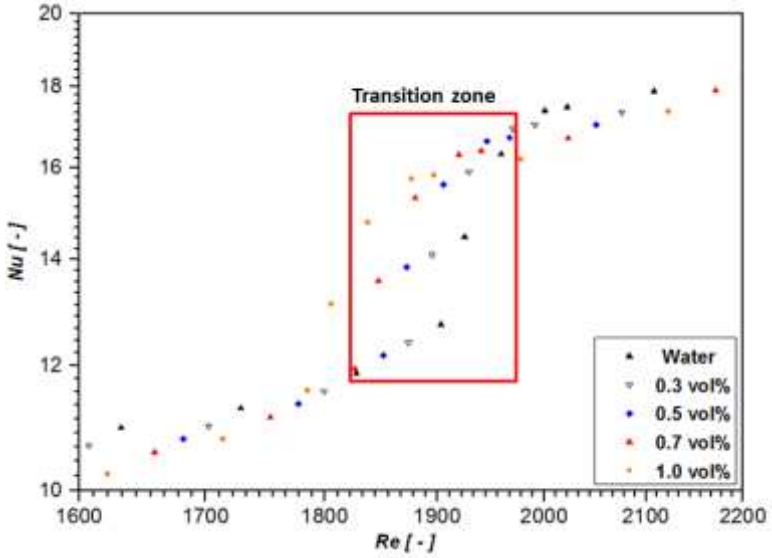

Figure 6.9**:** Nusselt number enhancement of TiO_2-water in trransition regime.

6.6 Pressure drop and friction coefficient results

The pressure drop of water compared with four TiO_2-water nanofluids is presented in Figure 6.10 to cover the full flow range span. Results showed that the pressure drop increased with an increase in the concentration and the Reynolds number, as it is observed to be 2.8%, 5.4%, 8.0% and 12.7% for the 0.3, 0.5, 0.7 and 1.0 vol% nanofluids. The penalty in the pressure in the transition flow regime was slightly higher than in the turbulent regime since it was 4.5% for the 0.3 vol% nanofluid, 11.3% for the 0.5 vol % nanofuid, 15.5% for the 0.7 vol% nanofluid and 22.5% for the 1.0 vol % nanofluid. The increase in the pressure drop was due to the particles interacting with the wall of the test section and due to the higher viscosity of the nanofluids compared with that of water.

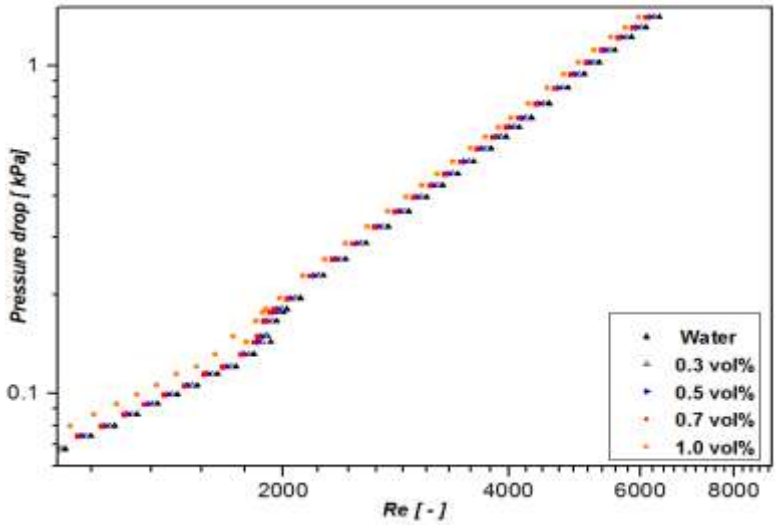

Figure 6.10**:** Pressure drop of TiO_2-water nanofluids and pure water as a function of Reynolds number.

The friction coefficients for various concentrations of titanium dioxide nanofluids and the water are displayed in Figure 6.11. The friction coefficients decreased with the rise in the volume concentration in the laminar regime, except for the weakest volume concentration nanofluid (0.3 vol%) because it was similar to the values of pure water. The friction coefficient data of the 0.5 and 0.7 vol% nanofluids were less than the values of pure water at the same Reynolds number throughout the turbulent regime, while the friction coefficient results for both 0.3 and 1.0% were higher than those of the water.

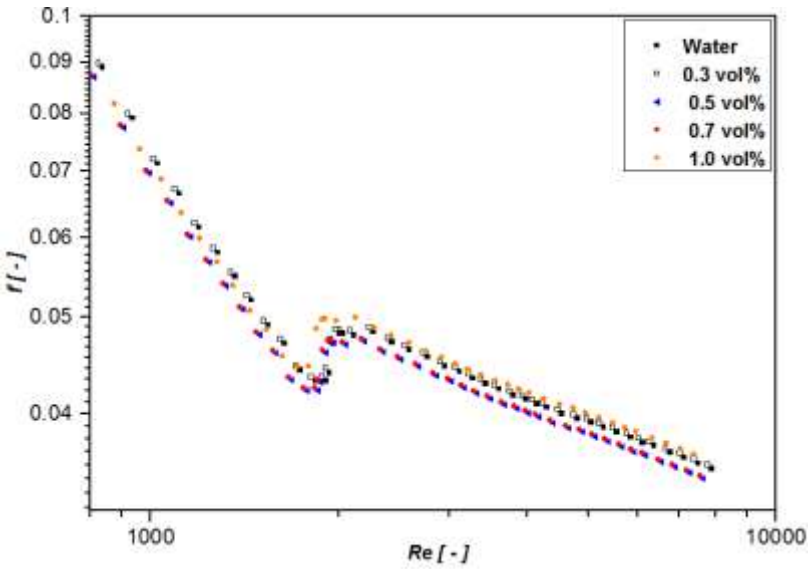

Figure 6.11**:** Variation of friction coefficient of TiO_2-water nanofluids and water with Reynolds number.

The friction factor coefficients in the transition flow regime were noticed to increase with volume and they were 2.3, 6.5, 7.7 and 15.2% for the 0.3, 0.5, 0.7 and 1.0 vol%. The start and the length of transition were identical in the heat transfer and the pressure drop results, as shown in Section 6.5 and Secion 6.6.

6.7 Evaluation of the heat transfer performance of nanofluids

The thermal performance factor used to evaluate the heat transfer performance of the titanium dioxide aqueous nanofluid was tested in this work and was defined by comparing the Nusselt number of the nanofluid and the water with the friction factor. The mathematical definition is shown in Equation 6.2 as suggested by karwa et al. [187] for the rectangular channels:

$$Thermal\ performance\ factor\ = \frac{\frac{Nu_{nf}}{Nu_f}}{\left(\frac{f_{nf}}{f_f}\right)^{1/3}} \qquad (\mathbf{6.2})$$

where Nu_{nf} and f_{nf} are the Nusselt number and the friction factor of the nanofluid, while Nu_f and f_f are the Nusselt number and the friction factor of the host fluid respectively.

The thermal performance factor, as outlined in Equation 6.2, was computed by calculating the average Nusselt number and the friction factor for all the concentrations of the nanofluids over Reynolds number values covering the transition and the turbulent regimes. The laminar flow measurements were not included because the heat transfer enhancement was negligible, as can be seen from Figure 6.7 and Figure 6.8.

Figure 6.12 shows that the thermal performance factor of the nanofluids in the transition regime was higher than the unity value and the maximum values were 1.07, 1.15, 1.25 and 1.19 for the 0.3, 0.5, 0.7 and 1.0 vol% nanofluid respectively. Therefore, in the transition regime, the nanofluids under investigation contributed to the heat transfer improvement more than the increase in the pumping power required due to the viscosity increase in the nanofluid. In the turbulent regime, the results of the thermal performance factor indicated that all the values for all the nanofluids were under the unity bar except for the 0.7 vol%.

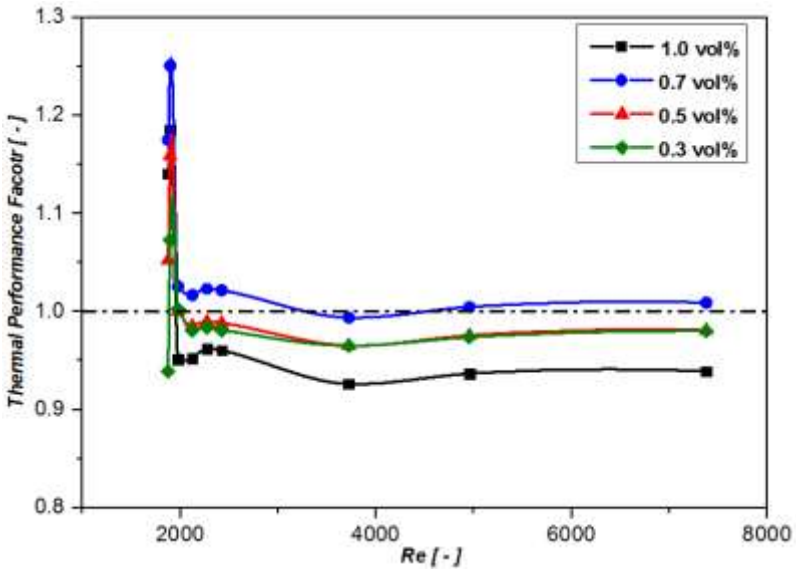

Figure 6.12: Thermal performance factor of TiO_2-water nanofluids over Reynolds number through the full flow range.

6.8 Comparison of the two nanofluids

6.8.1 Heat transfer coefficient and Nusselt number

The average heat transfer coefficient and Nusselt number for Al_2O_3- and TiO_2-water nanofluids compared with those of pure water over the Reynolds number range of 200 to

8 000 are displayed in Figure 6.13 and Figure 6.14. The heat transfer coefficient of TiO_2-water nanofluid at 0.3 vol% was identical with the pure water measurements at the laminar and the turbulent flow regimes, while an enhancement of 4% was noticed in the transition regime. The comparison of the heat transfer coefficients between TiO_2-water nanofluid and Al_2O_3-water nanofluid at the 0.3% vol% revealed that Al_2O_3 nanofluids had a higher heat transfer coefficient in the turbulent and the transition flow regimes (3.1 and 15.3% respectively). However, no change in the laminar regime was observed for both nanofluids, as shown in Figure 6.13.

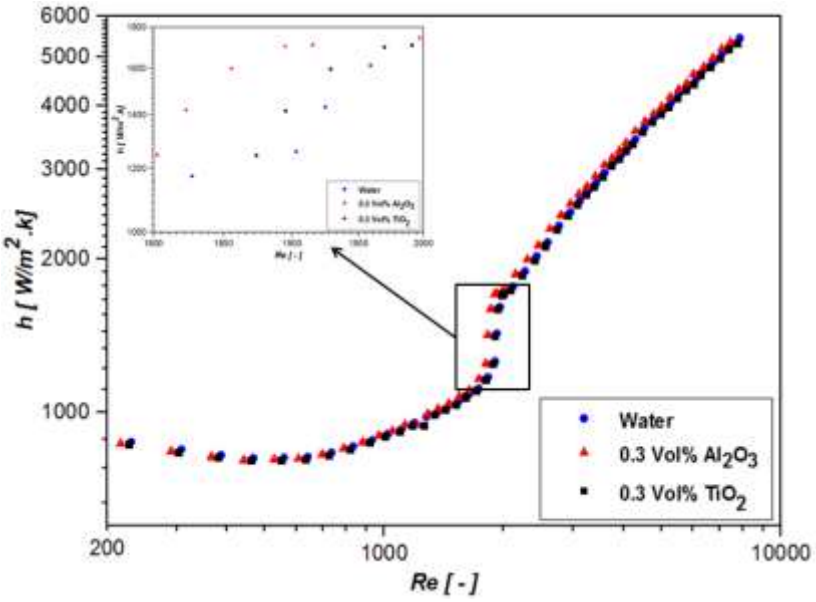

Figure 6.13: Comparison of heat transfer coefficient for Al_2O_3- and TiO_2-water nanofluids at 0.3 vol%.

Nusselt number measurements for both nanofluids at the 0.3 vol% are presented in Figure 6.14. Observations in the turbulent regime showed the lower Nusselt number for TiO_2-water nanofluid compared with that of pure water and Al_2O_3-water nanofluid. An average enhancement of 4% in Nusselt number for Al_2O_3-water in the turbulent regime was achieved compared with that of TiO2-water nanofluid. A significant increase was observed in the transition regime because it was 14% and 5% for Al_2O_3-water and TiO_2-water respectively. A magnified view of the transition regime in the graph is presented in both figures to show that the enhancement was noticeable. The reason for the superiority of Al_2O_3-water nanofluid in heat transfer enhancement could be the higher thermal conductivity of Al_2O_3 than that of TiO_2.

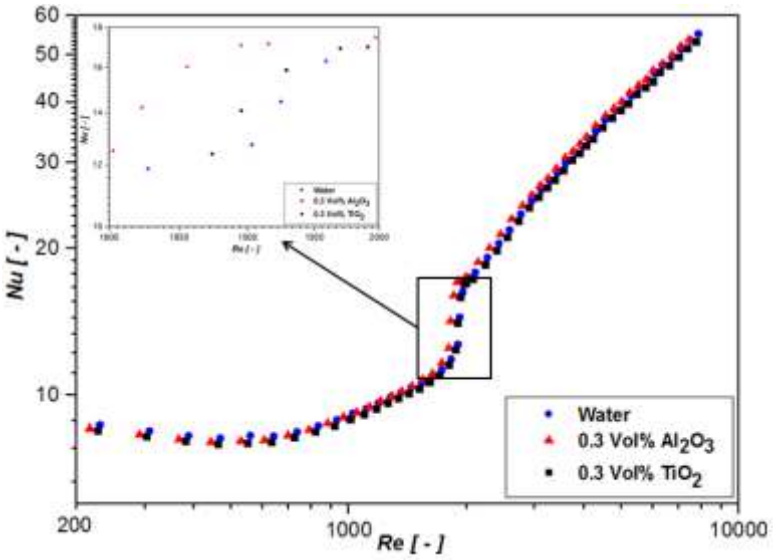

Figure 6.14: Nusselt number comparison of Al_2O_3- and TiO_2- water nanofluids at 0.3 vol%.

The heat transfer coefficient of the 0.5 vol% is presented in Figure 6.15. The comparison was conducted between both different nanofluids and pure water. The values of TiO_2-water nanofluids overlaid the pure water measurement indicating no increase in the heat transfer coefficient for TiO_2-water nanofluid when compared with that of base fluid in the turbulent regime. The same result was obtained in the laminar regime, but in the transition regime, an enhancement of 11.7% was earned from TiO_2-water against pure water. The aluminium oxide-water nanofluid exhibited a noticeable enhancement in the turbulent and the transition regimes, because the increases in the heat transfer coefficient were 6% and 24% respectively higher than that of TiO_2-water nanofluid. The higher increase in the transition measurements for Al2O3-water over TiO_2-water could be because of the shape and size of the particles, as indicated in Section 5.2.

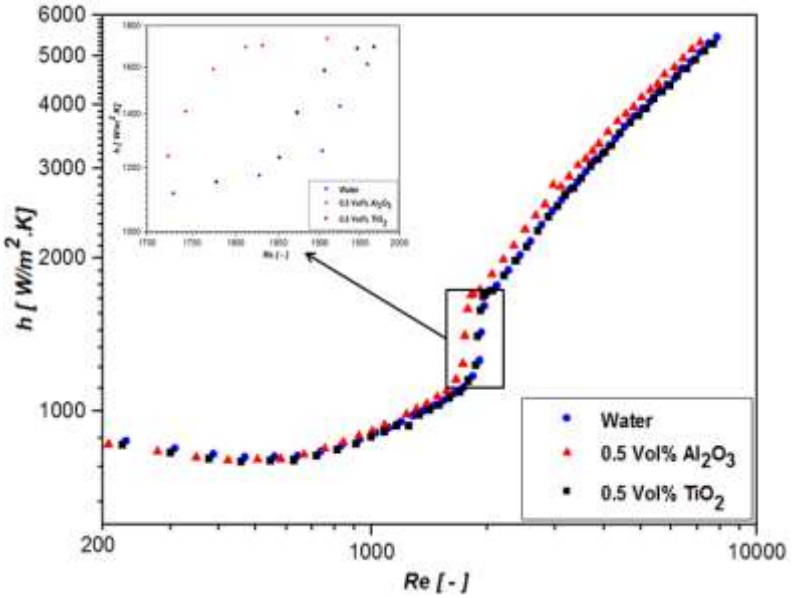

Figure 6.15: Comparison of heat transfer coefficient of Al_2O_3- and TiO_2-water nanofluids at 0.5 vol%.

The Nusselt number for both nanofluids was compared with that of water at the volume concentration of 0.5% and is shown in Figure 6.16. The Nusselt number for TiO_2-water nanofluids was lower than that of water by 2.6% at the turbulent regime, 11.7% higher in the transition regime, and 6% lower in the laminar regime. Al_2O_3-water nanofluids had a higher Nusselt number of 7.2% than that of TiO_2-water nanofluid in the turbulent regime and 33.9 % in the transition regime.

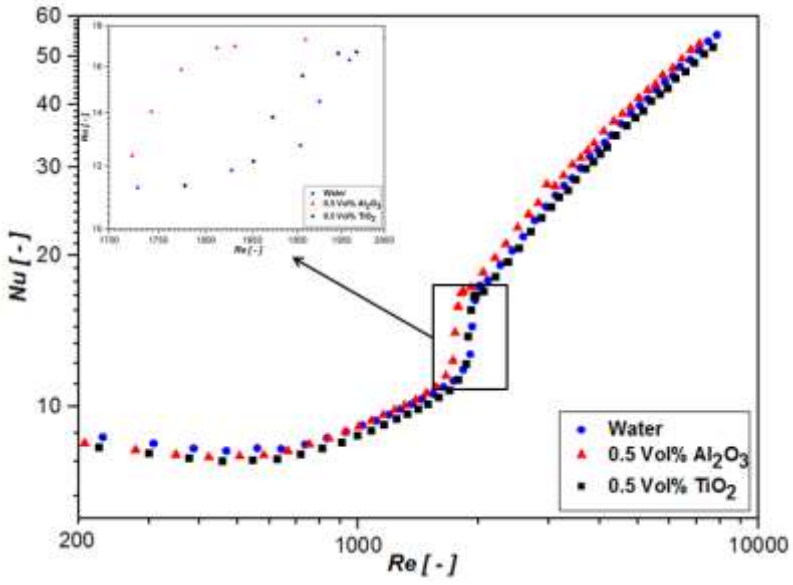

Figure 6.16: Nusselt number comparison of Al_2O_3- and TiO_2-water nanofluids at 0.5 vol%.

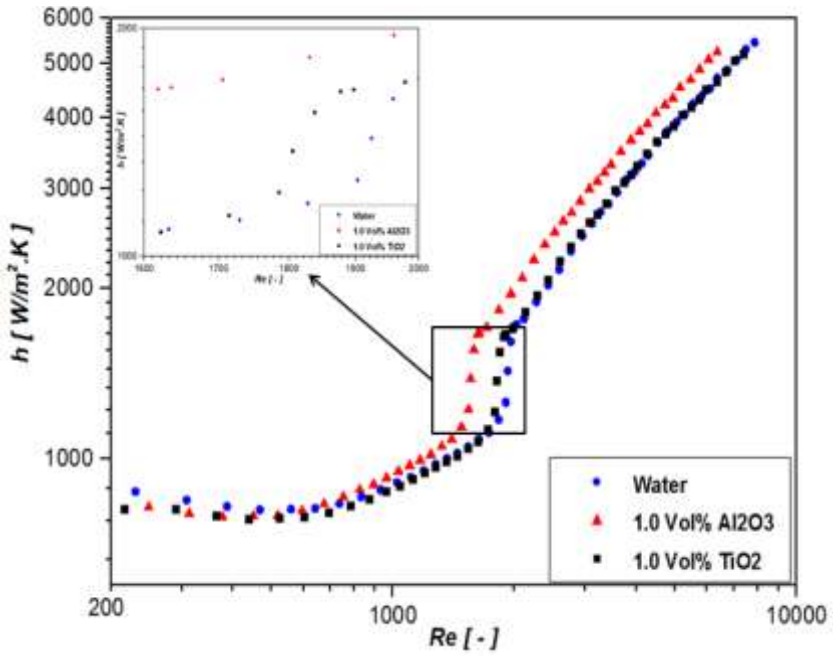

Figure 6.17: Comparison of (a) heat transfer coefficient and (b) Nusselt number for Al_2O_3- and TiO_2-water nanofluids at 1.0 vol%.

The average heat transfer coefficient for Al_2O_3- and TiO_2-water nanofluids at 1.0% compared with that of pure water over the Reynolds number range of 200 to 8 000 is displayed in Figure 6.17. TiO_2-water nanofluid showed an average improvement in the heat transfer coefficient in the turbulent and the transition flow regimes. The average enhancement was 1.1 and 21.9% respectively. The heat transfer coefficients of Al_2O_3-water nanofluids were 14.5% and 25% higher than those of TiO_2-water in the turbulent and the transition flow regimes respectively.

The Nusselt number of the two nanofluids at 1.0 vol% was compared with the base fluid over Reynold number span of 200 to 8 000 (see Figure 6.18). The enhancement by Al_2O_3-water nanofluids was 12.5% higher than water and 17.1% higher than TiO_2-water in the turbulent flow regime. In the transition, the enhancement was 50% and 28.1% higher than for water and TiO_2-water nanofluid respectively. In the laminar regime, no enhancement was observed for both nanofluids.

Magnified views are extracted from the transition regime and presented in Figure 6.13 to Figure 6.18. Two aspects were noticed when transitioning from laminar to turbulent in the rectangular channels by using TiO_2- and Al_2O_3-water nanofluids. The first aspect was that the nanofluid concentration influenced the onset of transition, and it was found to be taking place at a smaller Reynolds number with an increase in volume concentration. For TiO_2-water

nanofluids, the transition onset started at Reynolds number of 1 799 for the 0.3 vol% nanofluid, at Reynolds number of 1 778 for the 0.5 vol% nanofluid, and at Reynolds number of 1 714 when using 1.0 vol% nanofluid. The length of transition in terms of Reynolds number measure was 191, 189, 186 and 182 respectively, while for Al_2O_3-water nanofluid, the transition started at Reynolds number of 1 731, 1 723, and 1 705 respectively and the corresponding transition period lengths were 125, 110 and 125 respectively.

The transition flow regime for all the tested nanofluids started earlier than for pure water. The early transition was linked to the higher nanofluid viscosity, which shifted the position of transition from what it is in Figure 4.1 to a new transition situation, as presented in Figure 6.13 to Figure 18. The quicker transition agreed with the work of Meyer et al. [24]. The second feature that was observed concerning the transition behaviour of the current test nanofluids, was the significant enhancement of all the concentrations for both nanofluids.

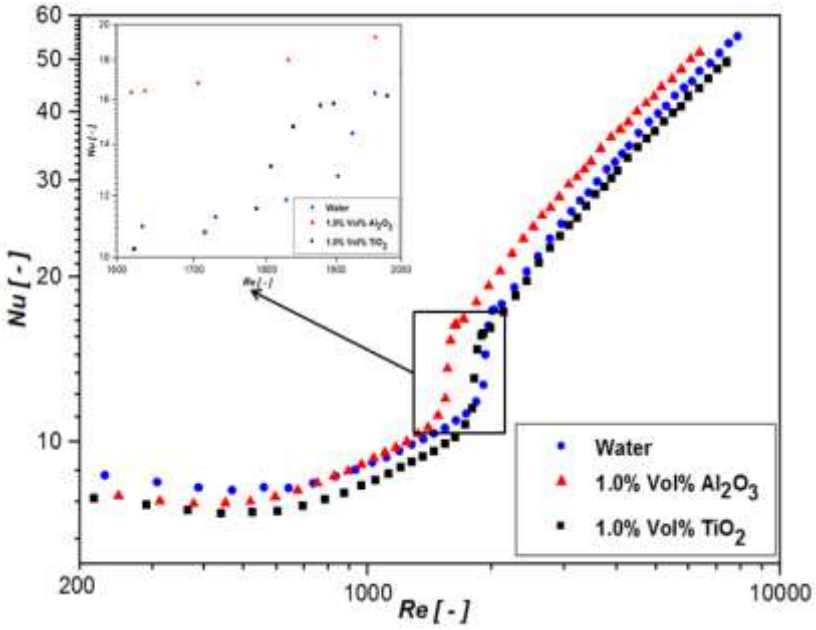

Figure 6.18: Comparison of (a) heat transfer coefficient and (b) Nusselt number for Al_2O_3- and TiO_2-water nanofluids at 1.0 vol%.

6.8.2 Pressure drop and friction coefficient results

The friction coefficients for various concentrations of water-based titanium and aluminium oxide nanofluids are displayed in Figure 6.19. The friction coefficients of both TiO_2-water and Al_2O_3-water nanofluids decreased with the rise in the volume concentration in the laminar regime, except for the weakest volume concentration nanofluid (0.3 vol%) because it was similar to the values of pure water. In the turbulent regime, the friction coefficient results

for the nanofluids and water became difficult to distinguish because of the effect of the nanoparticles on the flow physics at this regime.

The friction factor coefficients in the transition flow regime increased in volume, and they were 2.3, 6.5 and 15.2% for the 0.3, 0.5 and 1.0 vol% for TiO_2-water nanofluid, and 4, 10.5 and 25% for the 0.3, 0.5 and 1.0 vol% for Al_2O_3-water nanofluid. The onset and the length of transition happened at the same time as the heat transfer results, as shown in Section 6.8.1.

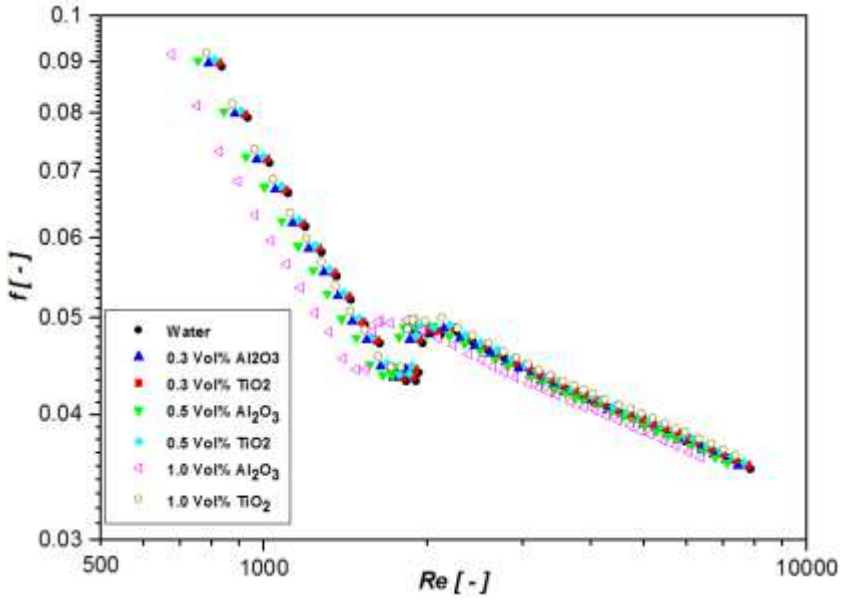

Figure 6.19: Variation of friction coefficients with Reynolds number for all nanofluids compared with water.

The pressure drop of water compared with that of Al_2O_3- and TiO_2-water nanofluids is presented in Figure 6.20 to cover the full flow range span. Results showed that the pressure drop for all nanofluids increased with an increase in the concentration and the Reynolds number. Al_2O_3-water nanofluids resulted in a higher pressure drop than for TiO_2-water nanofluids in the turbulent flow and the increase was 8.2%, 13.6% and 33.3% for the 0.3, 0.5 and 1.0 vol% nanofluid. The penalty in the pressure in the transition flow regime was slightly higher than in the turbulent regime since it was 3.4% for the 0.3 vol% nanofluid, 2.7% for the 0.5 vol% and 38.5% for the 1.0 vol% nanofluid. The increase in the pressure drop was due to the interaction of the particles with the wall of the test section and also the higher viscosity of the nanofluids than that of water.

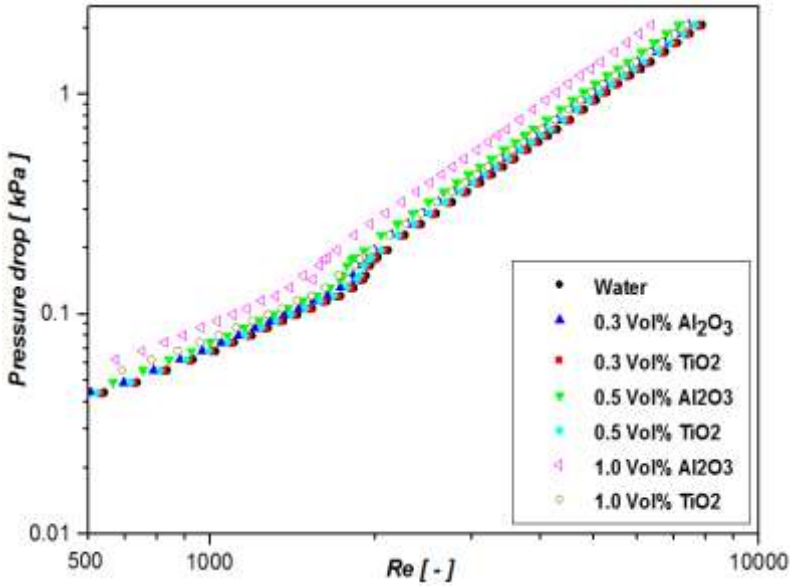

Figure 6.20: Variation of pressure drop with Reynolds number for all nanofluids compared with water.

6.8.3 Thermal performance evaluation of nanofluids

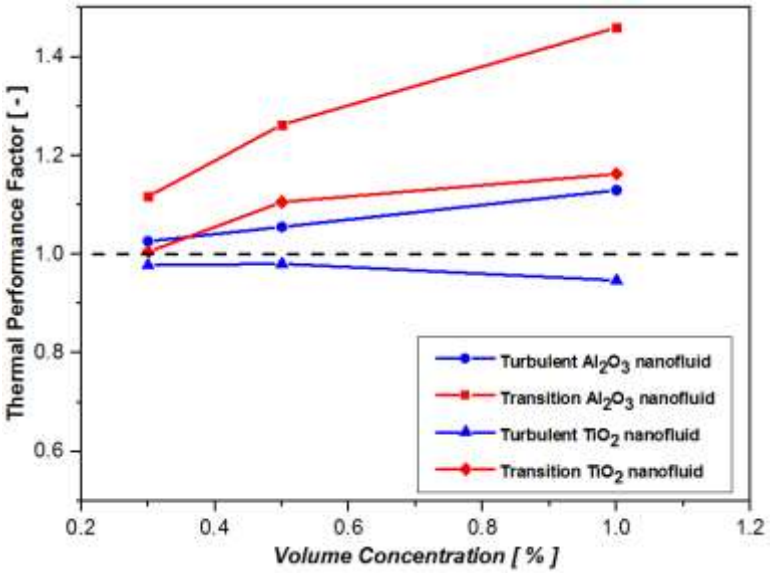

Figure 6.21: Thermal performance factor variation with volume concentration in the turbulent and the transition regimes for TiO_2- and Al_2O_3-water-based nanofluids.

The thermal performance factor, as outlined in Equation 6.2, was computed by calculating the average Nusselt number and friction factor for all the concentrations of the nanofluids over Reynolds number values covering the transition and turbulent regimes. The laminar flow measurements were not included because the heat transfer enhancement was negligible.

The thermal performance factor of the nanofluids in the transition regime was higher than the unity value for both nanofluids at all test concentrations, as indicated in Figure 6.21, and the maximum values were 1.47 and 1.14 at the 1.0 vol% for Al_2O_3-water and TiO_2-water nanofluids respectively. Therefore, in the transition regime, the nanofluids under investigation contributed to the heat transfer improvement more than the increase in the pumping power required due to the viscosity increase in the nanofluid. In the turbulent regime, the thermal performance factor indicated that all the concentrations of TiO_2-water nanofluids were not suitable to use due to the thermal performance factor of values lower than the unity. However, the thermal performance of Al_2O_3-water nanofluid in the turbulent regime was better and the maximum value was 1.1 at the volume concentration of 1%.

6.9 Heat transfer results of the porous media insert

6.9.1 Pressure drop across the test section with the nickel foam insert

Equation 6.3 represents the relation between the pressure gradient through the porous media and flow velocity. For the high fluid velocity, the inertial effect is dominant and the flow range is known as non-Darcy flow regime. The flow range in the test section under investigation falls under the non-Darcy flow regime:

$$\frac{dp}{dx} = \frac{\mu}{K}V + \frac{C_E}{\sqrt{K}}\rho V^2 \qquad (\mathbf{6.3})$$

where K is the permeability, which describes the conductivity of the porous media for the Newtonian permutation. The permeability value of a porous medium may vary with the geometrical characteristic. Therefore, it is necessary to calculate the nickel foam that is inserted into the rectangular test section. Equation 6.4 is a reformulation of Equation 6.3 for the purpose of the linearisation of the equation:

$$\frac{1}{\mu V}\left(\frac{dp}{dx}\right) = \frac{1}{K} + \frac{C_E}{\sqrt{K}}\frac{\rho V}{\mu} \qquad (\mathbf{6.4})$$

Figure 6.22 shows the linear relation between $\frac{1}{\mu V}\left(\frac{dp}{dx}\right)$ and $\frac{\rho V}{\mu}$. The values of the permeability (K) and Ergun coefficient (C_E) are extracted from the figure and are 0.000162 and 0.00078 respectively.

A common way to write Reynolds number is to define $\sqrt{K}$ as characteristic length, as follows:

$$Re = \frac{\rho V \sqrt{K}}{\mu} \qquad (6.5)$$

The friction coefficient is calculated by the measurements of the pressure drop using Equation 6.6:

$$f = \frac{\Delta P \, D_h}{\rho L V^2} \qquad (6.6)$$

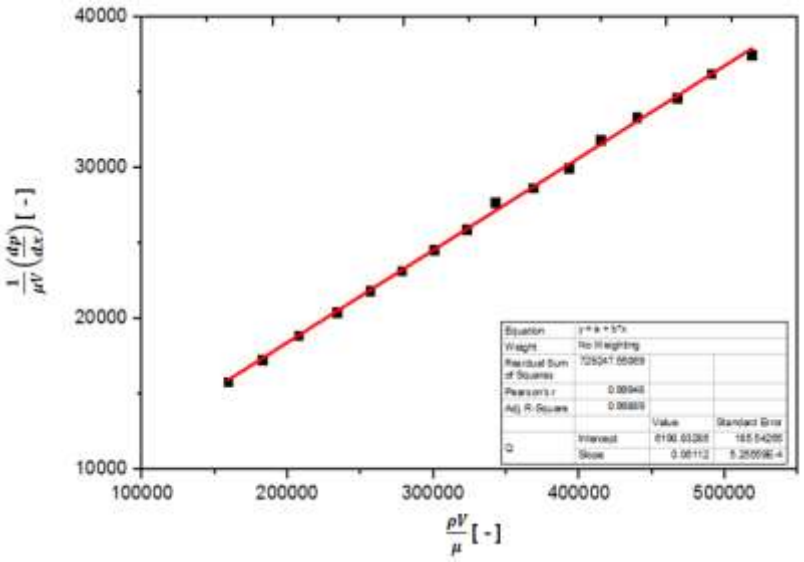

Figure 6.22: Linear relation of pressure gradient across the porous media with the velocity.

The friction coefficient variation with the Reynolds number for the test section with the nickel foam insert is shown in Figure 6.23. The permeability-based Reynolds number span ranged between 2 000 and 6 500. The range corresponded to the full flow range in the empty test section (laminar to turbulent including the transition regime). The friction coefficient of the foam-filled test section showed no change in the pattern of the measurements, which indicated no transition and the flow regime followed the non-Darcy flow regime. Moreover, the values of the friction coefficient were significantly higher than those for the empty test section value (24.5 times higher than the values of the empty test section), and this could be explained by the complicated structure of the nickel foam resulting in a flow fouling and therefore high pressure drop across the test section.

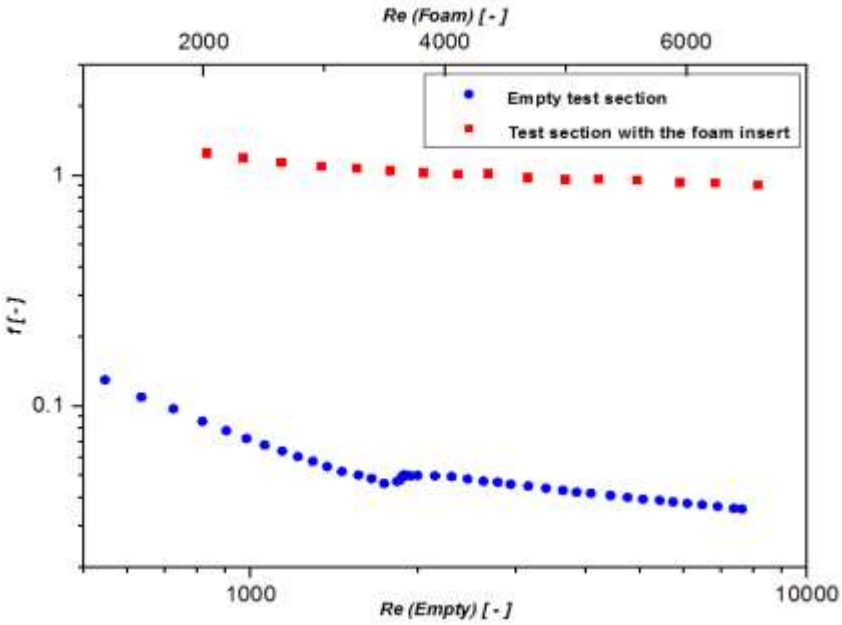

Figure 6.23: Friction coefficient variation with Reynolds number of the empty test section compared with the test section with nickel foam insert.

6.9.2 Heat transfer evaluation of the test section with the nickel foam insert

The variation of the local Nusselt number for two Reynolds numbers at seven various positions along the test section is presented in Figure 6.24. For both Reynolds numbers (higher and lower), the Nusselt number decreased until the value of x/d =30. This length was the entrance length, in which the flow was still thermally developing. These results indicated no effect of the foam in the thermal entrance length compared with the empty test section. The Nusselt number for the Re = 8 400 remained constant along the remaining length, while the Nusselt number at Reynolds number of 1 710 increased with the length of the tube, and it was 2.7 times higher than the value of Nusselt number at the position of x/d=30. Figure 6.25 shows the average Nusselt number variation with Reynolds number for the water flow across the nickel foam in the rectangular test section. The results were compared with the empty test section results. A drastic increase in Nusselt number was observed by using the nickel foam because the increase was three times on average compared with that of the empty test section. The Nusselt number for the foam-filled test section increased with a higher rate in lower Reynolds number, a 77% increase for the range of Reynolds number between 1 700 and 6 000 was observed, while the increase in Nusselt number for the higher Reynolds number range (6 000-10 000) was as little as 13%. This result could be justified by observing the behaviour of local heat transfer for the higher and low flow rate, as illustrated in Figure 6.24, because the increase in the Nusselt number was almost negligible at the higher Reynolds number compared with the lower Reynolds number. Another feature demonstrated in Figure

6.25 is the one pattern of Nusselt number variation with Reynolds number; because no transition was noticed in the tested flow range. The transition from the laminar to turbulent was observed for the flow in the empty test section at Reynolds number of 1 750 and ended at Reynolds number of 2 000. This showed the effect of the porous media on the transition because no transition occurred when inserting the nickel foam in the rectangular test section.

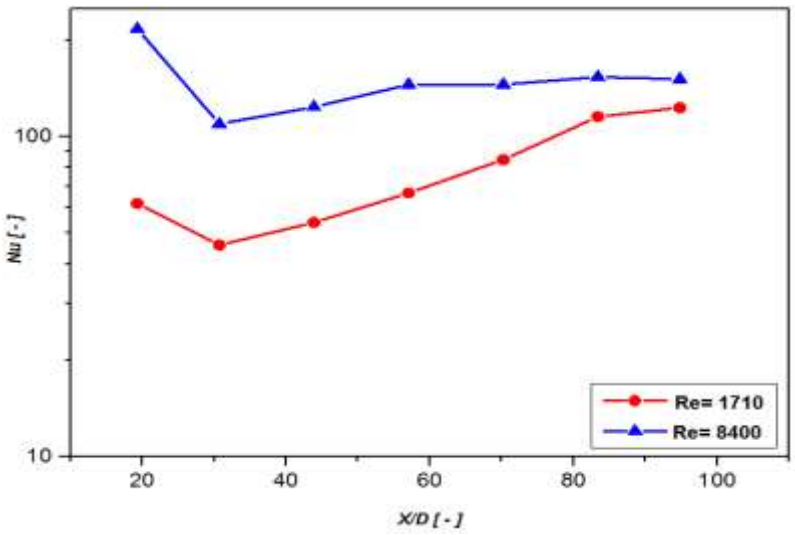

Figure 6.24: Local Nusselt number of two different flow rates through nickel foam in a rectangular test section.

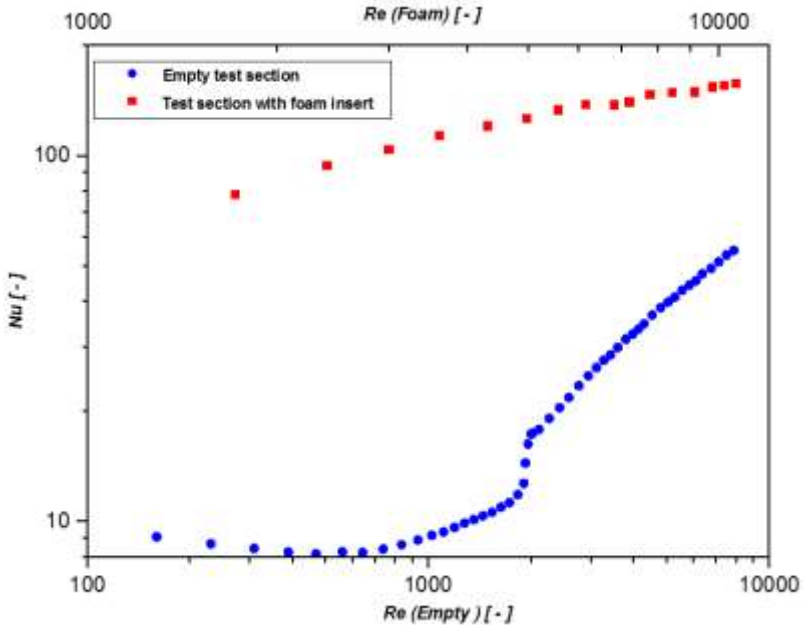

Figure 6.25: Nusselt number comparison of flow through an empty rectangular test section and nickel foam-inserted test section.

6.9.3 Heat transfer enhancement evaluation of the nickel foam test section

The thermal performance factor was used as heat transfer enhancement criteria, as stated in Equation 6.2, to compare between the obtained heat transfer enhancement and the penalty in the pressure drop. Figure 6.26 shows that the thermal performance factor was higher than the unity through the entire Reynolds number range of 2 000 to 6 500. The higher performance factor values proved the feasibility of using the nickel foam as a method of heat transfer enhancement although the high-pressure drop occurred when using the foam. The results also revealed that the operation of the foam-filled rectangular test section was better than at the lower flow rates because the thermal performance factor was observed to be 1.7.

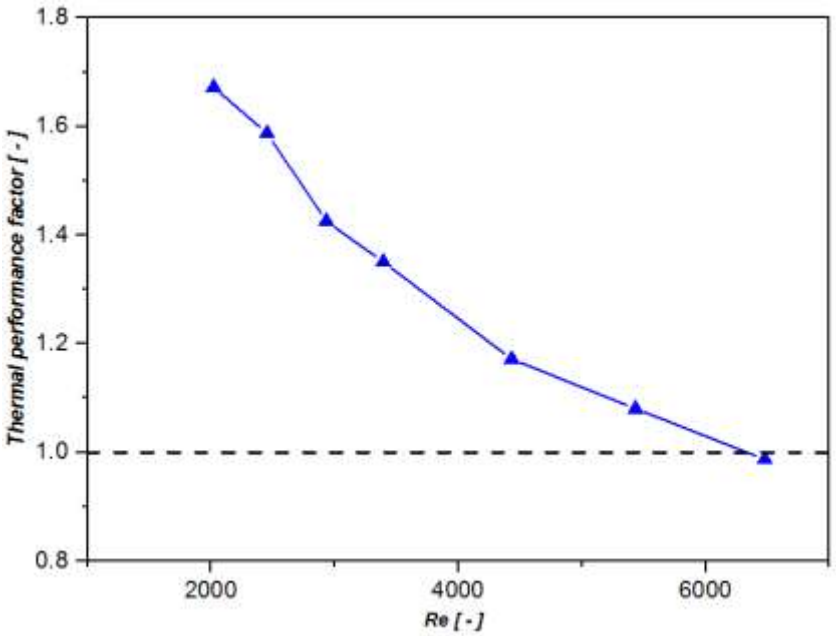

Figure 6.26: Thermal performance factor variation with Reynolds number for flow through nickel foam in a rectangular test section.

6.10 Conclusion

The pressure drop and the heat transfer for the water were measured and compared with three Al_2O_3-water nanofluids and four TiO_2-water nanofluids against the Reynolds number for the entire flow range. The increase in the pressure drop was significant in the transition flow regime for all the nanofluids. The maximum pressure drop for Al_2O_3-water nanofluids was

61% for the 1.0 vol%, while, for TiO_2-water nanofluids, the maximum increase in the pressure drop was 22.5% for the 1.0 vol%.

The enhancement of the heat transfer coefficients in the transition flow regime was higher than in the turbulent and laminar regimes for Al_2O_3- and TiO_2-water nanofluids. The maximum enhancement in the transition regime was 54% at the 1.0 vol%, while it was 29.3 % at 1.0 vol%. Both Al_2O_3- and TiO_2-water nanofluid results showed that the transition occurred earlier than with that of water. The foam-filled test section was constructed by ponding the foam strips to the channel, and the permeability was determined by linearising the no-Darcy flow pressure gradient equation. The pressure drop for the foam test section was 24.5 times higher than for the empty test section. However, the heat transfer in terms of Nusselt number showed an increase of three times of the empty test section value. The overall thermal performance factor showed the effectiveness of filling the test section with high-porosity nickel foam. No transition regime was noticed for the foam-filled test section on either the heat transfer results or the pressure drop results, while transition from laminar to turbulent was found for the empty test section.

CHAPTER 7

CONCLUSION AND RECOMMENDATIONS

7.1 Summary

Improvement in the heat transfer performance of heat exchangers can be achieved by two methods. The first approach is by using more effective heat transport fluids, which improve thermal properties such as nanofluids. The second approach is by increasing the heat transfer area of the heat exchanger itself, and this can be practically done by attaching fins or inserts to heat exchanger walls or by filling the heat exchanger tubes with porous media. In this study, both approaches were experimentally investigated with more focus on the nanofluids. The transition flow regime was specifically discussed because of a lack of research on nanofluids in this regime.

A rectangular test section of 450 mm was used with a hydrodynamic length of 600 mm attached to the test section. The test section was provided with two mixers at the inlet and the outlet, and seven thermocouples were attached to the outer surface of the test section to measure the average surface temperature. Two pressure taps were added to the two ends of the test section to measure the differential pressure across the test section. The test section was uniformly heated using an electrical power supply. Three concentrations of aluminium oxide-water nanofluids and four concentrations of titanium dioxide-water nanofluids were used.

The same test section was filled with a porous media insert of rectangular shape to assist in heat transfer enhancement. The porous media was high-porosity nickel foam. The heat transfer and pressure drop characteristics of water flowing through the nickel foam in the rectangular test section were investigated.

The results of the experiments of the nanofluids in the empty test section, and the water flowing in the porous media-filled test section are outlined in the following sections.

7.2 Conclusions

7.2.1 Conclusions on aluminium oxide-water nanofluids

Aluminium oxide-water nanofluids with volume concentrations of 0.3%, 0.5% and 1.0% were tested in a uniformly heated rectangular channel for the entire flow regime, and the following conclusions were made:

- The transition to turbulent flow in a rectangular channel started earlier than in conventional circular channels.
- The transition started earlier when using the nanofluids compared than when using water, as observed in both the heat transfer and pressure drop results.
- The enhancement of the heat transfer coefficient was 43% more in the transition regime than in the turbulent regime.
- The convective heat transfer efficiency was 1.3% at 1.0 vol% in the transition flow regime, whereas it was 0.55% at the same volume concentration in the turbulent flow regime. Therefore, the pressure drop in the turbulent flow regime was found to be greater than the heat transfer, whereas, in the transition regime, the heat transfer was found to be greater than the pressure drop.
- Enhancements of the heat transfer coefficients and Nusselt number were observed in the turbulent flow regime for all three nanofluids, with a maximum enhancement of 11% when using the 1.0 vol% nanofluid.
- No heat transfer enhancement occurred in the laminar regime for this nanofluid, and the friction factors for the nanofluids tested were significantly higher than for pure water.
- Pressure drop increased with the volume concentration.

7.2.2 Conclusions on titanium dioxide-water nanofluids

Titanium dioxide-aqueous nanofluids of 0.3, 0.5, 0.7 and 1.0 vol% were examined in a constantly heated rectangular channel for the full range of flow, and the following conclusions were made:

- The transition started earlier in the rectangular cross-section channels than in the conventional round channels.
- Using TiO_2-water nanofluids resulted in an earlier transition than for water.
- The heat transfer coefficient was significantly enhanced in the transition flow regime: a maximum average enhancement of 29.3% was achieved by using the 1.0 vol% nanofluid.
- A Nusselt number enhancement of 24.3% was obtained in the transition regime by using 0.7 vol% nanofluid.
- Heat transfer coefficient and Nusselt number results in the turbulent regime showed that all TiO_2-water nanofluids of volume concentrations of 0.7% and 1% enhanced the heat transfer.
- The thermal performance factor showed better performance of the nanofluids under investigation in the transition regime than in the turbulent and the laminar flow regimes.
- Improvement in heat transfer was negligible in the laminar regime for TiO_2-water nanofluid.
- The pressure drop and friction coefficient increased with an increase in the volume concentration and Reynolds number.
- The investigated nanofluids in the transition regime were more thermally efficient than in the laminar and turbulent regimes.

7.2.3 Conclusions on comparison of aluminum with titanium dioxide-water nanofluids

Titanium dioxide-aqueous nanofluids of 0.3, 0.5 and 1.0 vol% were examined and compared with the water-based aluminium oxide nanofluids at the same concentrations in a continuously heated rectangular channel for the full range of flow. The following conclusions were made:

i. Using TiO_2-water nanofluids resulted in an earlier transition than when using water and later transition than when using Al_2O_3-water nanofluid.
ii. Nusselt number and heat transfer coefficients were significantly enhanced in the transitional flow regime; maximum average enhancements of 21.9% and 29.3% were

respectively achieved at 1.0 vol% of TiO_2-water nanofluid. Maximum enhancements of 50% and 54.2% were respectively achieved at 1.0 vol% of Al_2O_3-water nanofluid.

iii. No enhancement was observed in Nusselt number in the turbulent regime for TiO_2-water nanofluids. However, a maximum enhancement of 12.5% was achieved for Al_2O_3-water nanofluid of 1.0 vol %, and the maximum enhancement in the heat transfer coefficients for TiO_2-water in the turbulent regime was 1.1% at 1.0 vol %, while it was 15.6% for Al_2O_3-water nanofluid at the same volume concentration.

iv. Improvement in heat transfer was negligible in the laminar regime for TiO_2-water and Al_2O_3-water nanofluids.

v. Thermal performance factor results showed that all the investigated nanofluids in the transition regime were thermally more efficient than in the laminar and turbulent regimes.

7.2.4 Conclusions on nickel foam-filled test section

The nickel foam-filled rectangular test section was subjected to uniform heat flux and the test was carried out in the range of the perambilty-based Reynolds number of 1 700 to 1 000, and the following conclusions were made from the results:

vi. A higher pressure drop when using the nickel foam was observed than when using the empty test section.

vii. The local heat transfer results for the nickel foam test section showed that the thermal entry length did not depend on the flow rate.

viii. The heat transfer increment was constant towards the exit of the test section at the higher flow rates, while it increased rapidly at the lower flow rates.

ix. Nusselt numbers for the foam-filled test were higher than for the empty test section indicating a heat transfer improvement when using nickel foam.

x. No transition regime was noticed for the foam-filled test section on either the heat transfer results or the pressure drop results, while transition from laminar to turbulent was found for the empty test section.

7.3 Recommendations

- Modification of the experimental system is necessary to investigate the transition flow regime for nanofluid volume concentrations of more than 1.0%.

- Conducting the experiment with nanofluids with other base fluids than water to generalise the obtained results and to obtain accurate correlations for the heat transfer enhancement in the transition flow regime is recommended.
- Experimenting with a long test section to investigate the transition flow regime when the flow is thermally fully developed and comparing this with the current results is recommended.
- Development of correlations in the transition flow regime by conducting experiments with different nanofluids with a wider concentration range.
- Investigating with hybrid nanofluids to explore the effect of mixing two different nanoparticles into the base fluid
- Inducing a magnetic field to influence the stability and heat transfer performance of the nanofluids.
- A comprehensive test conducted with a foam-filled test section by using different foam materials and different foam structures to conclude the effect of the foam in the heat transfer performance and the transition regime is recommended.
- An experimental comparison between the nanofluids and the porous media at the same equivalent concentration to determine the effectiveness of both of them in the heat transfer characteristics is recommended.

7.4 Challenges

- A blockage in the pressure taps was noticed when increasing the volume concentration of the nanofluids more than 1%.
- There was a restriction on using a base fluid other than the pure water because base fluids such as Ethylene and Propylene Glycol increase the viscosity. Therefore the pump cannot handle the nanofluids to reach the transition and the turbulent flow regimes.
- Inserting the Nickel foam in the test section was challenged by the fact that the structure of the foam could be slightly changed when using the mechanical ponding technique, and when using the soldering to close the channel, special care needs to be taken to avoid spelling the solder inside the channel and causing flow blockage.

REFERENCES

[1] S. U. S. Choi, "Enhancing thermal conductivity of fluids with nanoparticles," in *American Society of Mechanical Engineers, Fluids Engineering Division (Publication) FED*, 1995, vol. 231, pp. 99-105.

[2] S. A. Adio, M. Mehrabi, M. Sharifpur, and J. P. Meyer, "Experimental investigation and model development for effective viscosity of MgO–ethylene glycol nanofluids by using dimensional analysis, FCM-ANFIS and GA-PNN techniques," *International Communications in Heat and Mass Transfer*, vol. 72, no. Supplement C, pp. 71-83, 2016/03/01/ 2016.

[3] M. Sharifpur, S. A. Adio, and J. P. Meyer, "Experimental investigation and model development for effective viscosity of Al2O3–glycerol nanofluids by using dimensional analysis and GMDH-NN methods," *International Communications in Heat and Mass Transfer*, vol. 68, no. Supplement C, pp. 208-219, 2015/11/01/ 2015.

[4] M. Amiri, S. Movahedirad, and F. Manteghi, "Thermal conductivity of water and ethylene glycol nanofluids containing new modified surface SiO2-Cu nanoparticles: Experimental and modeling," *Applied Thermal Engineering*, vol. 108, no. Supplement C, pp. 48-53, 2016/09/05/ 2016.

[5] P. Garg, J. L. Alvarado, C. Marsh, T. A. Carlson, D. A. Kessler, and K. Annamalai, "An experimental study on the effect of ultrasonication on viscosity and heat transfer performance of multi-wall carbon nanotube-based aqueous nanofluids," *International Journal of Heat and Mass Transfer*, vol. 52, no. 21-22, pp. 5090-5101, 2009.

[6] O. A. Alawi, N. A. C. Sidik, H. W. Xian, T. H. Kean, and S. N. Kazi, "Thermal conductivity and viscosity models of metallic oxides nanofluids," *International Journal of Heat and Mass Transfer*, vol. 116, pp. 1314-1325, 2018/01/01/ 2018.

[7] Y. Ueki, T. Aoki, K. Ueda, and M. Shibahara, "Thermophysical properties of carbon-based material nanofluid," *International Journal of Heat and Mass Transfer*, vol. 113, pp. 1130-1134, 2017/10/01/ 2017.

[8] Q. Li and Y. Xuan, "Convective heat transfer and flow characteristics of Cu-water nanofluid," *Science in China, Series E: Technological Sciences*, vol. 45, no. 4, pp. 408-416, 2002.

[9] Y. Yang, Z. G. Zhang, E. A. Grulke, W. B. Anderson, and G. Wu, "Heat transfer properties of nanoparticle-in-fluid dispersions (nanofluids) in laminar flow," *International Journal of Heat and Mass Transfer*, vol. 48, no. 6, pp. 1107-1116, 2005.

[10] Y. Ding, H. Alias, D. Wen, and R. A. Williams, "Heat transfer of aqueous suspensions of carbon nanotubes (CNT nanofluids)," *International Journal of Heat and Mass Transfer*, vol. 49, no. 1-2, pp. 240-250, 2006.

[11] S. M. S. Murshed, K. C. Leong, C. Yang, and N. T. Nguyen, "Convective heat transfer characteristics of aqueous TiO2 nanofluid under laminar flow conditions," *International Journal of Nanoscience*, vol. 7, no. 6, pp. 325-331, 2008.

[12] A. A. Hussien, M. Z. Abdullah, N. M. Yusop, M. d. A. Al-Nimr, M. A. Atieh, and M. Mehrali, "Experiment on forced convective heat transfer enhancement using MWCNTs/GNPs hybrid nanofluid and mini-tube," *International Journal of Heat and Mass Transfer*, vol. 115, pp. 1121-1131, 2017/12/01/ 2017.

[13] M. Ahmadi and G. Willing, "Heat transfer measurment in water based nanofluids," *International Journal of Heat and Mass Transfer*, vol. 118, pp. 40-47, 2018/03/01/ 2018.

[14] J. Zhang, Y. Diao, Y. Zhao, and Y. Zhang, "Experimental study of TiO2–water nanofluid flow and heat transfer characteristics in a multiport minichannel flat tube," *International Journal of Heat and Mass Transfer*, vol. 79, pp. 628-638, 2014/12/01/ 2014.

[15] H. Ghodsinezhad, M. Sharifpur, and J. P. Meyer, "Experimental investigation on cavity flow natural convection of Al2O3–water nanofluids," *International Communications in Heat and Mass Transfer*, vol. 76, no. Supplement C, pp. 316-324, 2016/08/01/ 2016.

[16] A. Brusly Solomon, J. van Rooyen, M. Rencken, M. Sharifpur, and J. P. Meyer, "Experimental study on the influence of the aspect ratio of square cavity on natural

convection heat transfer with Al2O3/water nanofluids," *International Communications in Heat and Mass Transfer,* vol. 88, no. Supplement C, pp. 254-261, 2017/11/01/ 2017.
[17] I. V. Miroshnichenko, M. A. Sheremet, H. F. Oztop, and N. Abu-Hamdeh, "Natural convection of alumina-water nanofluid in an open cavity having multiple porous layers," *International Journal of Heat and Mass Transfer,* vol. 125, pp. 648-657, 2018/10/01/ 2018.
[18] B. C. Pak and Y. I. Cho, "Hydrodynamic and heat transfer study of dispersed fluids with submicron metallic oxide particles," *Experimental Heat Transfer,* vol. 11, no. 2, pp. 151-170, 1998.
[19] D. Wen and Y. Ding, "Experimental investigation into convective heat transfer of nanofluids at the entrance region under laminar flow conditions," *International Journal of Heat and Mass Transfer,* vol. 47, no. 24, pp. 5181-5188, 2004.
[20] K. B. Anoop, T. Sundararajan, and S. K. Das, "Effect of particle size on the convective heat transfer in nanofluid in the developing region," *International Journal of Heat and Mass Transfer,* vol. 52, no. 9-10, pp. 2189-2195, 2009.
[21] K. S. Hwang, S. P. Jang, and S. U. S. Choi, "Flow and convective heat transfer characteristics of water-based Al2O3 nanofluids in fully developed laminar flow regime," *International Journal of Heat and Mass Transfer,* vol. 52, no. 1, pp. 193-199, 2009/01/15/ 2009.
[22] B. Sahin, G. G. Gültekin, E. Manay, and S. Karagoz, "Experimental investigation of heat transfer and pressure drop characteristics of Al2O3–water nanofluid," *Experimental Thermal and Fluid Science,* vol. 50, no. Supplement C, pp. 21-28, 2013/10/01/ 2013.
[23] Liu Donga and Y. Leyuan, "Single-phase thermal transport of nanofluids in a minichannel " *Journal of Heat Transfer,* vol. 133, no. 3, 2011.
[24] J. P. Meyer, T. J. McKrell, and K. Grote, "The influence of multi-walled carbon nanotubes on single-phase heat transfer and pressure drop characteristics in the transitional flow regime of smooth tubes," *International Journal of Heat and Mass Transfer,* vol. 58, no. 1-2, pp. 597-609, 2013.
[25] M. H. Kayhani, H. Soltanzadeh, M. M. Heyhat, M. Nazari, and F. Kowsary, "Experimental study of convective heat transfer and pressure drop of TiO2/water nanofluid," *International Communications in Heat and Mass Transfer,* vol. 39, no. 3, pp. 456-462, 2012/03/01/ 2012.
[26] Y. He, Y. Jin, H. Chen, Y. Ding, D. Cang, and H. Lu, "Heat transfer and flow behaviour of aqueous suspensions of TiO2 nanoparticles (nanofluids) flowing upward through a vertical pipe," *International Journal of Heat and Mass Transfer,* vol. 50, no. 11-12, pp. 2272-2281, 2007.
[27] W. H. Azmi, K. V. Sharma, P. K. Sarma, R. Mamat, and S. Anuar, "Comparison of convective heat transfer coefficient and friction factor of TiO2 nanofluid flow in a tube with twisted tape inserts," *International Journal of Thermal Sciences,* vol. 81, pp. 84-93, 2014/07/01/ 2014.
[28] A. R. Sajadi and M. H. Kazemi, "Investigation of turbulent convective heat transfer and pressure drop of TiO2/water nanofluid in circular tube," *International Communications in Heat and Mass Transfer,* vol. 38, no. 10, pp. 1474-1478, 2011/12/01/ 2011.
[29] W. Duangthongsuk and S. Wongwises, "Heat transfer enhancement and pressure drop characteristics of TiO2–water nanofluid in a double-tube counter flow heat exchanger," *International Journal of Heat and Mass Transfer,* vol. 52, no. 7, pp. 2059-2067, 2009/03/01/ 2009.
[30] W. Duangthongsuk and S. Wongwises, "An experimental study on the heat transfer performance and pressure drop of TiO2-water nanofluids flowing under a turbulent flow regime," *International Journal of Heat and Mass Transfer,* vol. 53, no. 1-3, pp. 334-344, 2010.
[31] A. A. Abbasian Arani and J. Amani, "Experimental investigation of diameter effect on heat transfer performance and pressure drop of TiO2–water nanofluid," *Experimental Thermal and Fluid Science,* vol. 44, pp. 520-533, 2013/01/01/ 2013.
[32] A. A. Abbasian Arani and J. Amani, "Experimental study on the effect of TiO2–water nanofluid on heat transfer and pressure drop," *Experimental Thermal and Fluid Science,* vol. 42, pp. 107-115, 2012/10/01/ 2012.

[33] K. A. Hamid, W. H. Azmi, R. Mamat, and K. V. Sharma, "Experimental investigation on heat transfer performance of TiO2 nanofluids in water-ethylene glycol mixture," *International Communications in Heat and Mass Transfer*, vol. 73, pp. 16-24, 2016/04/01/ 2016.
[34] D. Seguin, A. Montillet, J. Comiti, and F. Huet, "Experimental characterization of flow regimes in various porous media—II: Transition to turbulent regime," *Chemical Engineering Science*, vol. 53, no. 22, pp. 3897-3909, 1998/11/01/ 1998.
[35] D. Seguin, A. Montillet, and J. Comiti, "Experimental characterisation of flow regimes in various porous media—I: Limit of laminar flow regime," *Chemical Engineering Science*, vol. 53, no. 21, pp. 3751-3761, 1998/11/01/ 1998.
[36] S. Rode, N. Midoux, M. A. Latifi, A. Storck, and E. Saatdjian, "Hydrodynamics of liquid flow in packed beds: an experimental study using electrochemical shear rate sensors," *Chemical Engineering Science*, vol. 49, no. 6, pp. 889-900, 1994/01/01/ 1994.
[37] I. Kececioglu and Y. Jiang, "Flow through porous media of packed spheres saturated with water," *Journal of Fluids Engineering*, vol. 116, no. 1, pp. 164-170, 1994.
[38] R. M. Fand, B. Y. K. Kim, A. C. C. Lam, and R. T. Phan, "Resistance to the flow of fluids through simple and complex porous media whose matrices are composed of randomly packed spheres," *Journal of Fluids Engineering*, vol. 109, no. 3, pp. 268-273, 1987.
[39] A. Dybbs and R. V. Edwards, "A New Look at Porous Media Fluid Mechanics — Darcy to Turbulent," in *Fundamentals of Transport Phenomena in Porous Media*, J. Bear and M. Y. Corapcioglu, Eds. Dordrecht: Springer Netherlands, 1984, pp. 199-256.
[40] D. A. Nield and A. Bejan, *Convection in Porous Media*, 4th ed. Springer, 2013.
[41] J. Bear, *Dynamics of Fluids in Porous Media*. American Elsevier Company, 1972.
[42] C. T'Joen, P. De Jaeger, H. Huisseune, S. Van Herzeele, N. Vorst, and M. De Paepe, "Thermo-hydraulic study of a single row heat exchanger consisting of metal foam covered round tubes," *International Journal of Heat and Mass Transfer*, vol. 53, no. 15, pp. 3262-3274, 2010/07/01/ 2010.
[43] G. S. Beavers and E. M. Sparrow, "Non-Darcy flow through fibrous porous media," *Journal of Applied Mechanics*, vol. 36, no. 4, pp. 711-714, 1969.
[44] J. W. Paek, B. H. Kang, S. Y. Kim, and J. M. Hyun, "Effective thermal conductivity and permeability of aluminum foam materials," *International Journal of Thermophysics*, journal article vol. 21, no. 2, pp. 453-464, March 01 2000.
[45] S. Miwa and S. T. Revankar, "Hydrodynamic characterization of nickel metal foam, Part 1: Single-phase permeability," *Transport in Porous Media*, vol. 80, no. 2, p. 269, 2009/03/03 2009.
[46] V. V. Calmidi and R. L. Mahajan, "Forced convection in high porosity metal foams," *Journal of Heat Transfer*, vol. 122, no. 3, pp. 557-565, 2000.
[47] S. Y. Kim, B. H. Kang, and J.-H. Kim, "Forced convection from aluminum foam materials in an asymmetrically heated channel," *International Journal of Heat and Mass Transfer*, vol. 44, no. 7, pp. 1451-1454, 2001/04/01/ 2001.
[48] M. Nazari, M. Ashouri, M. H. Kayhani, and A. Tamayol, "Experimental study of convective heat transfer of a nanofluid through a pipe filled with metal foam," *International Journal of Thermal Sciences*, vol. 88, pp. 33-39, 2015/02/01/ 2015.
[49] J.-S. Noh, K. B. Lee, and C. G. Lee, "Pressure loss and forced convective heat transfer in an annulus filled with aluminum foam," *International Communications in Heat and Mass Transfer*, vol. 33, no. 4, pp. 434-444, 2006/04/01/ 2006.
[50] H. Wang and L. Guo, "Experimental investigation on pressure drop and heat transfer in metal foam filled tubes under convective boundary condition," *Chemical Engineering Science*, vol. 155, pp. 438-448, 2016/11/22/ 2016.
[51] S. Mancin, C. Zilio, L. Rossetto, and A. Cavallini, "Foam height effects on heat transfer performance of 20 ppi aluminum foams," *Applied Thermal Engineering*, vol. 49, pp. 55-60, 2012/12/31/ 2012.
[52] A. Hamadouche, R. Nebbali, H. Benahmed, A. Kouidri, and A. Bousri, "Experimental investigation of convective heat transfer in an open-cell aluminum foam," *Experimental Thermal and Fluid Science*, vol. 71, pp. 86-94, 2016/02/01/ 2016.

[53] N. Dukhan and P. Patel, "Equivalent particle diameter and length scale for pressure drop in porous metals," *Experimental Thermal and Fluid Science,* vol. 32, no. 5, pp. 1059-1067, 2008/04/01/ 2008.
[54] M. Chandrasekar, S. Suresh, and A. Chandra Bose, "Experimental investigations and theoretical determination of thermal conductivity and viscosity of Al2O3/water nanofluid," *Experimental Thermal and Fluid Science,* vol. 34, no. 2, pp. 210-216, 2010.
[55] L. Syam Sundar and M. K. Singh, "Convective heat transfer and friction factor correlations of nanofluid in a tube and with inserts: A review," *Renewable and Sustainable Energy Reviews,* vol. 20, pp. 23-35, 2013.
[56] V. Trisaksri and S. Wongwises, "Critical review of heat transfer characteristics of nanofluids," *Renewable and Sustainable Energy Reviews,* vol. 11, no. 3, pp. 512-523, 2007.
[57] H. Chang, C. S. Jwo, P. S. Fan, and S. H. Pai, "Process optimization and material properties for nanofluid manufacturing," *International Journal of Advanced Manufacturing Technology,* vol. 34, no. 3-4, pp. 300-306, 2007.
[58] E. J. Swanson, J. Tavares, and S. Coulombe, "Improved dual-plasma process for the synthesis of coated or functionalized metal nanoparticles," *IEEE Transactions on Plasma Science,* vol. 36, no. 4 PART 1, pp. 886-887, 2008.
[59] X. Q. Wang and A. S. Mujumdar, "Heat transfer characteristics of nanofluids: a review," *International Journal of Thermal Sciences,* vol. 46, no. 1, pp. 1-19, 2007.
[60] Y. Hwang *et al.*, "Stability and thermal conductivity characteristics of nanofluids," *Thermochimica Acta,* vol. 455, no. 1, pp. 70-74, 2007/04/01/ 2007.
[61] J. Huang, X. Wang, Q. Long, X. Wen, Y. Zhou, and L. Li, "Influence of pH on the Stability Characteristics of Nanofluids," in *2009 Symposium on Photonics and Optoelectronics*, 2009, pp. 1-4.
[62] L. Jiang, L. Gao, and J. Sun, "Production of aqueous colloidal dispersions of carbon nanotubes," *Journal of Colloid and Interface Science,* vol. 260, no. 1, pp. 89-94, 2003/04/01/ 2003.
[63] I. Madani, C.-Y. Hwang, S.-D. Park, Y.-H. Choa, and H.-T. Kim, "Mixed surfactant system for stable suspension of multiwalled carbon nanotubes," *Colloids surface A: Physicochemical and Engineering Aspects,* vol. 358, no. 1-3, pp. 101-107, 2010.
[64] M. J. Assael, I. N. Metaxa, J. Arvanitidis, D. Christofilos, and C. Lioutas, "Thermal conductivity enhancement in aqueous suspensions of carbon multi-walled and double-walled nanotubes in the presence of two different dispersants," *International Journal of Thermophysics,* vol. 26, no. 3, pp. 647-664, 2005/05/01 2005.
[65] M. N. Pantzali, A. A. Mouza, and S. V. Paras, "Investigating the efficacy of nanofluids as coolants in plate heat exchangers (PHE)," *Chemical Engineering Science,* vol. 64, no. 14, pp. 3290-3300, 2009/07/15/ 2009.
[66] H. Xie, H. Lee, W. Youn, and M. Choi, "Nanofluids containing multiwalled carbon nanotubes and their enhanced thermal conductivities," *Journal of Applied Physics,* vol. 94, no. 8, pp. 4967-4971, 2003.
[67] Y. Hwang *et al.*, "Production and dispersion stability of nanoparticles in nanofluids," *Powder Technology,* vol. 186, no. 2, pp. 145-153, 2008/08/11/ 2008.
[68] S. M. S. Murshed, K. C. Leong, and C. Yang, "Thermophysical and electrokinetic properties of nanofluids: A critical review," *Applied Thermal Engineering,* vol. 28, no. 17-18, pp. 2109-2125, 2008.
[69] G. Paul, M. Chopkar, I. Manna, and P. K. Das, "Techniques for measuring the thermal conductivity of nanofluids: A review," *Renewable and Sustainable Energy Reviews,* vol. 14, no. 7, pp. 1913-1924, 2010.
[70] S. K. Das, S. U. S. Choi, and H. E. Patel, "Heat transfer in nanofluids: A review," *Heat Transfer Engineering,* vol. 27, no. 10, pp. 3-19, 2006.
[71] A. Amrollahi, A. A. Hamidi, and A. M. Rashidi, "The effects of temperature, volume fraction and vibration time on the thermo-physical properties of a carbon nanotube suspension (carbon nanofluid)," *Nanotechnology,* vol. 19, no. 31, 2008, Art. no. 315701.

[72] L. Li, Y. Zhang, H. Ma, and M. Yang, "An investigation of molecular layering at the liquid-solid interface in nanofluids by molecular dynamics simulation," *Physics Letters, Section A: General, Atomic and Solid State Physics,* vol. 372, no. 25, pp. 4541-4544, 2008.
[73] Y. Ren, H. Xie, and A. Cai, "Effective thermal conductivity of nanofluids containing spherical nanoparticles," *Journal of Physics D: Applied Physics,* vol. 38, no. 21, pp. 3958-3961, 2005.
[74] P. Tillman and J. M. Hill, "Determination of nanolayer thickness for a nanofluid," *International Communications in Heat and Mass Transfer,* vol. 34, no. 4, pp. 399-407, 2007.
[75] Q. Xue and W. M. Xu, "A model of thermal conductivity of nanofluids with interfacial shells," *Materials Chemistry and Physics,* vol. 90, no. 2-3, pp. 298-301, 2005.
[76] F. Achard, "Chapter 44 - James Clerk Maxwell, A treatise on electricity and magnetism,," in *Landmark Writings in Western Mathematics 1640-1940,* I. G.-G. C. C. C. Guicciardini, Ed.

ed. Amsterdam: Elsevier Science, 2005, pp. 564-587.
[77] A. D. Sommers and K. L. Yerkes, "Experimental investigation into the convective heat transfer and system-level effects of Al2O3-propanol nanofluid," *Journal of Nanoparticle Research,* vol. 12, no. 3, pp. 1003-1014, 2010.
[78] D. Wen, G. Lin, S. Vafaei, and K. Zhang, "Review of nanofluids for heat transfer applications," *Particuology,* vol. 7, no. 2, pp. 141-150, 2009.
[79] W. Evans, R. Prasher, J. Fish, P. Meakin, P. Phelan, and P. Keblinski, "Effect of aggregation and interfacial thermal resistance on thermal conductivity of nanocomposites and colloidal nanofluids," *International Journal of Heat and Mass Transfer,* vol. 51, no. 5-6, pp. 1431-1438, 2008.
[80] P. E. Gharagozloo, J. K. Eaton, and K. E. Goodson, "Diffusion, aggregation, and the thermal conductivity of nanofluids," *Applied Physics Letters,* vol. 93, no. 10, 2008, Art. no. 103110.
[81] P. E. Gharagozloo and K. E. Goodson, "Aggregate fractal dimensions and thermal conduction in nanofluids," *Journal of Applied Physics,* vol. 108, no. 7, 2010, Art. no. 074309.
[82] K. S. Hong, T. K. Hong, and H. S. Yang, "Thermal conductivity of Fe nanofluids depending on the cluster size of nanoparticles," *Applied Physics Letters,* vol. 88, no. 3, pp. 1-3, 2006, Art. no. 031901.
[83] S. Özerinç, S. Kakaç, and A. G. YazIcIoğlu, "Enhanced thermal conductivity of nanofluids: A state-of-the-art review," *Microfluidics and Nanofluidics,* vol. 8, no. 2, pp. 145-170, 2010.
[84] L. Gao, X. Zhou, and Y. Ding, "Effective thermal and electrical conductivity of carbon nanotube composites," *Chemical Physics Letters,* vol. 434, no. 4-6, pp. 297-300, 2007.
[85] L. Gao and X. F. Zhou, "Differential effective medium theory for thermal conductivity in nanofluids," *Physics Letters, Section A: General, Atomic and Solid State Physics,* vol. 348, no. 3-6, pp. 355-360, 2006.
[86] X. F. Zhou and L. Gao, "Effective thermal conductivity in nanofluids of nonspherical particles with interfacial thermal resistance: Differential effective medium theory," *Journal of Applied Physics,* vol. 100, no. 2, 2006, Art. no. 024913.
[87] J. Koo and C. Kleinstreuer, "Laminar nanofluid flow in microheat-sinks," *International Journal of Heat and Mass Transfer,* vol. 48, no. 13, pp. 2652-2661, 2005.
[88] H. Zhu, C. Zhang, S. Liu, Y. Tang, and Y. Yin, "Effects of nanoparticle clustering and alignment on thermal conductivities of Fe3O4 aqueous nanofluids," *Applied Physics Letters,* vol. 89, no. 2, 2006, Art. no. 023123.
[89] N. R. Karthikeyan, J. Philip, and B. Raj, "Effect of clustering on the thermal conductivity of nanofluids," *Materials Chemistry and Physics,* vol. 109, no. 1, pp. 50-55, 2008.
[90] P. Vadasz, "Heat conduction in nanofluid suspensions," *Journal of Heat Transfer,* vol. 128, no. 5, pp. 465-477, 2006.
[91] H. A. Mintsa, G. Roy, C. T. Nguyen, and D. Doucet, "New temperature dependent thermal conductivity data for water-based nanofluids," *International Journal of Thermal Sciences,* vol. 48, no. 2, pp. 363-371, 2009/02/01/ 2009.
[92] N. A. Roberts and D. G. Walker, "Convective performance of nanofluids in commercial electronics cooling systems," *Applied Thermal Engineering,* vol. 30, no. 16, pp. 2499-2504, 2010.

[93] S. M. S. Murshed, K. C. Leong, and C. Yang, "Enhanced thermal conductivity of TiO2 - Water based nanofluids," *International Journal of Thermal Sciences,* vol. 44, no. 4, pp. 367-373, 2005.

[94] W. Yu, H. Xie, L. Chen, and Y. Li, "Enhancement of thermal conductivity of kerosene-based Fe3O4 nanofluids prepared via phase-transfer method," *Colloids and Surfaces A: Physicochemical and Engineering Aspects,* vol. 355, no. 1-3, pp. 109-113, 2010.

[95] D. Lee, J. W. Kim, and B. G. Kim, "A new parameter to control heat transport in nanofluids: Surface charge state of the particle in suspension," *Journal of Physical Chemistry B,* vol. 110, no. 9, pp. 4323-4328, 2006.

[96] B. Yang and Z. H. Han, "Temperature-dependent thermal conductivity of nanorod-based nanofluids," *Applied Physics Letters,* vol. 89, no. 8, 2006, Art. no. 083111.

[97] D. W. Oh, A. Jain, J. K. Eaton, K. E. Goodson, and J. S. Lee, "Thermal conductivity measurement and sedimentation detection of aluminum oxide nanofluids by using the 3ω method," *International Journal of Heat and Fluid Flow,* vol. 29, no. 5, pp. 1456-1461, 2008.

[98] S. Lee, S. U. S. Choi, S. Li, and J. A. Eastman, "Measuring Thermal Conductivity of Fluids Containing Oxide Nanoparticles," *Journal of Heat Transfer,* vol. 121, no. 2, pp. 280-288, 1999.

[99] X. J. Wang, D. S. Zhu, and S. Yang, "Investigation of pH and SDBS on enhancement of thermal conductivity in nanofluids," *Chemical Physics Letters,* vol. 470, no. 1-3, pp. 107-111, 2009.

[100] Y. Xuan, Q. Li, and W. Hu, "Aggregation structure and thermal conductivity of nanofluids," *AIChE Journal,* vol. 49, no. 4, pp. 1038-1043, 2003.

[101] X. F. Li, D. S. Zhu, X. J. Wang, N. Wang, J. W. Gao, and H. Li, "Thermal conductivity enhancement dependent pH and chemical surfactant for Cu-H2O nanofluids," *Thermochimica Acta,* vol. 469, no. 1-2, pp. 98-103, 2008.

[102] Y. Xuan and Q. Li, "Heat transfer enhancement of nanofluids," *International Journal of Heat and Fluid Flow,* vol. 21, no. 1, pp. 58-64, 2// 2000.

[103] H. Xie, J. Wang, T. Xi, Y. Liu, F. Ai, and Q. Wu, "Thermal conductivity enhancement of suspensions containing nanosized alumina particles," *Journal of Applied Physics,* vol. 91, no. 7, pp. 4568-4572, 2002.

[104] H. E. Patel, S. K. Das, T. Sundararajan, A. Sreekumaran Nair, B. George, and T. Pradeep, "Thermal conductivities of naked and monolayer protected metal nanoparticle based nanofluids: Manifestation of anomalous enhancement and chemical effects," *Applied Physics Letters,* vol. 83, no. 14, pp. 2931-2933, 2003.

[105] S. U. S. Choi, Z. G. Zhang, W. Yu, F. E. Lockwood, and E. A. Grulke, "Anomalous thermal conductivity enhancement in nanotube suspensions," *Applied Physics Letters,* vol. 79, no. 14, pp. 2252-2254, 2001.

[106] J. C. Maxwell, "A Treatise on Electricity and Magnetism, Clarendon," *Oxford, UK,,* 1891.

[107] R. L. Hamilton and O. K. Crosser, "Thermal Conductivity of Heterogeneous Two-Component Systems," *I & EC Fundamentals,* vol. 1, pp. 182–191, 1962.

[108] P. Keblinski, S. R. Phillpot, S. U. S. Choi, and J. A. Eastman, "Mechanisms of heat flow in suspensions of nano-sized particles (nanofluids)," *International Journal of Heat and Mass Transfer,* vol. 45, no. 4, pp. 855-863, 2001.

[109] B. X. Wang, L. P. Zhou, and X. F. Peng, "A fractal model for predicting the effective thermal conductivity of liquid with suspension of nanoparticles," *International Journal of Heat and Mass Transfer,* vol. 46, no. 14, pp. 2665-2672, 2003.

[110] Q. Z. Xue, "Model for effective thermal conductivity of nanofluids," *Physics Letters, Section A: General, Atomic and Solid State Physics,* vol. 307, no. 5-6, pp. 313-317, 2003.

[111] W. Yu and S. U. S. Choi, "The role of interfacial layers in the enhanced thermal conductivity of nanofluids: A renovated Maxwell model," *Journal of Nanoparticle Research,* vol. 5, no. 1-2, pp. 167-171, 2003.

[112] S. P. Jang and S. U. S. Choi, "Role of Brownian motion in the enhanced thermal conductivity of nanofluids," *Applied Physics Letters,* vol. 84, no. 21, pp. 4316-4318, 2004.

[113] C. T. Nguyen *et al.*, "Temperature and particle-size dependent viscosity data for water-based nanofluids: Hysteresis phenomenon," *International Journal of Heat and Fluid Flow,* vol. 28, no. 6, pp. 1492-1506, 2007.
[114] M. Kole and T. K. Dey, "Viscosity of alumina nanoparticles dispersed in car engine coolant," *Experimental Thermal and Fluid Science,* vol. 34, no. 6, pp. 677-683, 2010.
[115] L. Chen, H. Xie, Y. Li, and W. Yu, "Nanofluids containing carbon nanotubes treated by mechanochemical reaction," *Thermochimica Acta,* vol. 477, no. 1-2, pp. 21-24, 2008.
[116] C. T. Nguyen *et al.*, "Viscosity data for Al2O3-water nanofluid-hysteresis: Is heat transfer enhancement using nanofluids reliable?," *International Journal of Thermal Sciences,* vol. 47, no. 2, pp. 103-111, 2008.
[117] K. B. Anoop, S. Kabelac, T. Sundararajan, and S. K. Das, "Rheological and flow characteristics of nanofluids: Influence of electroviscous effects and particle agglomeration," *Journal of Applied Physics,* vol. 106, no. 3, 2009, Art. no. 034909.
[118] M. T. Naik, G. Ranga Janardhana, K. Vijaya Kumar Reddy, and B. Subba Reddy, "Experimental investigation into rheological property of copper oxide nanoparticles suspended in propylene glycol-water based fluids," *Journal of Engineering and Applied Sciences,* vol. 5, no. 6, pp. 29-34, 2010.
[119] P. K. Namburu, D. P. Kulkarni, D. Misra, and D. K. Das, "Viscosity of copper oxide nanoparticles dispersed in ethylene glycol and water mixture," *Experimental Thermal and Fluid Science,* vol. 32, no. 2, pp. 397-402, 2007.
[120] P. K. Namburu, D. P. Kulkarni, A. Dandekar, and D. K. Das, "Experimental investigation of viscosity and specific heat of silicon dioxide nanofluids," *Micro & Nano Letters,* vol. 2, no. 3, pp. 67-71, 2007.
[121] D. P. Kulkarni, D. K. Das, and R. S. Vajjha, "Application of nanofluids in heating buildings and reducing pollution," *Applied Energy,* vol. 86, no. 12, pp. 2566-2573, 2009.
[122] W. Q. Lu and Q. M. Fan, "Study for the particle's scale effect on some thermophysical properties of nanofluids by a simplified molecular dynamics method," *Engineering Analysis with Boundary Elements,* vol. 32, no. 4, pp. 282-289, 2008.
[123] J. Chevalier, O. Tillement, and F. Ayela, "Rheological properties of nanofluids flowing through microchannels," *Applied Physics Letters,* vol. 91, no. 23, 2007, Art. no. 233103.
[124] M. J. Pastoriza-Gallego, C. Casanova, J. L. Legido, and M. M. Piñeiro, "CuO in water nanofluid: Influence of particle size and polydispersity on volumetric behaviour and viscosity," *Fluid Phase Equilibria,* vol. 300, no. 1-2, pp. 188-196, 2011.
[125] R. Prasher, D. Song, J. Wang, and P. Phelan, "Measurements of nanofluid viscosity and its implications for thermal applications," *Applied Physics Letters,* vol. 89, no. 13, 2006, Art. no. 133108.
[126] E. V. Timofeeva, W. Yu, D. M. France, D. Singh, and J. L. Routbort, "Nanofluids for heat transfer: An engineering approach," *Nanoscale Research Letters,* vol. 6, no. 1, pp. X1-7, 2011.
[127] E. V. Timofeeva, J. L. Routbort, and D. Singh, "Particle shape effects on thermophysical properties of alumina nanofluids," *Journal of Applied Physics,* vol. 106, no. 1, 2009, Art. no. 014304.
[128] S. K. Das, N. Putra, and W. Roetzel, "Pool boiling characteristics of nano-fluids," *International Journal of Heat and Mass Transfer,* vol. 46, no. 5, pp. 851-862, 2003.
[129] W. J. Tseng and K. C. Lin, "Rheology and colloidal structure of aqueous TiO2 nanoparticle suspensions," *Materials Science and Engineering A,* vol. 355, no. 1-2, pp. 186-192, 2003.
[130] S. W. Lee, S. D. Park, S. Kang, I. C. Bang, and J. H. Kim, "Investigation of viscosity and thermal conductivity of SiC nanofluids for heat transfer applications," *International Journal of Heat and Mass Transfer,* vol. 54, no. 1-3, pp. 433-438, 2011.
[131] A. Einstein, "Eine neue bestimmung der moleküldimensionen,," *Ann. Phys,* vol. 324, no. 2, pp. 289–306, 1906.
[132] H. Brinkman, "The viscosity of concentrated suspensions and solutions," *J.Chem. Phys.,* vol. 20, 1952.
[133] I. M. Krieger, "A mechanism for non Newtonian flow in suspensions of rigid spheres,," *Trans. Soc. Rheol.,* no. 3, pp. 137–152, 1959.

[134] T. S. Lundgren, "Slow flow through stationary random beds and suspensions of spheres," *J. Fluid Mech.*, vol. 51, no. 2, pp. 273–299, 1972.
[135] G. Batchelor, "The effect of Brownian motion on the bulk stress in a suspension of spherical particles," *J. Fluid Mech.*, vol. 83, no. 01, pp. 97–117., 1977.
[136] A. L. Graham, "On the viscosity of suspensions of solid spheres," *Appl. Sci. Res.*, vol. 37, no. 3, pp. 275-286, 1981.
[137] D. Kim *et al.*, "Convective heat transfer characteristics of nanofluids under laminar and turbulent flow conditions," *Current Applied Physics*, vol. 9, no. 2 SUPPL., pp. e119-e123, 2009.
[138] S. Suresh, K. P. Venkitaraj, P. Selvakumar, and M. Chandrasekar, "Effect of Al2O3–Cu/water hybrid nanofluid in heat transfer," *Experimental Thermal and Fluid Science*, vol. 38, pp. 54-60, 2012/04/01/ 2012.
[139] U. Rea, T. McKrell, L.-w. Hu, and J. Buongiorno, "Laminar convective heat transfer and viscous pressure loss of alumina–water and zirconia–water nanofluids," *International Journal of Heat and Mass Transfer*, vol. 52, no. 7, pp. 2042-2048, 2009/03/01/ 2009.
[140] R. S. Vajjha, D. K. Das, and D. P. Kulkarni, "Development of new correlations for convective heat transfer and friction factor in turbulent regime for nanofluids," *International Journal of Heat and Mass Transfer*, vol. 53, no. 21-22, pp. 4607-4618, 2010.
[141] S. Ferrouillat, A. Bontemps, J. P. Ribeiro, J. A. Gruss, and O. Soriano, "Hydraulic and heat transfer study of SiO2/water nanofluids in horizontal tubes with imposed wall temperature boundary conditions," *International Journal of Heat and Fluid Flow*, vol. 32, no. 2, pp. 424-439, 2011.
[142] L. Syam Sundar, N. T. Ravi Kumar, M. T. Naik, and K. V. Sharma, "Effect of full length twisted tape inserts on heat transfer and friction factor enhancement with Fe 3O 4 magnetic nanofluid inside a plain tube: An experimental study," *International Journal of Heat and Mass Transfer*, vol. 55, no. 11-12, pp. 2761-2768, 2012.
[143] W. H. Azmi, K. V. Sharma, P. K. Sarma, R. Mamat, S. Anuar, and V. Dharma Rao, "Experimental determination of turbulent forced convection heat transfer and friction factor with SiO2 nanofluid," *Experimental Thermal and Fluid Science*, vol. 51, pp. 103-111, 2013.
[144] M. H. Kayhani, H. Soltanzadeh, M. M. Heyhat, M. Nazari, and F. Kowsary, "Experimental study of convective heat transfer and pressure drop of TiO 2/water nanofluid," *International Communications in Heat and Mass Transfer*, vol. 39, no. 3, pp. 456-462, 2012.
[145] B. Sahin, G. G. Gültekin, E. Manay, and S. Karagoz, "Experimental investigation of heat transfer and pressure drop characteristics of Al2O3-water nanofluid," *Experimental Thermal and Fluid Science*, vol. 50, pp. 21-28, 2013.
[146] S. Suresh, M. Chandrasekar, and S. Chandra Sekhar, "Experimental studies on heat transfer and friction factor characteristics of CuO/water nanofluid under turbulent flow in a helically dimpled tube," *Experimental Thermal and Fluid Science*, vol. 35, no. 3, pp. 542-549, 2011.
[147] W. Yu, E. V. Timofeeva, D. Singh, D. M. France, and R. K. Smith, "Investigations of heat transfer of copper-in-Therminol 59 nanofluids," *International Journal of Heat and Mass Transfer*, vol. 64, no. 1, pp. 1196-1204, 2013.
[148] L. G. Asirvatham, B. Raja, D. Mohan Lal, and S. Wongwises, "Convective heat transfer of nanofluids with correlations," *Particuology*, vol. 9, no. 6, pp. 626-631, 2011/12/01/ 2011.
[149] Y. Li, J. Fernández-Seara, K. Du, Á. Á. Pardiñas, L. L. Latas, and W. Jiang, "Experimental investigation on heat transfer and pressure drop of ZnO/ethylene glycol-water nanofluids in transition flow," *Applied Thermal Engineering*, vol. 93, pp. 537-548, 2016/01/25/ 2016.
[150] M. T. Naik and L. S. Sundar, "Heat Transfer and Friction Factor with Water/Propylene Glycol-Based CuO Nanofluid in Circular Tube with Helical Inserts under Transition Flow Regime," (in English), *Heat Transfer Engineering*, Article vol. 35, no. 1, pp. 53-62, 2014.
[151] X. Y. Ma Jie, Li Wenlie,Zhao Jiantao ,Zhang Shuping , and Basov Sergey, "Experimental investigation into the forced convective heat transfer of aqueous Fe3O4 nanofluids under transition region," *Journal of Nanoparticles*, vol. 2013, 2013.
[152] S. S. Chougule and S. K. Sahu, "Heat transfer and friction characteristics of Al2O3/water and CNT/water nanofluids in transition flow using helical screw tape inserts: A comparative

study," *Chemical Engineering and Processing: Process Intensification*, vol. 88, pp. 78-88, 2015/02/01/ 2015.
[153] H. K. Tam, L. M. Tam, and A. J. Ghajar, "Effect of inlet geometries and heating on the entrance and fully-developed friction factors in the laminar and transition regions of a horizontal tube," *Experimental Thermal and Fluid Science*, vol. 44, pp. 680-696, 2013.
[154] L. M. Tam and A. J. Ghajar, "Transitional heat transfer in plain horizontal tubes," *Heat Transfer Engineering*, vol. 27, no. 5, pp. 23-38, 2006/06/01 2006.
[155] A. J. Ghajar and K. F. Madon, "Pressure drop measurements in the transition region for a circular tube with three different inlet configurations," *Experimental Thermal and Fluid Science*, vol. 5, no. 1, pp. 129-135, 1992/01/01/ 1992.
[156] A. J. Ghajar and L.-M. Tam, "Heat transfer measurements and correlations in the transition region for a circular tube with three different inlet configurations," *Experimental Thermal and Fluid Science*, vol. 8, no. 1, pp. 79-90, 1// 1994.
[157] A. J. Ghajar and L.-M. Tam, "Flow regime map for a horizontal pipe with uniform wall heat flux and three inlet configurations," *Experimental Thermal and Fluid Science*, vol. 10, no. 3, pp. 287-297, 4// 1995.
[158] L.-M. Tam and A. J. Ghajar, "Effect of inlet geometry and heating on the fully developed friction factor in the transition region of a horizontal tube," *Experimental Thermal and Fluid Science*, vol. 15, no. 1, pp. 52-64, 7// 1997.
[159] J. A. Olivier and J. P. Meyer, "Single-phase heat transfer and pressure drop of the cooling of water inside smooth tubes for transitional flow with different inlet geometries," *HVAC and Refrigration*, vol. 16, no. 4, pp. 471 - 496 2010.
[160] J. P. Meyer and J. A. Olivier, "Heat transfer and pressure drop characteristics of smooth horizontal tubes in the transitional flow regime," *Heat Transfer Engineering*, vol. 35, no. 14-15, pp. 1246-1253, 2014.
[161] J. P. Meyer and J. A. Olivier, "Transitional flow inside enhanced tubes for fully developed and developing flow with different types of inlet disturbances: Part II–heat transfer," *International Journal of Heat and Mass Transfer*, vol. 54, no. 7-8, pp. 1598-1607, 2011.
[162] M. Everts and J. P. Meyer, "Heat transfer of developing and fully developed flow in smooth horizontal tubes in the transitional flow regime," *International Journal of Heat and Mass Transfer*, vol. 117, pp. 1331-1351, 2018/02/01/ 2018.
[163] J. P. Meyer and M. Everts, "Single-phase mixed convection of developing and fully developed flow in smooth horizontal circular tubes in the laminar and transitional flow regimes," *International Journal of Heat and Mass Transfer*, vol. 117, pp. 1251-1273, 2018/02/01/ 2018.
[164] M. Everts and J. P. Meyer, "Relationship between pressure drop and heat transfer of developing and fully developed flow in smooth horizontal circular tubes in laminar, transitional, quasi-turbulent and turbulent flow regimes " *International Journal of Heat and Mass Transfer*, vol. 117, no. 2018, pp. 1231 - 1250, 2017.
[165] M. Everts and J. P. Meyer, "Flow regime maps for smooth horizontal tubes at a constant heat flux," *International Journal of Heat and Mass Transfer*, vol. 117, pp. 1274-1290, 2018/02/01/ 2018.
[166] W. M. Kays and M. E. Crawford, *Convective Heat and Mass Transfer.*, 3rd ed. McGraw Hill, New York., 1993.
[167] O. S. Galaktionov and P. D. Anderson, "Analysis and optimization of kenics static mixers.," *International Polymer Processing,*, vol. 18, no. 2, pp. 138–150, 2003.
[168] R. E. Rayle, "An investigation of the influence of orifice geometry on static pressure measurements.," Master's, Massachusetts Institute of Technology, October 1949.
[169] P. F. Dunn, *Measurement and Data Analysis for Engineering and Science*, 2nd ed. Boca Raton: CRC Press, 2010.
[170] T. Leon and U. Roman, "Two-phase gas-liquid flow in rectangular channels " *Chem. Eng. Sc.* , vol. 39, no. 4, pp. 751-765, 1984.
[171] J. L. M. Poiseuille, "Recherches expérimentelles sur le mouvement des liquids dans le tubes detrés petits diamétres," *Comptes Rendu*, vol. 11, pp. 961-967, 1041-1048, 1840.

[172] P. R. H. Blasius, "Das Aehnlichkeitsgesetz bei Reibungsvorgangen in Flüssigkeiten," *Forschungsheft,* vol. 131, pp. 1-41, 1913.
[173] Y. A. Cengel, *Heat and Mass Transfer: A Practical Approach* 3rd ed. McGraw-Hill, 2007.
[174] S. Morcos and A. Bergles, "Experimental investigation of combined forced and free laminar convection in horizontal tubes " *Journal of Heat Transfer,* vol. 97, no. 2, pp. 212-219, 1975.
[175] V. Gnielinski, "New equations for heat and mass transfer in turbulent pipe and channel flow " *Int. Chem. Eng.,* vol. 16, no. 2, p. 10, 1976.
[176] Y. He, Y. Men, Y. Zhao, H. Lu, and Y. Ding, "Numerical investigation into the convective heat transfer of TiO2 nanofluids flowing through a straight tube under the laminar flow conditions," *Applied Thermal Engineering,* vol. 29, no. 10, pp. 1965-1972, 2009/07/01/ 2009.
[177] C. Popiel and J. Wojtkowiak, "Simple formulas for thermophysical properties of liquid water for heat transfer calculations " *Heat Transfer Engineering,* vol. 19, no. 3, pp. 87-101, 1998.
[178] J. C. Joubert, M. Sharifpur, A. B. Solomon, and J. P. Meyer, "Enhancement in heat transfer of a ferrofluid in a differentially heated square cavity through the use of permanent magnets," *Journal of Magnetism and Magnetic Materials,* vol. 443, pp. 149-158, 2017/12/01/ 2017.
[179] I. D. Garbadeen, M. Sharifpur, J. M. Slabber, and J. P. Meyer, "Experimental study on natural convection of MWCNT-water nanofluids in a square enclosure," *International Communications in Heat and Mass Transfer,* vol. 88, pp. 1-8, 2017/11/01/ 2017.
[180] M. Sharifpur, N. Tshimanga, J. P. Meyer, and O. Manca, "Experimental investigation and model development for thermal conductivity of α-Al2O3-glycerol nanofluids," *International Communications in Heat and Mass Transfer,* Article vol. 85, pp. 12-22, 2017.
[181] S. A. Adio, M. Mehrabi, M. Sharifpur, and J. P. Meyer, "Experimental investigation and model development for effective viscosity of MgO-ethylene glycol nanofluids by using dimensional analysis, FCM-ANFIS and GA-PNN techniques," *International Communications in Heat and Mass Transfer,* Article vol. 72, pp. 71-83, 2016.
[182] N. Tshimanga, M. Sharifpur, and J. P. Meyer, "Experimental investigation and model development for thermal conductivity of glycerol-MgO nanofluids," *Heat Transfer Engineering,* Article vol. 37, no. 18, pp. 1538-1553, 2016.
[183] S. A. Adio, M. Sharifpur, and J. P. Meyer, "Influence of ultrasonication energy on the dispersion consistency of Al2O3–glycerol nanofluid based on viscosity data, and model development for the required ultrasonication energy density," *Journal of Experimental Nanoscience,* Article vol. 11, no. 8, pp. 630-649, 2016.
[184] S. A. Adio, M. Sharifpur, and J. P. Meyer, "Electrical conductivity and pH of γ-Al2O3-glycerol nanofluids in Einstein concentration regime," *Heat Transfer Engineering,* Article vol. 36, no. 14-15, pp. 1241-1251, 2015.
[185] G. Hetsroni, "Particles-turbulence interaction," *International Journal of Multiphase Flow,* vol. 15, no. 5, pp. 735-746, 1989/09/01/ 1989.
[186] A. Meriläinen *et al.*, "Influence of particle size and shape on turbulent heat transfer characteristics and pressure losses in water-based nanofluids," *International Journal of Heat* and Mass Transfer, vol. 61, pp. 439-448, 2013/06/01/ 2013.
[187] R. Karwa et al., "performance evaluation criterion at equal pumping power for enhanced performance heat transfer surfaces," Journal of Solar Energy, vol. 2013, 2013/05/015/ 2013.

Appendix A

Calibration of thermocouple and pressure transducers

Calibration of thermocouples was accomplished by comparing the measurements of the thermocouples while they were attached to the test section with a PT-100 measurement. A water bath was used to vary the temperature of the water. The results are represented in this section because each station of the seven stations consists of four thermocouples, namely T for the top, B for the bottom, W for the west side of the channel, and E for the east side of the channel. Pressure transducers were also calibrated by using a manometer to correct the transducers' measurements, and two transducers were used and calibrated (PT1 and PT2).

A.1 Results of thermocouple calibration

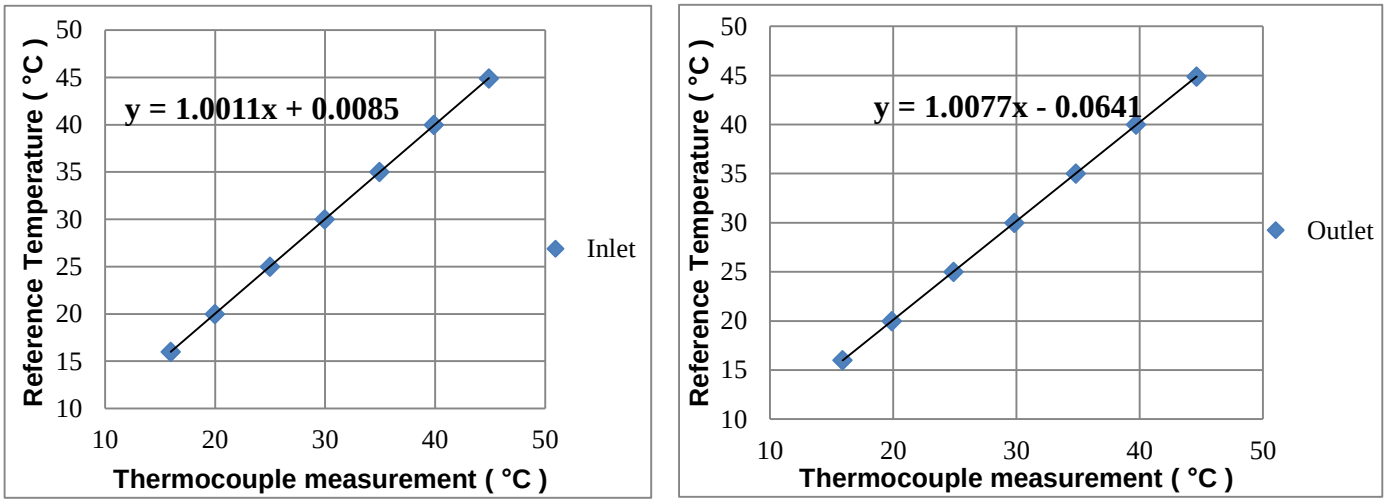

A. 1(a) **A. 1(b)**

Figure A.1: Calibration of the thermocouples used to measure the water temperature at (a) the inlet and (b) the outlet of the test section.

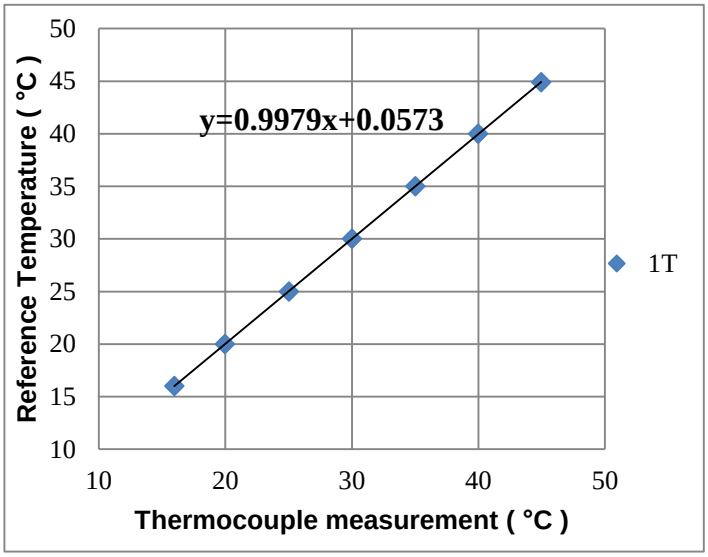

A. 2(a)

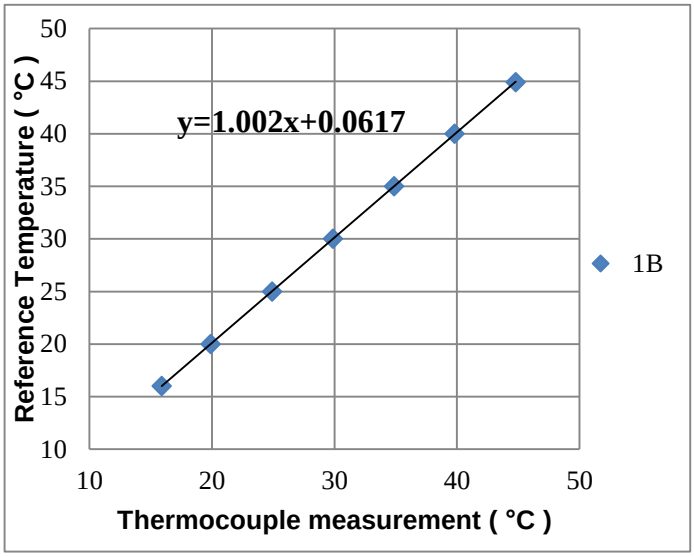

A. 2(b)

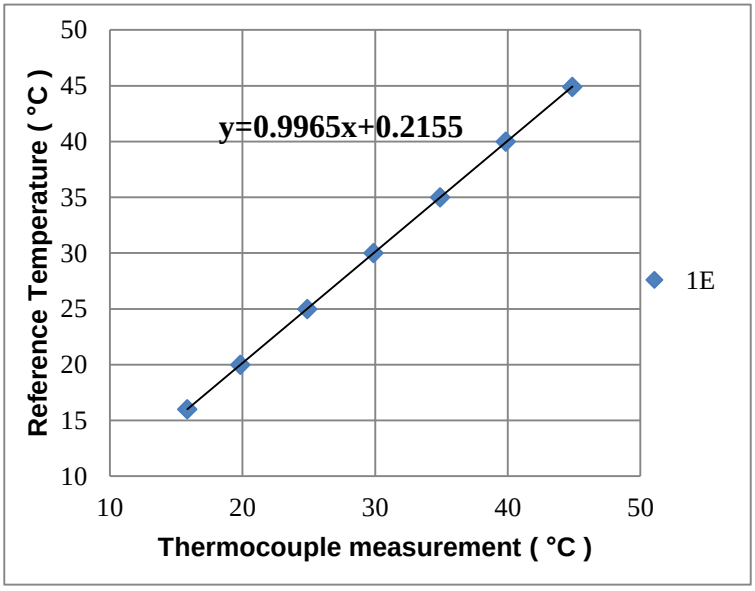

A. 2(c)

Figure A.2: Calibration of the four thermocouples in the first station: (a) top thermocouple, (b) thermocouple on the bottom side and (c) thermocouple on the eastern side of the test section.

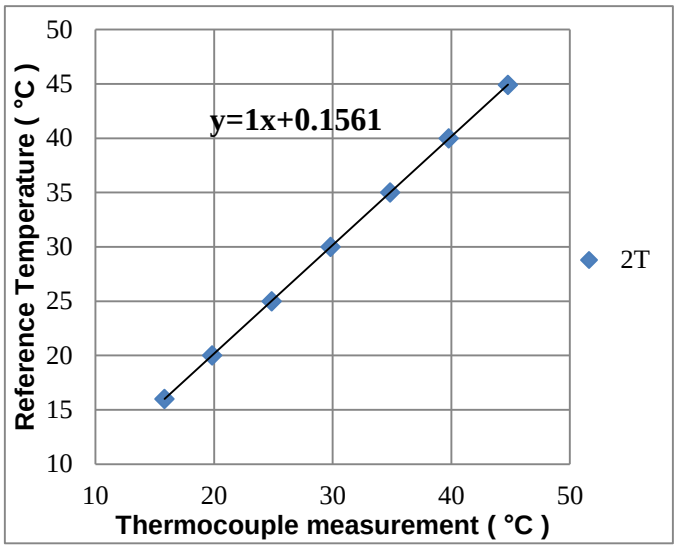

A. 3(a)

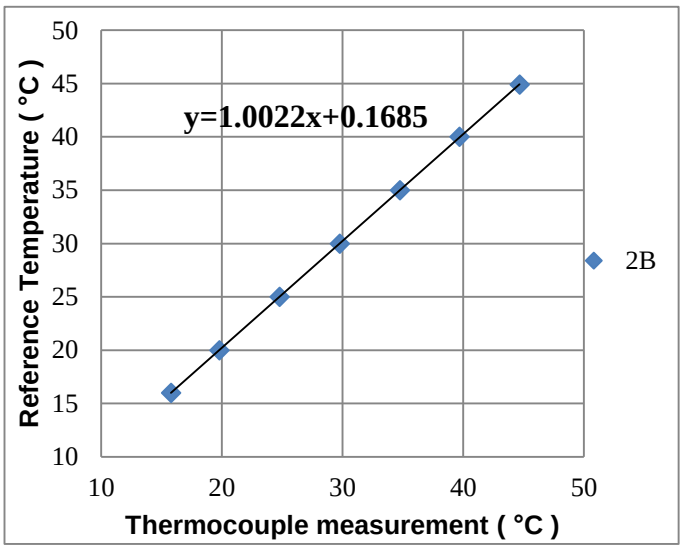

A. 3(b)

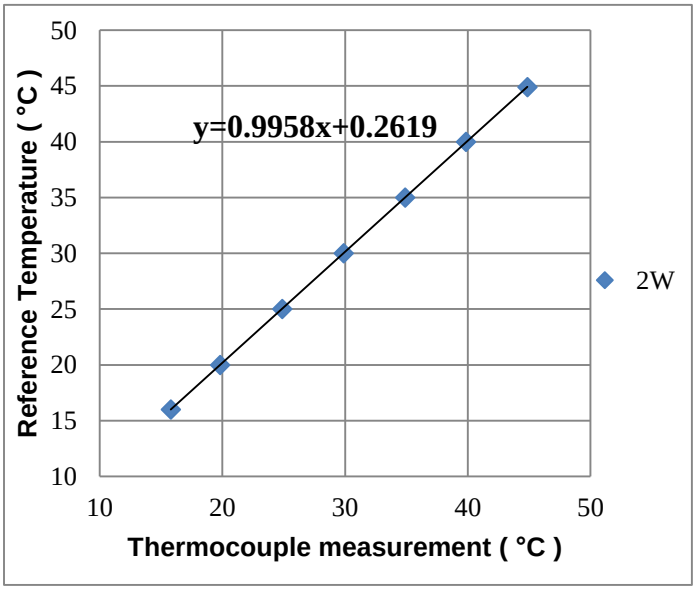

A. 3(c)

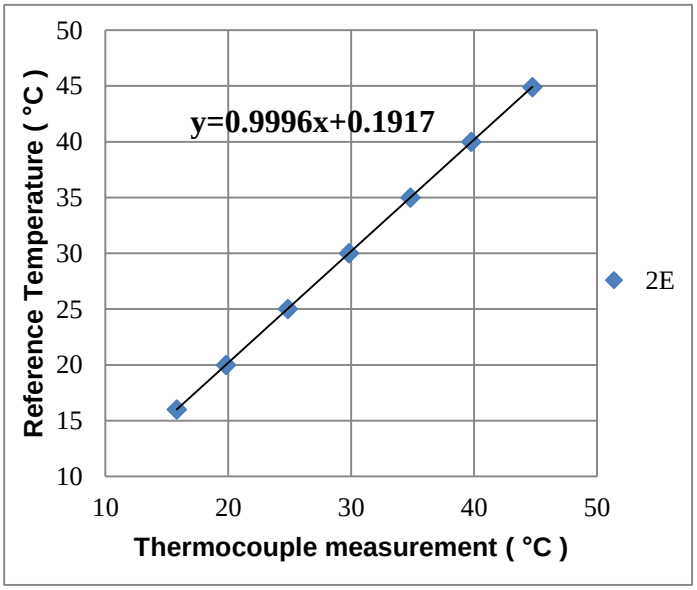

A. 3(d)

Figure A.3: Calibration of the four thermocouples in the second station: (a) top thermocouple, (b) thermocouple on the bottom side and (c) thermocouple on the eastern side of the test section.

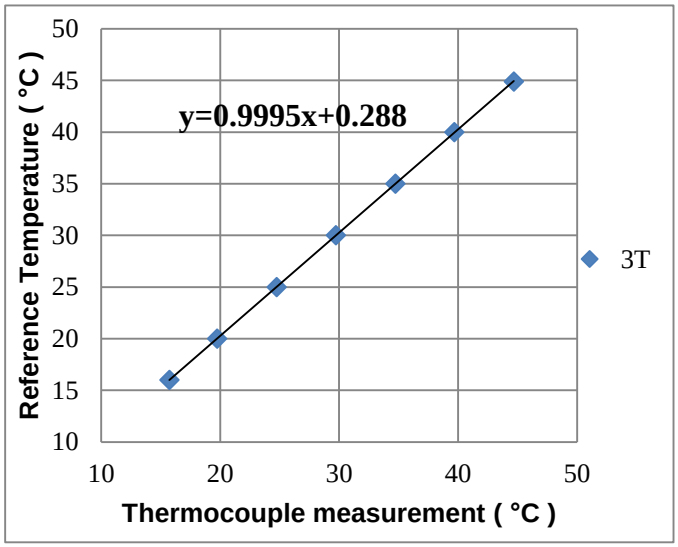

A. 4(a)

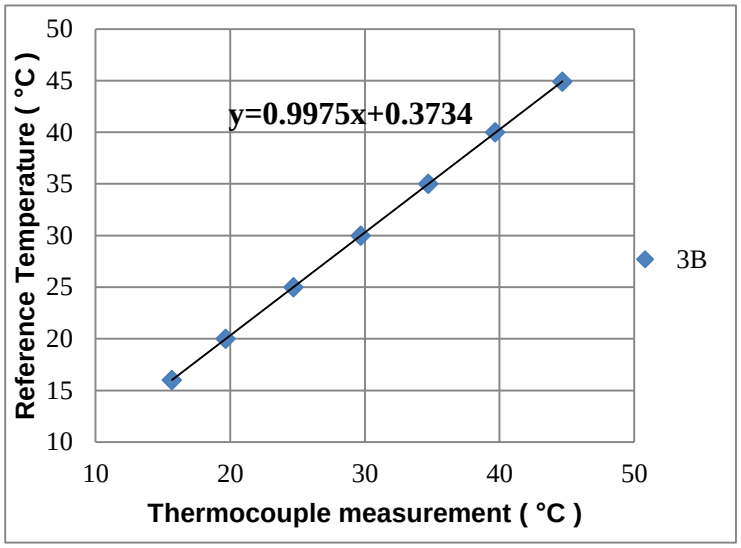

A. 4(b)

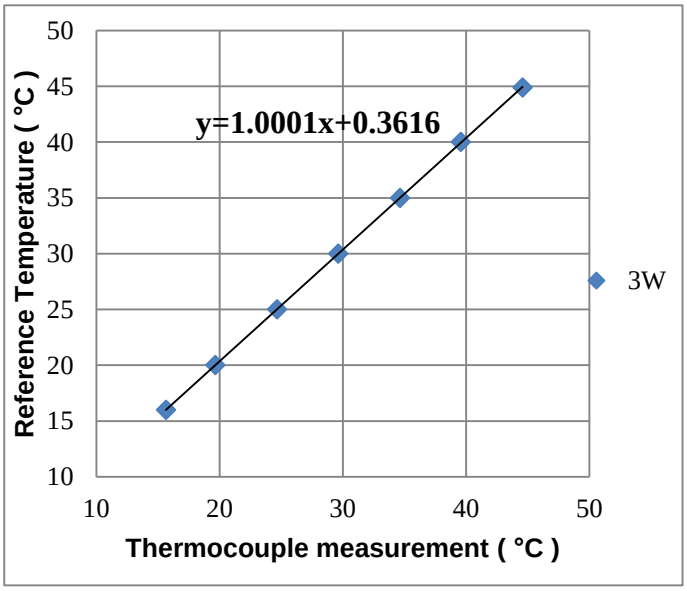

A. 4(c)

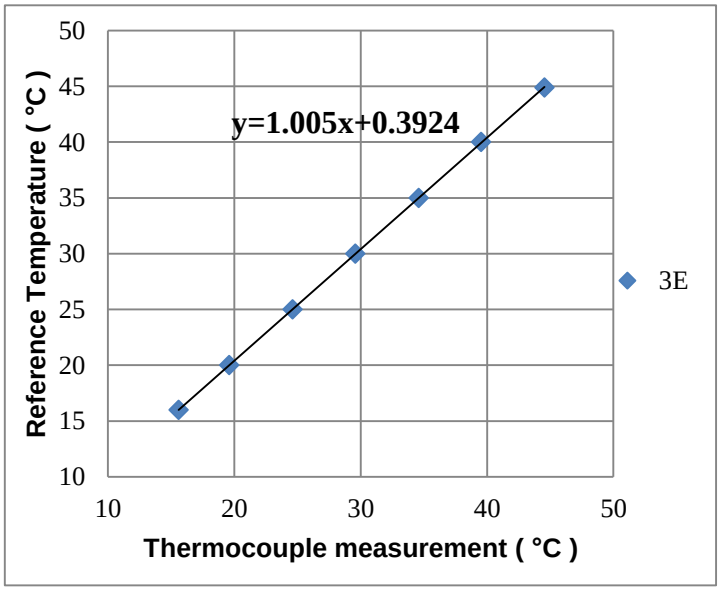

A. 4(d)

Figure A.4: Calibration of the four thermocouples in the third station: (a) top thermocouple, (b) thermocouple on the bottom side and (c) thermocouple on the eastern side of the test section.

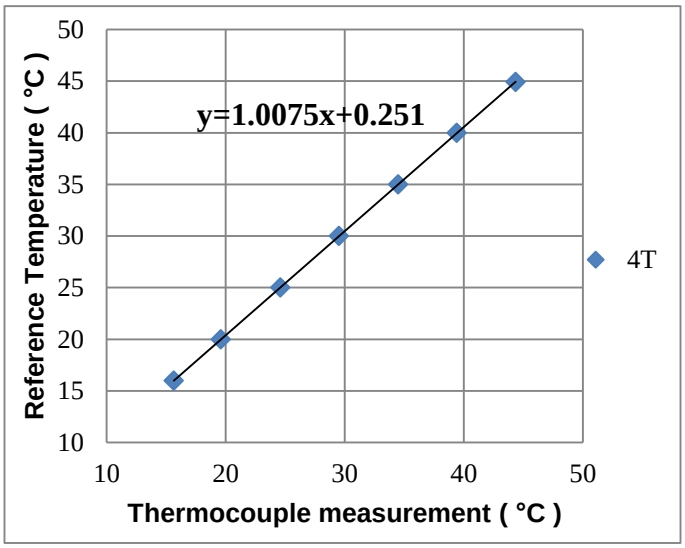

A. 5(a)

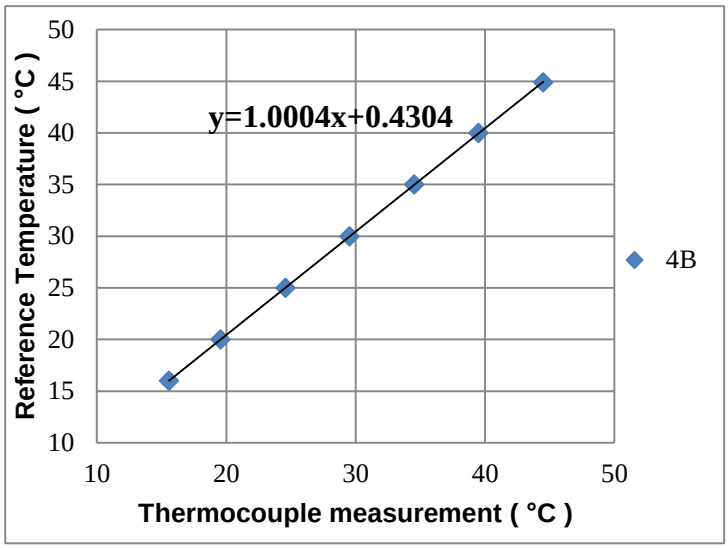

A. 5(b)

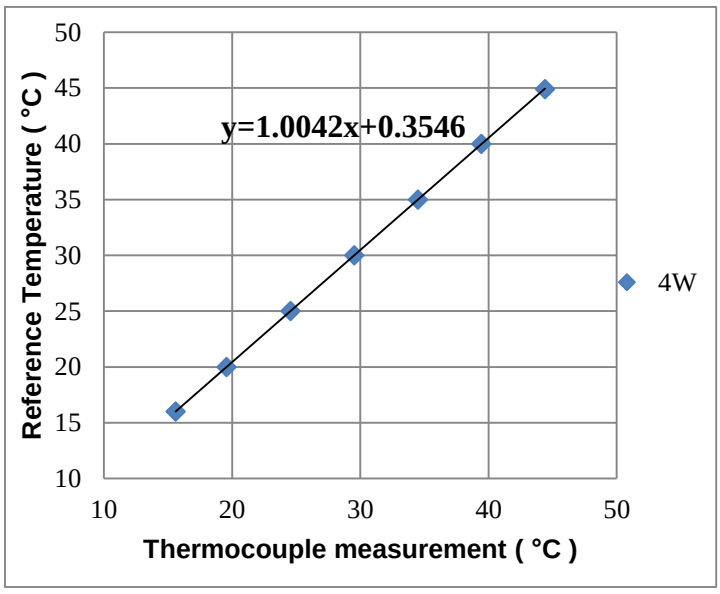

A. 5(c)

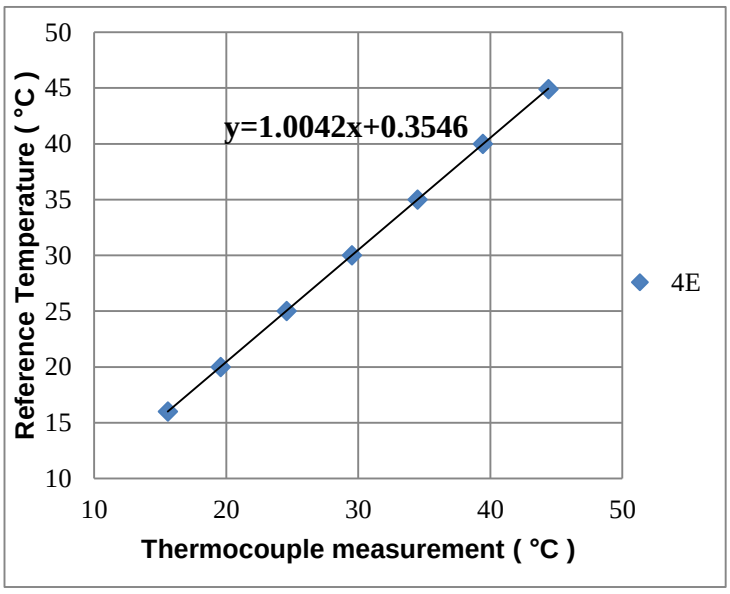

A. 5(d)

Figure A.5: Calibration of the four thermocouples in the fourth station: (a) top thermocouple, (b) thermocouple on the bottom side and (c) thermocouple on the eastern side of the test section.

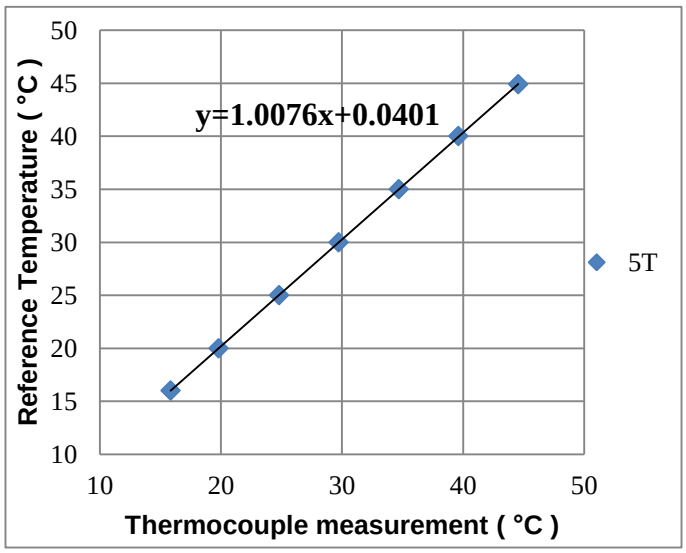

A. 6(a)

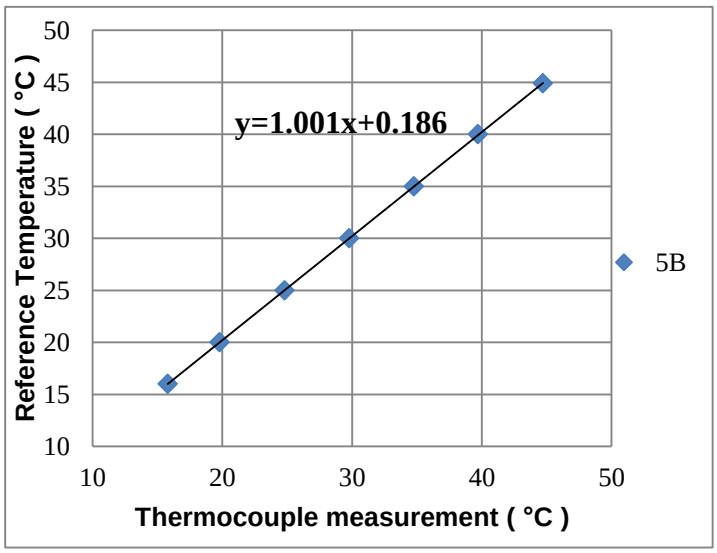

A. 6(b)

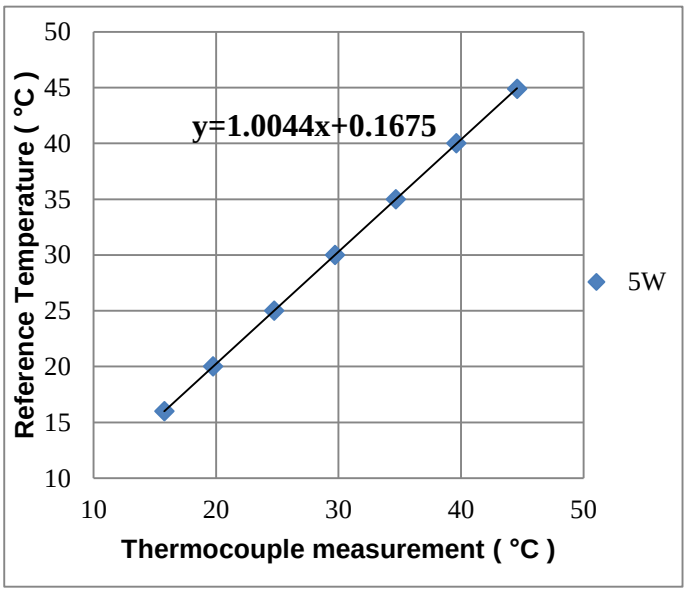

A. 6(c)

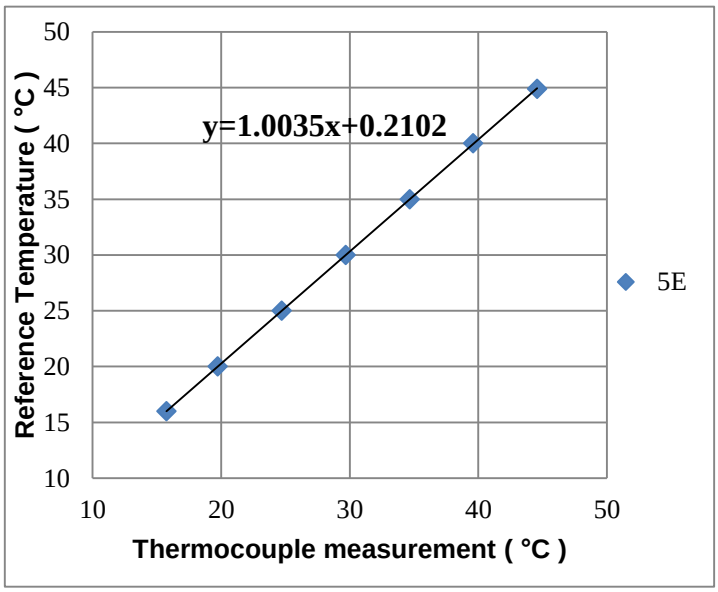

A. 6(d)

Figure A.6: Calibration of the four thermocouples in the fifth station: (a) top thermocouple, (b) thermocouple on the bottom side and (c) thermocouple on the eastern side of the test section.

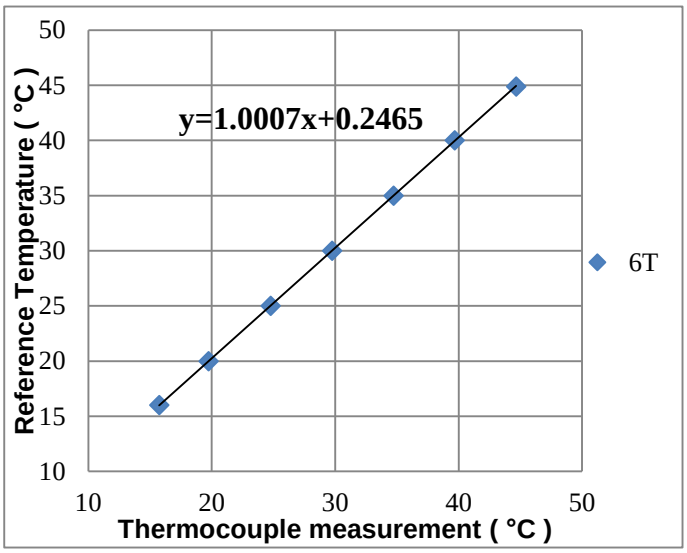

A. 7(a)

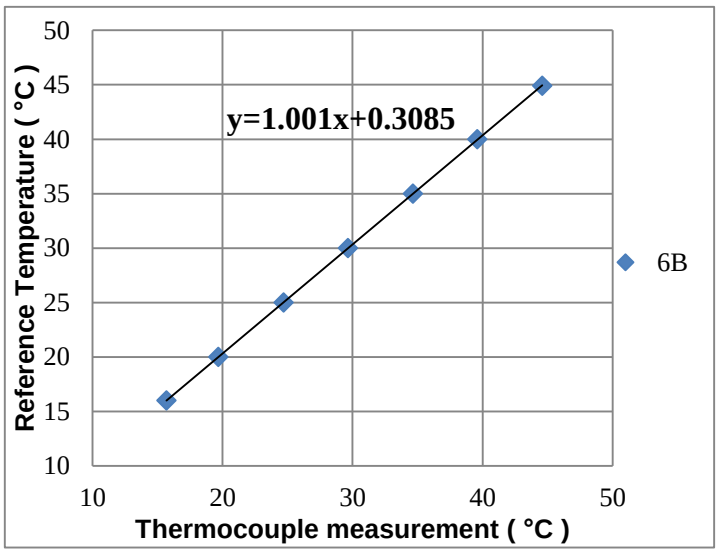

A. 7(b)

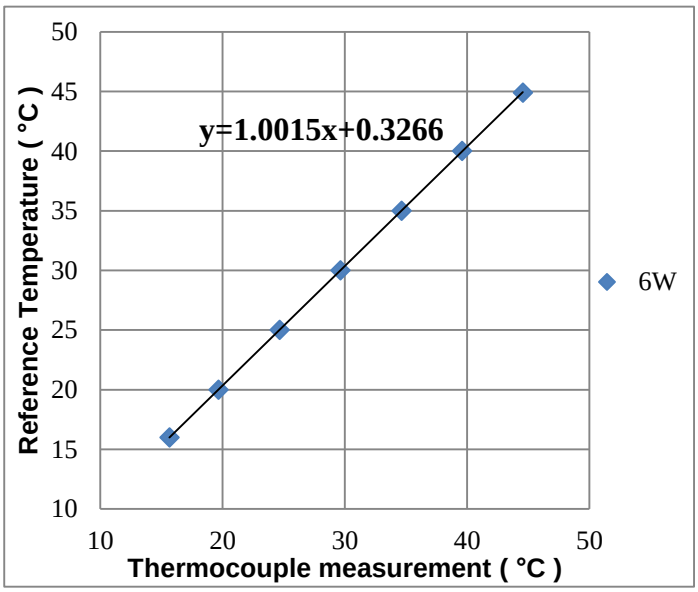

A. 7(c)

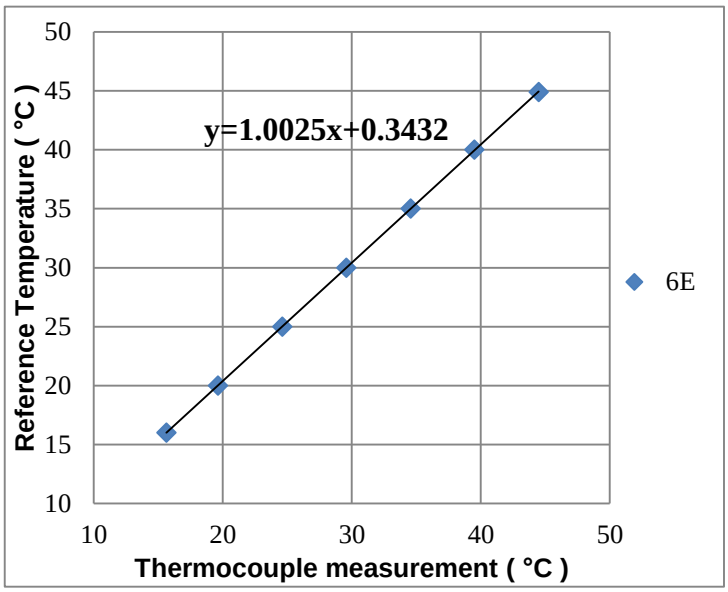

A. 7(d)

Figure A.7: Calibration of the four thermocouples in the sixth station: (a) top thermocouple, (b) thermocouple on the bottom side and (c) thermocouple on the eastern side of the test section.

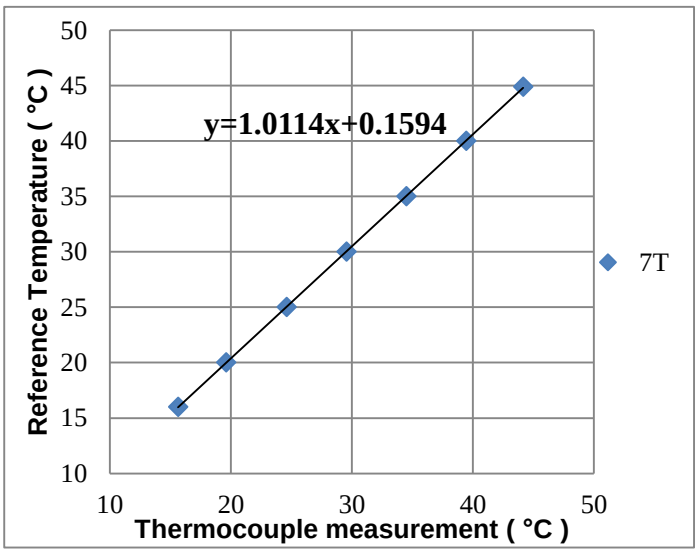

A. 8(a)

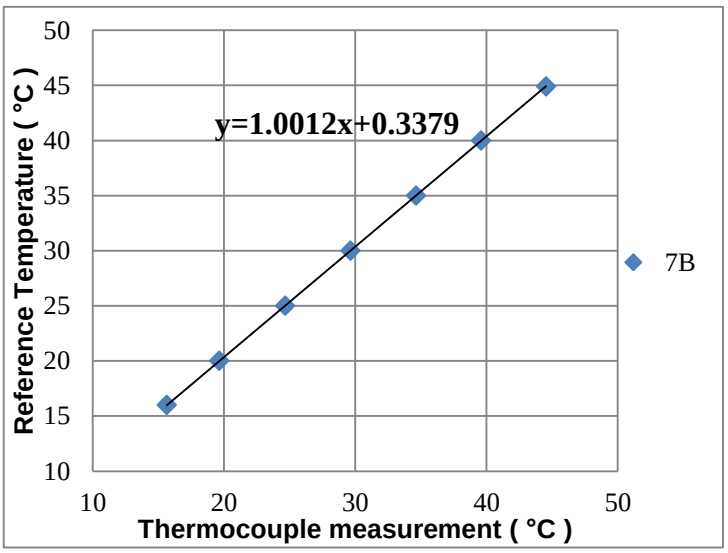

A. 8(b)

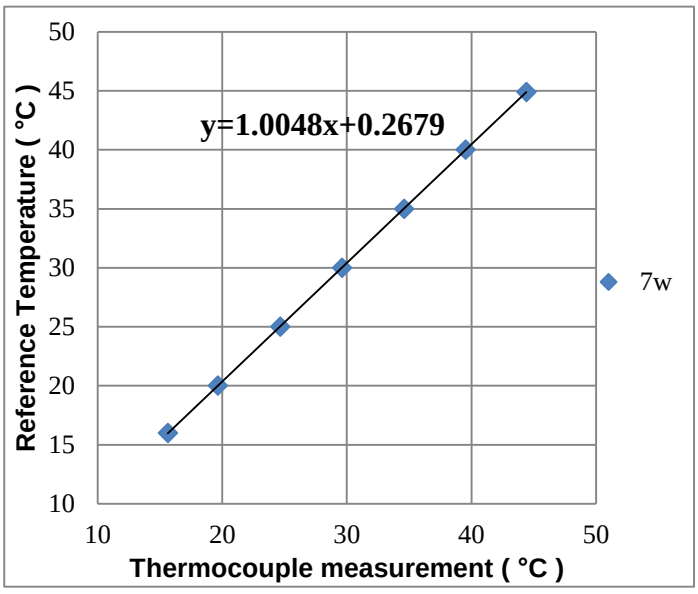

A. 8(c)

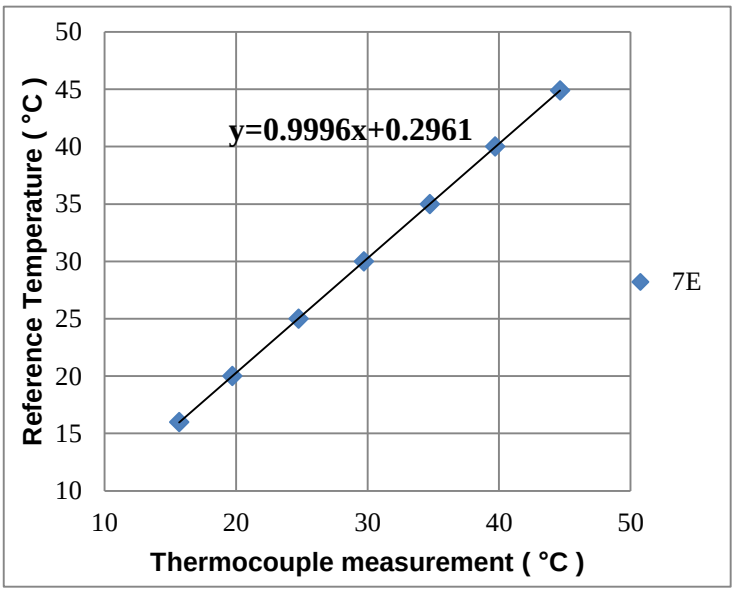

A. 8(d)

Figure A.8: Calibration of the four thermocouples in the seventh station: (a) top thermocouple, (b) thermocouple on the bottom side and (c) thermocouple on the eastern side of the test section.

A.2 Results of pressure transducer calibration

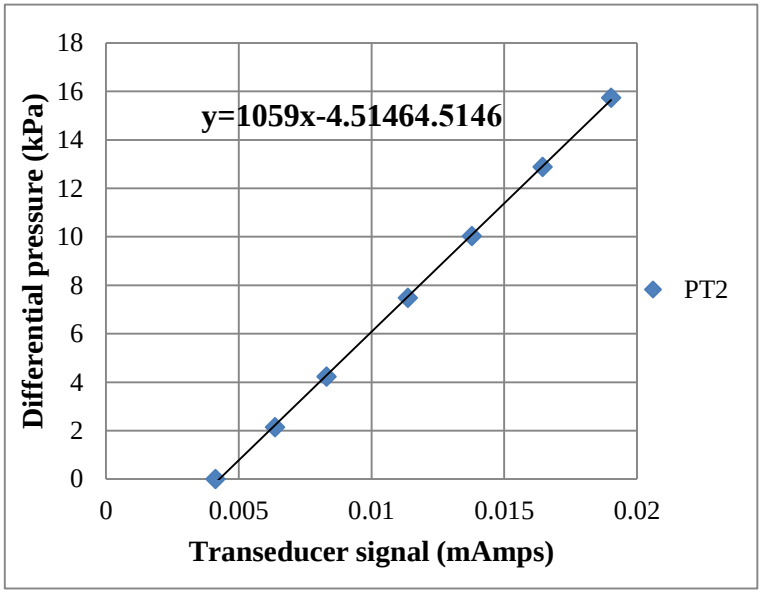

Figure A.9: Calibration of high-range pressure transducer (PT2).

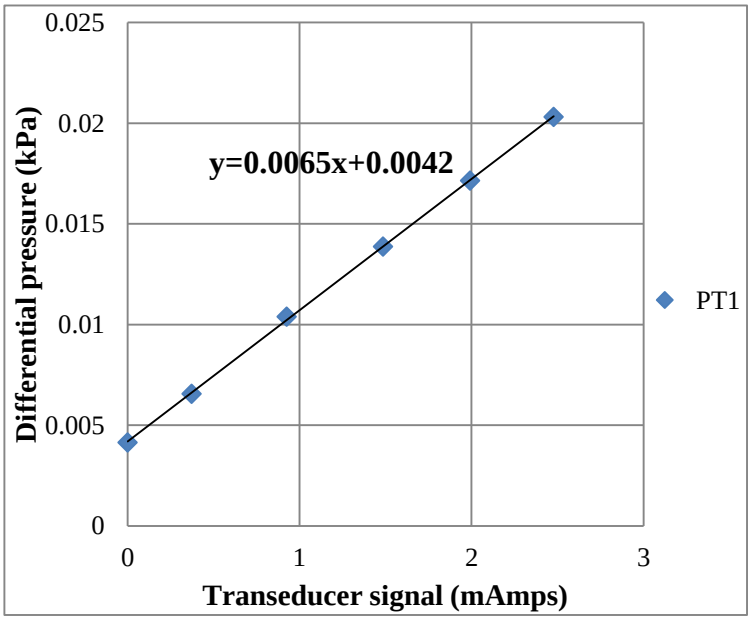

Figure A.10: Calibration of low-range pressure transducer (PT1).

Appendix B

Error estimation and uncertainty analysis

B.1 Introduction

Uncertainty and error analyses are necessary for any experimental work. In this study, the uncertainty of the pressure drop and the heat transfer parameters were calculated to know the reliability level of the measurements, which was the base of the current study.

The error in each measured value (x) was divided into (i) bias error, which is always a constant value caused by sensor calibration or the initial fixed operating conditions, (ii) random error, and the sensor sensitivity causes it, and it is also known as the accuracy.

The uncertainty in a measurement of a variable is the deviation of the true value of that variable for the mean measured value of the same variable.

B.2 Background

The uncertainty, u_x, is obtained from the bias error and estimates of the random error in the measured data set of x:

$$u_x = \sqrt{u_B^2 + u_p^2} \ , P\%$$

where u_B and u_P are bias error and precision error in x with P% probability respectively.

The uncertainty of parameter derived from measured variables can be calculated from a group of equations as follows:

$R(x) = f(x_1, x_2, \ldots\ldots x_n)$, where x_i is the measured variable. The uncertainty in R about the mean value $\bar{R}$ and the actual value R_{actual} is defined as follows:

$R_{actual} = \overline{R} + \delta R$ where δR is the uncertainty in R, and can be calculated as follows:

$$\delta R = \sqrt{\left(\delta x_1 \frac{\partial R}{\partial x_1}\right)^2 + \left(\delta x_2 \frac{\partial R}{\partial x_2}\right)^2 + \ldots\ldots\ldots + \left(\delta x_n \frac{\partial R}{\partial x_n}\right)^2} \qquad (\boldsymbol{B.1})$$

where δx_i is the uncertainty of the measured variable x_i

Perimeter of the test section:

$$p = (2W + 2H)$$

$$\boldsymbol{\delta p} = \sqrt{\left(\frac{\boldsymbol{\delta p}}{\boldsymbol{\delta W}}.\boldsymbol{\delta W}\right)^{\mathbf{2}} + \left(\frac{\boldsymbol{\delta p}}{\boldsymbol{\delta H}}.\boldsymbol{\delta H}\right)^{\mathbf{2}}}$$

$$\boldsymbol{\delta p} = \sqrt{(\mathbf{2}.\boldsymbol{\delta W})^{\mathbf{2}} + (\mathbf{2}.\boldsymbol{\delta H})^{\mathbf{2}}}$$

$$\frac{\boldsymbol{\delta p}}{\boldsymbol{p}} = \sqrt{\left(\frac{\boldsymbol{\delta W}}{\boldsymbol{W}+\boldsymbol{H}}\right)^{\mathbf{2}} + \left(\frac{\boldsymbol{\delta H}}{\boldsymbol{W}+\boldsymbol{H}}\right)^{\mathbf{2}}} \qquad (\boldsymbol{B}.\mathbf{2})$$

Heat transfer area:

$$A_s = (2z + 2h)L$$

$$\delta \mathrm{A_s} = \sqrt{\left(\frac{\delta \mathrm{A_s}}{\delta \mathrm{W}}.\delta \mathrm{W}\right)^{2} + \left(\frac{\delta \mathrm{A_s}}{\delta \mathrm{H}}.\delta \mathrm{H}\right)^{2} + \left(\frac{\delta \mathrm{A_s}}{\delta \mathrm{L}}.\delta \mathrm{L}\right)^{2}}$$

$$\delta A_s = \sqrt{(2L.\delta W)^2 + (2L.\delta H)^2 + \big((2W + 2H).\delta L\big)^2}$$

$$\frac{\delta A_s}{A_s} = \sqrt{\left(\frac{\delta W}{W+H}\right)^2 + \left(\frac{\delta H}{W+H}\right)^2 + \left(\frac{\delta L}{L}\right)^2}$$

$$\frac{\delta A_s}{A_s} = \sqrt{\left(\frac{\boldsymbol{\delta p}}{\boldsymbol{p}}\right)^2 + \left(\frac{\delta L}{L}\right)^2} \qquad (\boldsymbol{B}.\mathbf{3})$$

Flow velocity:

$$V = \frac{\dot{m}}{\rho\, WH}$$

$$\boldsymbol{\delta V} = \sqrt{\left(\frac{\boldsymbol{\delta V}}{\boldsymbol{\delta \dot{m}}}.\boldsymbol{\delta \dot{m}}\right)^{\mathbf{2}} + \left(\frac{\boldsymbol{\delta V}}{\boldsymbol{\delta \rho}}.\boldsymbol{\delta \rho}\right)^{\mathbf{2}} + \left(\frac{\boldsymbol{\delta V}}{\boldsymbol{\delta W}}.\boldsymbol{\delta W}\right)^{\mathbf{2}} + \left(\frac{\boldsymbol{\delta V}}{\boldsymbol{\delta h}}.\boldsymbol{\delta H}\right)^{\mathbf{2}}}$$

$$\boldsymbol{\delta}\mathrm{V} = \sqrt{\left(\frac{\mathbf{1}}{\boldsymbol{\rho WH}}.\boldsymbol{\delta}\dot{\mathrm{m}}\right)^{\mathbf{2}} + \left(\frac{-\dot{\mathbf{m}}\mathbf{WH}}{(\boldsymbol{\rho WH})^{\mathbf{2}}}.\boldsymbol{\delta}\rho\right)^{\mathbf{2}} + \left(\frac{-\dot{\mathbf{m}}\boldsymbol{\rho}\mathbf{H}}{(\boldsymbol{\rho WH})^{\mathbf{2}}}.\boldsymbol{\delta}\mathrm{W}\right)^{\mathbf{2}} + \left(\frac{-\dot{\mathbf{m}}\boldsymbol{\rho}\mathbf{W}}{(\boldsymbol{\rho WH})^{\mathbf{2}}}.\boldsymbol{\delta}\mathrm{H}\right)^{\mathbf{2}}}$$

$$\frac{\boldsymbol{\delta}\mathrm{V}}{\mathrm{V}} = \sqrt{\left(\frac{\boldsymbol{\delta}\dot{\mathrm{m}}}{\dot{\mathrm{m}}}\right)^{\mathbf{2}} + \left(\frac{\boldsymbol{\delta}\rho}{\rho}\right)^{\mathbf{2}} + \left(\frac{\boldsymbol{\delta}\mathrm{W}}{\boldsymbol{W}}\right)^{\mathbf{2}} + \left(\frac{\boldsymbol{\delta}\mathrm{H}}{\boldsymbol{H}}\right)^{\mathbf{2}}} \qquad (\boldsymbol{B}.\mathbf{4})$$

Fluid means temperature:

$$T_m(x) = T_i + \frac{\dot{q}\ x\ p}{\dot{m}C_P}$$

$$\boldsymbol{\delta}\,T_m(x) = \sqrt{\begin{aligned}&\left(\frac{\boldsymbol{\delta}T_m(x)}{\boldsymbol{\delta}T_i}.\boldsymbol{\delta}T_i\right)^{\mathbf{2}} + \left(\frac{\boldsymbol{\delta}T_m(x)}{\boldsymbol{\delta}\dot{q}}.\boldsymbol{\delta}\dot{q}\right)^{\mathbf{2}} + \left(\frac{\boldsymbol{\delta}T_m(x)}{\boldsymbol{\delta}x}.\boldsymbol{\delta}x\right)^{\mathbf{2}} + \left(\frac{\boldsymbol{\delta}T_m(x)}{\boldsymbol{\delta}p}.\boldsymbol{\partial}p\right)^{\mathbf{2}} \\ &+\left(\frac{\boldsymbol{\delta}T_m(x)}{\boldsymbol{\delta}\dot{m}}.\boldsymbol{\partial}\dot{m}\right)^{\mathbf{2}} + \left(\frac{\boldsymbol{\delta}T_m(x)}{\boldsymbol{\delta}C_P}.\boldsymbol{\delta}C_P\right)^{\mathbf{2}}\end{aligned}}$$

$$\boldsymbol{\delta}\,T_m(x) = \sqrt{(\boldsymbol{\delta}T_i)^{\mathbf{2}} + \left(\frac{x.p}{\dot{m}C_P}.\boldsymbol{\delta}\dot{q}\right)^{\mathbf{2}} + \left(\frac{\dot{q}\ .\ p}{\dot{m}C_P}.\boldsymbol{\delta}x\right)^{\mathbf{2}} + \left(\frac{\dot{q}.x}{\dot{m}C_P}.\boldsymbol{\delta}p\right)^{\mathbf{2}} + \left(\frac{\dot{q}\ x\ p}{\dot{m}^2C_P}.\boldsymbol{\delta}\dot{m}\right)^{\mathbf{2}} + \left(-\frac{\dot{q}\ x\ p}{\dot{m}{C_P}^2}.\boldsymbol{\delta}C_P\right)^{\mathbf{2}}}$$

$$\frac{\boldsymbol{\delta}\,T_m(x)}{T_m(x)} = \sqrt{\begin{aligned}&\left(\frac{\dot{m}C_P}{\dot{m}C_PT_i + \dot{q}\ x\ p}.\boldsymbol{\delta}T_i\right)^{\mathbf{2}} + \left(\frac{x.p}{\dot{m}C_PT_i + \dot{q}\ x\ p}.\boldsymbol{\delta}\dot{q}\right)^{\mathbf{2}} + \left(\frac{\dot{q}\ .\ p}{\dot{m}C_PT_i + \dot{q}\ x\ p}.\boldsymbol{\delta}x\right)^{\mathbf{2}} + \left(\frac{\dot{q}.x}{\dot{m}C_PT_i + \dot{q}\ x\ p}.\boldsymbol{\delta}p\right)^{\mathbf{2}} \\ &+\left(\frac{\dot{q}\ x\ p}{\dot{m}C_PT_i + \dot{q}\ x\ p}.\frac{\boldsymbol{\delta}\dot{m}}{\dot{m}}\right)^{\mathbf{2}} + \left(\frac{\dot{q}\ x\ p}{\dot{m}C_PT_i + \dot{q}\ x\ p}.\frac{\boldsymbol{\delta}C_P}{C_P}\right)^{\mathbf{2}}\end{aligned}}$$

$$(\boldsymbol{B}.\mathbf{5})$$

Heat transfer input to the test section:

$$Q_w = \dot{m} \,.\, C_P \,.\, (T_e - T_i)$$

$$\boldsymbol{\delta} Q_w = \sqrt{\left(\frac{\boldsymbol{\delta}\dot{Q_w}}{\boldsymbol{\delta}\dot{m}} . \boldsymbol{\delta}\dot{m}\right)^2 + \left(\frac{\boldsymbol{\delta}\dot{Q_w}}{\boldsymbol{\delta} c_p} . \boldsymbol{\delta} c_p\right)^2 + \left(\frac{\boldsymbol{\delta}\dot{Q_w}}{\boldsymbol{\delta} T_e} . \boldsymbol{\delta} T_e\right)^2 + \left(\frac{\boldsymbol{\delta}\dot{Q_w}}{\boldsymbol{\delta} T_i} . \boldsymbol{\delta} T_i\right)^2}$$

$$\boldsymbol{\delta} Q_w = \sqrt{\left(\boldsymbol{c_p}(\boldsymbol{T_e} - \boldsymbol{T_i}) . \boldsymbol{\delta}\dot{m}\right)^2 + \left(\dot{\boldsymbol{m}}(\boldsymbol{T_e} - \boldsymbol{T_i}) . \boldsymbol{\delta} c_p\right)^2 + \left(\dot{\boldsymbol{m}}\boldsymbol{c_p} . \boldsymbol{\delta} T_e\right)^2 + \left(-\dot{\boldsymbol{m}}\boldsymbol{c_p} . \boldsymbol{\delta} T_i\right)^2}$$

$$\frac{\boldsymbol{\delta} Q_w}{Q_w} = \sqrt{\left(\frac{\boldsymbol{\delta}\dot{m}}{\dot{m}}\right)^2 + \left(\frac{\boldsymbol{\delta} c_p}{c_p}\right)^2 + \left(\frac{\boldsymbol{\delta} T_e}{\boldsymbol{T_e} - \boldsymbol{T_i}}\right)^2 + \left(\frac{\boldsymbol{\delta} T_i}{\boldsymbol{T_e} - \boldsymbol{T_i}}\right)^2} \qquad (\boldsymbol{B.6})$$

Heat flux:

$$\dot{q} = \frac{Q_w}{A_S}$$

$$\boldsymbol{\delta}\,\dot{q} = \sqrt{\left(\frac{\boldsymbol{\delta}\dot{q}}{\boldsymbol{\delta} Q_w} . \boldsymbol{\delta} Q_w\right)^2 + \left(\frac{\boldsymbol{\delta}\dot{q}}{\boldsymbol{\delta} A_S} . \boldsymbol{\delta} A_S\right)^2}$$

$$\boldsymbol{\delta}\,\dot{q} = \sqrt{\left(\frac{\boldsymbol{1}}{\boldsymbol{A_S}} . \boldsymbol{\delta} Q_w\right)^2 + \left(\frac{\boldsymbol{Q_W}}{\boldsymbol{A_S^2}} . \boldsymbol{\delta} A_S\right)^2}$$

$$\frac{\boldsymbol{\delta}\,\dot{q}}{\dot{q}} = \sqrt{\left(\frac{\boldsymbol{\delta} Q_w}{Q_w}\right)^2 + \left(\frac{\boldsymbol{\delta} A_S}{A_S}\right)^2} \qquad (\boldsymbol{B.7})$$

Local and average heat transfer coefficient:

$$h(x) = \frac{\dot{q}}{[T_{wi}(x) - T_m(x)]}$$

$$\delta\, h(x) = \sqrt{\left(\frac{\delta h(x)}{\delta\dot{q}} . \partial\dot{q}\right)^2 + \left(\frac{\delta h(x)}{\delta T_{wi}} . \partial T_{wi}\right)^2 + \left(\frac{\delta h(x)}{\delta T_m} . \delta T_m\right)^2}$$

$$\partial\, h(x) = \sqrt{\left(\frac{\delta \dot{q}}{T_{wi} - T_m}\right)^2 + \left(\frac{-\dot{q}}{(T_{wi} - T_m)^2}.\partial T_{wi}\right)^2 + \left(\frac{\dot{q}}{(T_{wi} - T_m)^2}.\delta T_m\right)^2}$$

$$\frac{\partial\, h(x)}{h(x)} = \sqrt{\left(\frac{\delta \dot{q}}{\dot{q}}\right)^2 + \left(\frac{\partial T_{wi}}{T_{wi} - T_m}\right)^2 + \left(\frac{\delta T_m}{T_{wi} - T_m}\right)^2} \qquad (\boldsymbol{B}.\mathbf{8})$$

For the average heat transfer:

$$h_{avg} = \frac{h(x_1) + \cdots \ldots \ldots \ldots + h(x_n)}{n}$$

$$\delta\, \mathrm{h_{avg.}} = \sqrt{\left(\frac{\delta\, \mathrm{h_{avg.}}}{\delta \mathrm{h(x_1)}}\right)^2 . \delta \mathrm{h(x_n)} + \cdots + \left(\frac{\delta\, \mathrm{h_{avg.}}}{\delta \mathrm{h(x_n)}}\right)^2 . \delta \mathrm{h(x_n)}}$$

$$\frac{\delta\, h_{avg.}}{h_{avg.}} = \sqrt{\frac{1}{n}\left(\left(\frac{\delta\, h(x_1)}{h(x_1)}\right)^2 + \left(\frac{\delta\, h(x_2)}{h(x_2)}\right)^2 + \cdots + \left(\frac{\delta\, h(x_n)}{h(x_n)}\right)^2\right)} \qquad (\boldsymbol{B}.\mathbf{9})$$

Reynolds number:

$$Re = \frac{\rho V D_h}{\mu}$$

$$\delta Re = \sqrt{\left(\frac{\delta Re}{\delta \rho}.\delta \rho\right)^2 + \left(\frac{\delta Re}{\delta V}.\delta V\right)^2 + \left(\frac{\delta Re}{\delta D_h}.\delta D_h\right)^2 + \left(\frac{\delta Re}{\delta \mu}.\delta \mu\right)^2}$$

$$\delta Re = \sqrt{\left(\frac{V D_h}{\mu}.\delta \rho\right)^2 + \left(\frac{\rho D_h}{\mu}.\delta V\right)^2 + \left(\frac{\rho V}{\mu}.\delta D_h\right)^2 + \left(-\frac{\rho V D_h}{\mu^2}.\delta \mu\right)^2}$$

$$\frac{\delta Re}{Re} = \sqrt{\left(\frac{\delta \rho}{\rho}\right)^2 + \left(\frac{\delta V}{V}\right)^2 + \left(\frac{\delta D_h}{D_h}\right)^2 + \left(\frac{\delta \mu}{\mu}\right)^2} \qquad (\boldsymbol{B}.\mathbf{10})$$

Friction coefficient:

$$f = \frac{2\,\Delta P\,D_h}{\rho L\,V^2}$$

$$\boldsymbol{\delta} f = \sqrt{\left(\frac{\boldsymbol{\delta} f}{\boldsymbol{\delta}\Delta P}.\boldsymbol{\delta}\Delta P\right)^{\mathbf{2}} + \left(\frac{\boldsymbol{\delta} f}{\boldsymbol{\delta} D_h}.\boldsymbol{\delta} D_h\right)^{\mathbf{2}} + \left(\frac{\boldsymbol{\delta} f}{\boldsymbol{\delta}\rho}.\boldsymbol{\delta}\rho\right)^{\mathbf{2}} + \left(\frac{\boldsymbol{\delta} f}{\boldsymbol{\delta} L}.\boldsymbol{\delta} L\right)^{\mathbf{2}} + \left(\frac{\boldsymbol{\delta} f}{\boldsymbol{\delta} V}.\boldsymbol{\delta} V\right)^{\mathbf{2}}}$$

$$\boldsymbol{\delta} f = \sqrt{\begin{aligned}&\left(\frac{\mathbf{2} D_h}{\rho L V^2}.\boldsymbol{\delta}\Delta P\right)^{\mathbf{2}} + \left(\frac{\mathbf{2}\Delta P}{\rho L V^2}.\boldsymbol{\delta} D_h\right)^{\mathbf{2}} + \left(\frac{-\mathbf{2}\Delta P D_h L V^2}{(\rho L V^2)^2}.\boldsymbol{\delta}\rho\right)^{\mathbf{2}} + \left(\frac{-\mathbf{2}\Delta P D_h \rho V^2}{(\rho L V^2)^2}.\boldsymbol{\delta} L\right)^{\mathbf{2}} \\ &+ \left(\frac{-\mathbf{4}\Delta P D_h \rho L V}{(\rho L V^2)^2}.\boldsymbol{\delta} V\right)^{\mathbf{2}}\end{aligned}}$$

$$\frac{\boldsymbol{\delta} f}{f} = \sqrt{\left(\frac{\boldsymbol{\delta}\Delta P}{\Delta P}\right)^{\mathbf{2}} + \left(\frac{\boldsymbol{\delta} D_h}{D_h}\right)^{\mathbf{2}} + \left(\frac{\boldsymbol{\delta}\rho}{\rho}\right)^{\mathbf{2}} + \left(\frac{\boldsymbol{\delta} L}{L}\right)^{\mathbf{2}} + \left(\frac{\mathbf{2}\boldsymbol{\delta} V}{V}\right)^{\mathbf{2}}} \qquad (\boldsymbol{B}.\mathbf{11})$$

Hydraulic diameter:

$$\mathrm{D_h} = \frac{2\mathrm{WH}}{(\mathrm{W}+\mathrm{H})}$$

$$\boldsymbol{\delta}\mathrm{D_h} = \sqrt{\left(\frac{2\mathrm{H}^2}{(\mathrm{W}+\mathrm{H})^2}.\delta\mathrm{W}\right)^2 + \left(\frac{2\mathrm{W}^2\mathrm{H}}{(\mathrm{W}+\mathrm{H})^2}.\delta\mathrm{W}\right)^2}$$

$$\frac{\boldsymbol{\delta}\mathrm{D_h}}{\mathrm{D_h}} = \sqrt{\left(\frac{\mathrm{H}}{(\mathrm{W}+\mathrm{H})}.\delta\mathrm{W}\right)^2 + \left(\frac{\mathrm{W}}{(\mathrm{W}+\mathrm{H})}.\delta\mathrm{W}\right)^2} \qquad (\boldsymbol{B}.\mathbf{12})$$

Nusselt number:

$$Nu = \frac{h_{avg} D_h}{k}$$

$$\boldsymbol{\delta} Nu = \sqrt{\left(\frac{\boldsymbol{\delta} Nu}{\boldsymbol{\delta} h_{avg.}}.\boldsymbol{\delta} h_{avg.}\right)^{\mathbf{2}} + \left(\frac{\boldsymbol{\delta} Nu}{\boldsymbol{\delta} D_h}.\boldsymbol{\delta} D_h\right)^{\mathbf{2}} + \left(\frac{\boldsymbol{\delta} Nu}{\boldsymbol{\delta} k}.\boldsymbol{\delta} k\right)^{\mathbf{2}}}$$

$$\boldsymbol{\delta Nu} = \sqrt{\left(\frac{D_h}{k}.\boldsymbol{\delta} h_{avg.}\right)^{\mathbf{2}} + \left(\frac{h_{avg.}}{k}.\boldsymbol{\delta} D_h\right)^{\mathbf{2}} + \left(\frac{-\,h_{avg.}\,D_h}{k^2}.\boldsymbol{\delta} k\right)^{\mathbf{2}}}$$

$$\frac{\boldsymbol{\delta Nu}}{Nu} = \sqrt{\left(\frac{\boldsymbol{\delta} h_{avg.}}{h_{avg.}}\right)^{\mathbf{2}} + \left(\frac{\boldsymbol{\delta} D_h}{D_h}\right)^{\mathbf{2}} + \left(\frac{\boldsymbol{\delta} k}{\boldsymbol{k}}\right)^{\mathbf{2}}} \qquad (\boldsymbol{B.13})$$

Prandtl number:

$$pr = \frac{\mu c_p}{k}$$

$$\boldsymbol{\delta} pr = \sqrt{\left(\frac{\boldsymbol{\delta} pr}{\boldsymbol{\delta}\mu}.\boldsymbol{\delta}\mu\right)^{\mathbf{2}} + \left(\frac{\boldsymbol{\delta} pr}{\boldsymbol{\delta} c_p}.\boldsymbol{\delta} c_p\right)^{\mathbf{2}} + \left(\frac{\boldsymbol{\delta} pr}{\boldsymbol{\delta} k}.\boldsymbol{\delta} k\right)^{\mathbf{2}}}$$

$$\boldsymbol{\delta} pr = \sqrt{\left(\frac{\boldsymbol{c_p}}{\boldsymbol{k}}.\boldsymbol{\delta}\mu\right)^{\mathbf{2}} + \left(\frac{\boldsymbol{\mu}}{\boldsymbol{k}}.\boldsymbol{\delta} c_p\right)^{\mathbf{2}} + \left(\frac{-\boldsymbol{\mu c_p}}{\boldsymbol{k^2}}.\boldsymbol{\delta} k\right)^{\mathbf{2}}} \qquad (\boldsymbol{B.14})$$

$$\frac{\boldsymbol{\delta} pr}{pr} = \sqrt{\left(\frac{\boldsymbol{\delta}\mu}{\mu}\right)^{\mathbf{2}} + \left(\frac{\boldsymbol{\delta} c_p}{c_p}\right)^{\mathbf{2}} + \left(\frac{\boldsymbol{\delta} k}{k}\right)^{\mathbf{2}}} \qquad (\boldsymbol{B.14})$$

B.3 Uncertainty results

Table B.1: Uncertainty of the instruments used in the tests.

Instrument	**Range**	**Uncertainty**
Flow meter	0 – 0.07 kg/s	0.1 %
Pressure sensor	0 – 17 kPa	0.21%
Thermocouples	-200 – 350 °C	0.1 °C
Power supply	0 – 320 V 0 – 12.5 A	0.33 V 0.04 A

Table B.2: Uncertainty of pure water properties.

Instrument	**Uncertainty**
Specific heat	0.1 %
Viscosity	0.21%
Density	0.1 °C
Thermal conductivity	0.33 V

Table B.3: Uncertainty of heat transfer and pressure drop parameters for pure water.

Parameter	**Uncertainty (Re=600)**	**Uncertainty (Re=7000)**
h	1.7 %	2.3 %
Nu	2.3 %	5 %
Re	2.1 %	1.7 %
f	18.6 %	1.9 %

Appendix C

Thermal properties of the working fluids

The polynomial equation of Popiel and Wojtkowiak [177] is used to estimate the properties of the water.

C.1 Water properties

C.1.1 Density of saturated liquid water

$$\rho = a + bT + cT^{2} + dT^{2.5} + eT^{3} \qquad \textbf{(C.1)}$$

where

a = 999.79684, b = 0.068317355, c = −0.010740248, d = 0.00082140905 and

$e = -2.3030988 \times 10^{-5}$. uncertainty for Equation C.1 is ±0.004%.

C.1.2 Specific heat of water at constant pressure

$$\rho = a + bT + cT^{1.5} + dT^{2} + eT^{2.5} \qquad \textbf{(C.2)}$$

where

a = 4.2174356, b = −0.0056181625, c = 0.0012992528, d = −0.00011535353 and

$e = 4.14964 \times 10^{-6}$. The estimated uncertainty for Equation C.2 is ±0.04%.

C.1.3 Thermal conductivity of water

$$k = a + bT + cT^{1.5} + dT^{2} + eT^{0.5} \qquad \textbf{(C.3)}$$

where

a = 0.5650285, b = 0.0026363895, c = −0.00012516934, $d = -1.5154918 \times 10^{-6}$ and

e = −0.0009412945. The estimated uncertainty for Equation C.3 is ±2%.

C.1.4 Dynamic viscosity of water

$$\mu = \frac{1}{a+bT+cT^{2}+dT^{3}} \qquad \textbf{(C.4)}$$

where

a = 557.82468, b = 19.408782, c = 0.1360459, d = −3.1160832×10^{-4}. The estimated uncertainty for Equation C.4 is ±1%.

C.2 Nanofluid properties

The viscosity of nanofluids used in the testing was measured, while the density and the specific heat were calculated using the mixture theory, which is valid for any mixture of two or more fluids. The thermal conductivity is predicted by using correlations from the literature for similar nanofluid types and concentrations.

C.2.1 Density of the nanofluids

The density of the nanofluids are calculated from the equation used in the literature:

$$\rho_{nf} = \emptyset.\rho_p + (1 - \emptyset) * \rho_{bf} \quad \textit{(C.5)}$$

C.2.2 Specific heat of the nanofluid

The specific heat is calculated based on the mixture theory as used in the literature:

$$\left(C_p\right)_{nf} = \frac{\emptyset.\left(\rho.C_p\right)_p + (1-\emptyset).\left(\rho.C_p\right)_{bf}}{\rho_{nf}} \quad \textit{(C.6)}$$

C.2.3 Thermal conductivity of the nanofluid

Mintsa et al. [91] developed a correlation for the effective thermal conductivity of Al_2O_3-water nanofluids, The correlation is valid for concentrations up to 9%, as shown in Eq. (1):

$$\frac{K_{nf}}{K_{bf}} = 1.72\emptyset + 1 \quad \textit{(C.7)}$$

The model of He et al. [176] was considered for the thermal conductivity of the nanofluids in this work, which was developed for different TiO_2-water-based nanofluids, as shown in Eq. (1):

$$\frac{K_{nf}}{K_{bf}} = 125.62\emptyset^2\ 4.82\emptyset + 1 \quad \textit{(C.8)}$$